2016

Effects of rhodopsin phosphorylation on dark adaptation and the recovery of sensitivity

BOSTON UNIVERSITY

SCHOOL OF MEDICINE

Dissertation

EFFECTS OF RHODOPSIN PHOSPHORYLATION ON DARK ADAPTATION AND THE RECOVERY OF SENSITIVITY

by

JUSTIN DAVID BERRY

B.S., Illinois State University, 2007
M.S., Northern Illinois University, 2010

Submitted in partial fulfillment of the

requirements for the degree of

Doctor of Philosophy

2016

Approved by

First Reader _____

M. Carter Cornwall, Ph.D.
Professor of Physiology and Biophysics

Second Reader _____

Clint Makino, Ph.D.
Associate Professor of Physiology and Biophysics

Third Reader _____

Jeannie Chen, Ph.D.
Professor of Cell & Neurobiology
University of Southern California, Keck School of Medicine

Wisdom must be intuitive reason combined with scientific knowledge.
— Aristotle

DEDICATION

I would like to dedicate this research to all the people that have made it possible. First, to my friends and family for their love and support over these many years. I also dedicate this to my advisor and colleagues that made me a better scientist.

ACKNOWLEDGMENTS

This work would not have been possible without contributions from the following people:

In Chapter 2, Soile Nymark performed the MSP recordings presented in Figure 2.2, which she also created. The data supporting this figure came from a previously published work, but the figure was not published along with the manuscript.

In Chapter 3, the IEF measurements were performed by Yun Yao. Yun also digitalized these IEF gels. Jeannie Chen performed the quantification of the IEF data using ImageJ. Likewise, ROS analysis used to track transducin translocation and arrestin translocation was performed by Yun Yao and Jeannie Chen. *In vivo* measurements of rhodopsin phosphorylation were performed at University of Southern California, Keck School of Medicine. Helen He, Tian Wang, and Kasey Rose provided assistance is performing these experiments. Rikard Frederiksen provided assistance with the microspectrophotometry and suction electrode experimental analysis. Additionally he created the software used to analyze the single quantal responses and he performed analysis of the variance.

Specific thanks to Maureen Estevez Stabio for early support in my graduate studies and continued friendship. Thanks to Howard Cohen for assistance with our electronics.

I would like to thank the Sampath lab at the University of Southern California (now at UCLA) for allowing me to work out of the lab in summer 2013. The Sampath lab provided instruments, animals, and assistance with performing proof of concept ERG recordings on Gnat2$^{-/-}$ retinae that allowed me to conduct further experiments at Boston University to determine the recovery of flash sensitivity during dark adaptation. I would like to thank Sam and Johan Pahlberg for their time and special assistance. I would also like to thank Kate Fehlhaber and Dutch Ratliff for their help while I visited the lab.

Thanks to the Chen lab at the University of Southern California for being exceptional collaborators, and providing me with a space to work out of for a few weeks in spring 2014. Special thanks, in particular, to Jeannie Chen and her family, who were gracious hosts while I performed experiments at the University of Southern California over two these occasions.

Many thanks to my dissertation committee: Chris Gabel, Clint Makino, Jeannie Chen and Jeff Moore. Each member of the committee provided me with valuable feedback and support at various points along the way.

I would like to convey special thanks to Rikard Frederiksen for being a superb colleague over the past five years in the Cornwall Lab. Rikard was instrumental in providing on the job training, critical analysis of the data, and real time experiment troubleshooting. These experiments would not have been nearly as successful without his advice and guidance.

Finally, I would like to thank my advisor, Carter Cornwall. His contributions greatly improved my experimental designs and research, and I thank him for his contributions in data analysis. He was an excellent mentor throughout this process and he challenged me to become a better scientist: for this, I am grateful.

EFFECTS OF RHODOPSIN PHOSPHORYLATION ON DARK ADAPTATION AND THE RECOVERY OF SENSITIVITY

JUSTIN DAVID BERRY

Boston University School of Medicine, 2016

Major Professor: M. Carter Cornwall Ph.D., Professor of Physiology and Biophysics

ABSTRACT

Vision requires the photoreceptors in the eye to rapidly respond to changes in light intensity. These processes are accomplished within rod photoreceptors by the visual pigment rhodopsin that initiates a downstream signaling cascade called phototransduction. Rhodopsin is composed of an apoprotein opsin that is covalently bonded with light sensitive 11-*cis* retinal. Rhodopsin is activated when 11-*cis* retinal is photoisomerized into all-trans retinal. This isomerization initiates the phototransduction cascade that culminates in a change in current at the plasma membrane. Rhodopsin, once activated ("bleached"), can no longer absorb photons to activate phototransduction, and must be regenerated through the visual cycle.

To enable the photoreceptors to respond to rapid changes in light intensities, phototransduction must terminate in a timely manner. Deactivation involves phosphorylation of activated rhodopsin by rhodopsin kinase, and then binding of visual arrestin. Exposing rods to daylight bleaches a large proportion of rhodopsin molecules. This exposure leads to desensitization of the photoreceptors and phosphorylation of bleached rhodopsin. Full recovery of receptor sensitivity is achieved when rhodopsin is

recycled and regenerated through a series of steps to its ground state. The last step in this process is the dephosphorylation of rhodopsin. This dissertation focuses on how rhodopsin dephosphorylation affects rod sensitivity.

I exploited a novel observation; mouse retinae when isolated from the retinal pigment epithelium (and eye cup), display blunted rhodopsin dephosphorylation. Isoelectric focusing followed by Western blot analysis of retinal homogenate from bleached isolated retinae showed little dephosphorylation of rhodopsin for up to four hours in darkness, even under conditions when rhodopsin was completely regenerated. Microspectrophotometric measurements of rhodopsin spectra show that regenerated phospho-rhodopsin has the same molecular photosensitivity as unphosphorylated rhodopsin and that flash responses measured by trans-retinal electroretinogram or single cell suction electrode recording displayed dark-adapted kinetics. Single quantal responses displayed normal dark-adapted kinetics, but rods were only half as sensitive as those containing exclusively unphosphorylated rhodopsin. I propose a revised model in which light-exposed retinae contain a mixed population of phosphorylated and unphosphorylated rhodopsin. Moreover, complete dark-adaptation can only occur when all rhodopsin has been dephosphorylated, a process that requires more than three hours in complete darkness.

TABLE OF CONTENTS

LIST OF TABLES

LIST OF FIGURES

LIST OF ABBREVIATIONS

Arr1 ..... Visual Arrestin

$Arr1^{-/-}$ ..... Homozygous Visual Arrestin Knockout

BU ..... Boston University

CNG ..... Cyclic Nucleotide Gated

Cpfl3 ..... Cone Photoreceptor Functional Loss 3

GAP ..... GTPase Accelerating Protein

GC ..... Guanylate Cyclase

GCAP ..... Guanylate Cyclase Activated Protein

Gnat2 ..... Guanine Nucleotide Binding Protein 2

$Gnat2^{-/-}$ ..... Homozygous Guanine Nucleotide Binding Protein 2 Knockout

Grk1 ..... G-Protein Receptor Kinase 1, Rhodopsin Kinase

$Grk1^{-/-}$ ..... Homozygous Rhodopsin Kinase Knockout

IEF ..... Isoelectric Focusing Western Blot

ISO ..... International Standards Organization

MII ..... Photo-activated Rhodopsin (Metarhodopsin II)

MSP ..... Microspectrophotometry

P-rhodopsin ..... Phosphorylated Rhodopsin

PDE ..... Phosphodiesterase

Rh ..... Rhodopsin

Rh* ..... Photo-activated Rhodopsin

ROS ..... Isolated Rod Outer Segment

SQR ..... Single Quantal Response

USC ..... University of Southern California

CHAPTER ONE: INTRODUCTION

All vision begins with a single event, the detection of a photon. In our eyes, photon detection occurs within rod and cone photoreceptors in the retina by a process that activates the visual pigment rhodopsin in rods and iodopsin in cones. This process, photoactivation, produces a cascade of cellular events known as phototransduction. Collectively, photoactivation and phototransduction allow visual information transmitted by light to be converted into electro-chemical signals that are interpreted by the retina and the brain.

Anatomy of the Retina

The retina is a layer of tissue that resides in the distal area of the eye (see Figure 1.1). Within the plane of this tissue, optical images are brought to focus. Photons from these images are collected by photoreceptors and retinal neurons convey this visual information to the brain. Visual information is relayed through three stratified layers of highly segregated and highly specialized retinal neurons, as illustrated in Figure 1.1 and Figure 1.2. At the most distal layer of the retina are the rod and cone photoreceptors. Humans possess a single class of rod photoreceptor, and three different subtypes of cone photoreceptors. Within these photoreceptor cells, light is absorbed by the visual pigment rhodopsin and converted into an electrochemical signal through the phototransduction cascade. Rod photoreceptors are highly sensitive and dynamic detectors that react with a graded response to light; an individual rod photoreceptor is sensitive to a wide range of

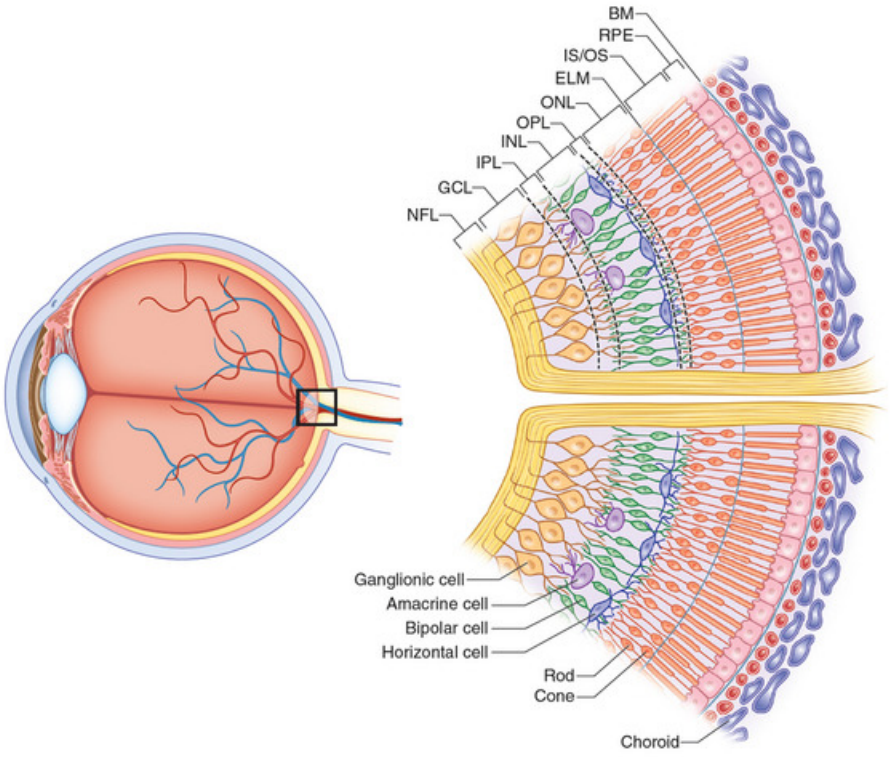

Figure 1.1: Anatomy of the mammalian eye. The cornea and the lens focus visual images onto the retina, which is located at back of the eye. In the retina, light is detected using photoreceptors located in the most distal portion of the eye. Visual signals are transmitted to the inner retinal neurons, then transmitted to the brain via the optic nerve. Abbreviations: nerver fiber layer (NFL), ganglion cell layer (GCL), inner plexiform layer (IPL), inner nuclear layer (INL), outer plexiform layer (OPL), outer nuclear layer (ONL), external limiting membrane (ELM), rod and cone inner and outer segment (IS/OS), retinal pigment epithelium (RPE), and Bruch membrane (BM) This illustration has been reproduced with permission from David J. Browning, MD, PhD (Browning), and the Springer Publishing Company**.**

light intensities, from a single photon to several thousand photons per second. Cones behave in a similar fashion, but operate at brighter light intensities. The signals created by photoreceptor cells are relayed synaptically, to inner retinal neurons.

The inner neurons in the retina are designed to process the visual information before it is communicated to the brain. In general, inner neurons collectively parse neurosynaptic signals that are generated by the photoreceptors (Masland, 2001a, b; Sampath and Rieke, 2004). Horizontal cells within the inner retina affect visual perception by detecting contrast. Specifically, horizontal cells receive synaptic input from multiple photoreceptors, and suppress the synaptic output of individual photoreceptors through a feedback mechanism that effectively subtracts the mean response from neighboring photoreceptor cells. Horizontal cell inhibition takes place at the bipolar cell synaptic junction. Retinal bipolar cells also collect signals from the photoreceptors. There is a single type of rod bipolar cell, while there are several subclasses of cone bipolar cells, each with their own function in how they process the visual data. Next, the inner retina contains amacrine cells. Amacrine cells function at the cone bipolar to ganglion junction. In rod mediated visual processes, AII amacrine cells bridge rod bipolar cells to ganglion cells, allowing rod bipolar cells to use the cone visual pathways since no direct connection between rod bipolar and ganglion cells exists. Collectively, cone bipolar and amacrine cells parse visual information into a series of events. When these events occur within predefined conditions, they trigger the excitation of retinal ganglion cells. The specific conditions required to trigger a response are in part reflected in the morphology

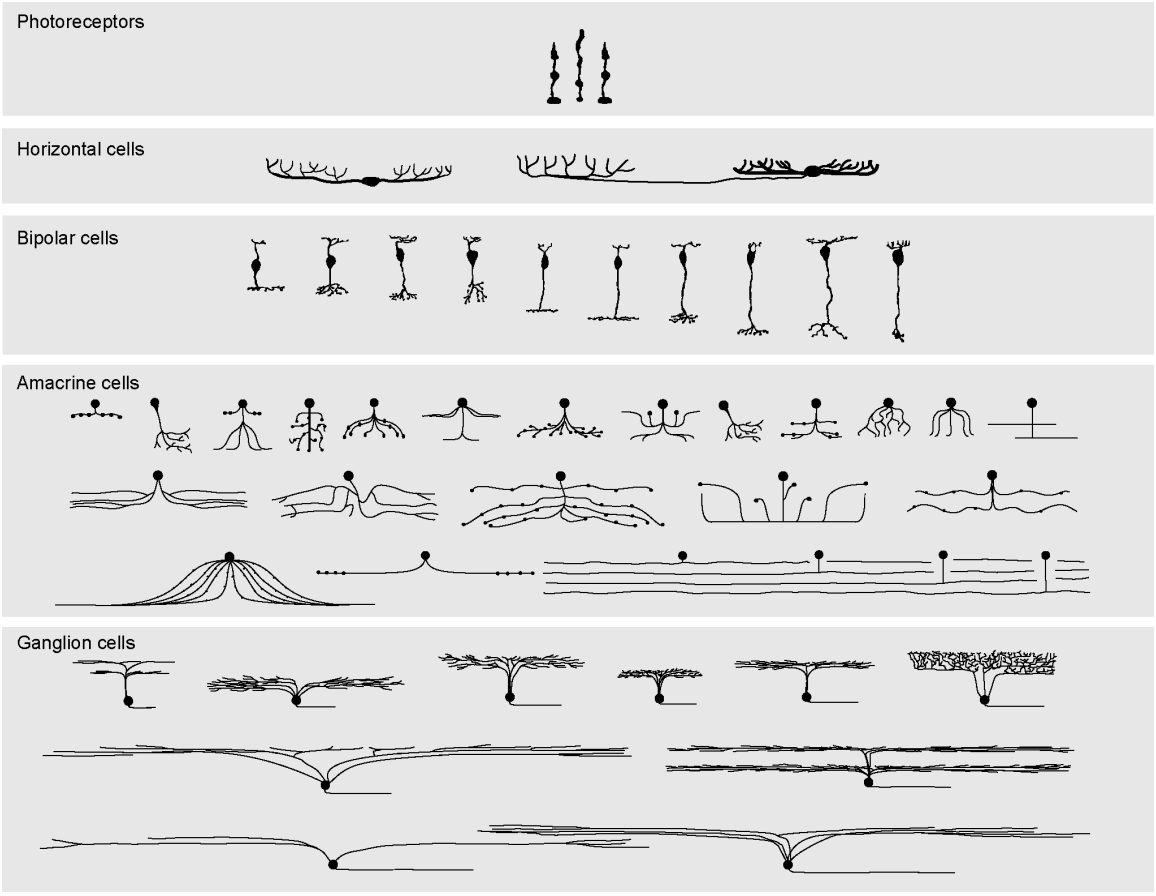

Figure 1.2: Diversity of the retinal stratification and morphology. From top panel to bottom panel, the retina contains photoreceptors, horizontal cells, bipolar cells, amacrine cells, and ganglion cells. The different morphologies within each subset of cells reflect the diversity of their specific functions. This illustration is based on work performed primarily on rabbit retina. Reproduced with permission from Richard H. Masland (Masland, 2001a, b).

Visual Pigment: Rhodopsin

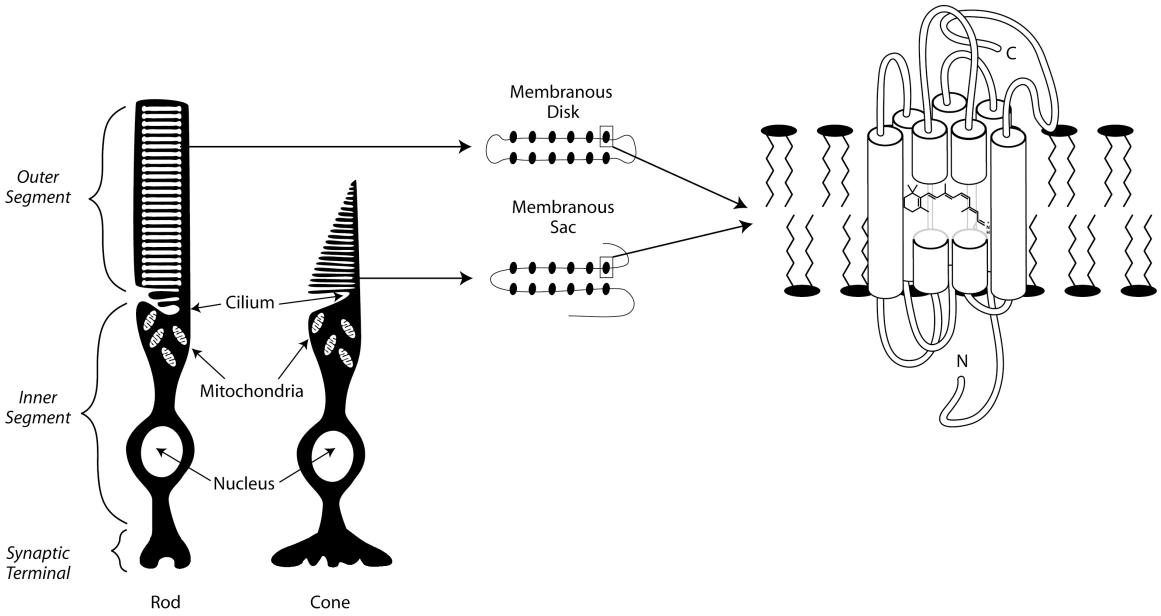

Figure 1.3: Rod and cone photoreceptor morphology. On the left is an illustration of a rod and a cone photoreceptor. Both of these cells contain synaptic terminals, inner segments, and outer segments. The synaptic terminal contains the cellular machinery that relays visual information to bipolar cells. The inner segment is the metabolic energy production center for the entire cell and the outer segments contain the visual pigment rhodopsin. In rod photoreceptors, rhodopsin is bound to membranous lipid disks. Rods contain numerous disks in their outer segment. In cone photoreceptors, the visual pigment iodopsin is bound to the plasma membrane. The plasma membrane in cones is invaginated numerous times to create membranous sacs that increase the likeliness of photon absorption. The visual pigment is composed of 7 trans-membrane helices, with a light sensitive visual chromophore, 11-*cis* retinal. This figure modified from a figure designed by Karen Moore. Figure is a reproduction from Maureen Estevez Stabio's Ph.D. dissertation (Estevez, 2007).

of each subclass of ganglion cell, and the subsequent excitation sends a specific set of visual information to the brain.

The protagonist of this dissertation is the visual pigment rhodopsin. It is the singular protein that renders photoreceptors susceptible to excitation by light. Rhodopsin is a classic and prototypical G-Protein coupled receptor (GPCR); it is composed of a membrane bound protein, opsin, which is bound through a Schiff base linkage to a light-sensitive chromophore, 11-*cis* retinal. Rhodopsin is found in high concentrations in membrane disks located in the outer segment at 3.5 mM concentration (Harosi, 1975). In the case of cones, iodopsin is embedded in the plasma membrane. Hereafter, the attention of this dissertation will be focused entirely on rods and rhodopsin, rather than cones.

Structurally, rhodopsin is comprised of 7 transmembrane helical domains. A lysine residue (Lys296), located on the seventh transmembrane helix provides a substrate for the Schiff base linkage with the chromophore, while a glutamate (Glu113) on helix 3 acts as a stabilizing counter-ion (Sakmar et al., 1989; Zhukovsky and Oprian, 1989; Nathans, 1990a, b). In darkness, when bound with 11-*cis* retinal (the ground state), the Schiff base is protonated (Oseroff and Callender, 1974). In this configuration, the visual pigment is very stable (Ebrey and Koutalos, 2001; Ala-Laurila et al., 2004; Ala-Laurila et al., 2007).

The typical absorbance spectrum of rhodopsin is shown in Figure 1.4. Most commonly, the absorbance for rhodopsin is maximal around 500 nm light (Govardovskii et al., 2000), but has the ability to capture photons at other wavelengths, albeit at a lower probability (Cornwall et al., 1984). This absorbance spectrum only holds true while opsin

is covalently bound with 11-*cis* retinal. Site-specific mutagenesis studies have conversely shown that specific residues on helices 3, 4, and 5 affect rhodopsin's spectrum (Baldwin, 1993; Tang et al., 1995; Rao and Oprian, 1996; Sakmar, 1998).

Activation of rhodopsin (R*) occurs when 11-*cis* retinal absorbs a photon. As a result, the chromophore undergoes a *cis* to *trans* photoisomerization resulting in deprotonation (Doukas et al., 1978) and breakup of the anionic counterion-cationic Schiff base (Cohen et al., 1992; Robinson et al., 1992). In addition the counterion Glu113 becomes protonated, resulting in additional conformation changes within rhodopsin (Jager et al., 1994). These events lead to an activating conformational change within rhodopsin, which initiates a sequence of events that are collectively known as phototransduction.

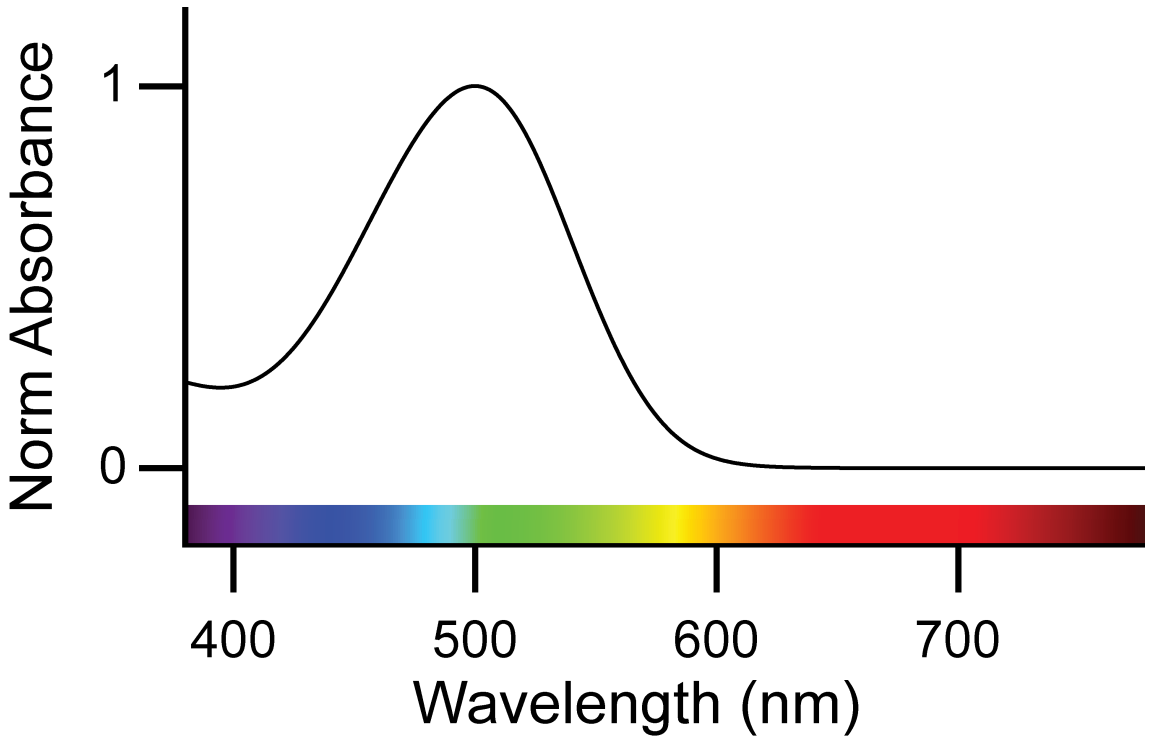

Figure 1.4: Spectral properties of rhodopsin. Rhodopsin has a spectral absorbance to light that typically peaks around 500 nm. The normalized spectrum has been plotted using a template for rhodopsin (Govardovskii et al., 2000).

Phototransduction

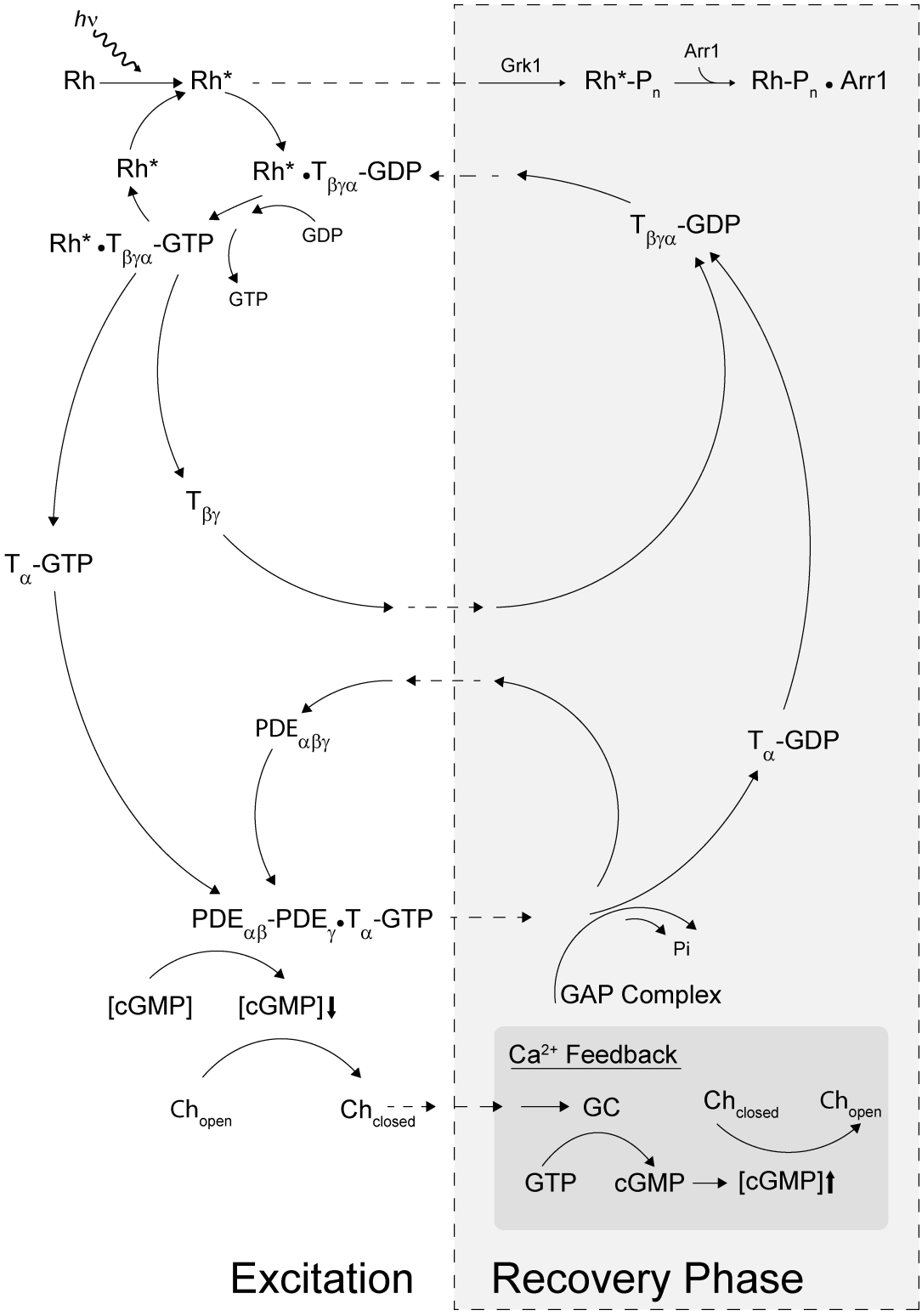

Figure 1.5: A schematic of phototransduction, separated into excitation (or activation) and recovery phases. *(Excitation Phase):* Rhodopsin becomes activated following photon absorption, and initiates phototransduction. Activated rhodopsin (Rh*) interacts with the G-protein transducin ($T_{\alpha\beta\gamma}$), and catalyzes a GDP to GTP exchange on the T_α subunit. Afterwards Rh* dissociates from transducin, and T_α-GTP dissociates from $T_{\beta\gamma}$. T_α-GTP then interacts with phosphodiesterase ($PDE_{\alpha\beta\gamma}$), and binds to PDE_γ to expose the catalytic subunit $PDE_{\alpha\beta}$. $PDE_{\alpha\beta}$ converts intracellular cGMP to GMP. The decrease in cGMP causes cyclic-nucleotide-gated (CNG) channels to close. Channel closure prevents cations from entering the outer segment, and the closure of these channels also hyperpolarizes the cell. *(Recovery Phase):* First, rhodopsin needs to deactivate in a two-step process before the physiological response can be terminated. To do this, Rh* is phosphorylated by rhodopsin kinase (Grk1). In humans (and in mice), rhodopsin can be phosphorylated up to 6 times. Next, visual arrestin (Arr1) binds phosphorylated rhodopsin, and quenches all of rhodopsin's activity. Likewise, transducin and PDE are deactivated in the recovery phase, in a simultaneous process. These two proteins combine with a GTPase accelerating protein (GAP) complex, which hydrolyzes T_α-GTP to T_α-GDP. Afterwards, T_α-GDP dissociates from PDEγ, and T_α-GDP can either recombine with a free $T_{\beta\gamma}$ or it becomes solubilized in the cytoplasm (not illustrated). The recovery phase also requires that the CNG channels reopen. The excitation phase causes intracellular free calcium concentrations to drop, and this induces a calcium feedback mechanism. Calcium feedback causes guanylate cyclase (GC) activity to rapidly increase. Guanylate cyclase then enzymatically converts GTP to cGMP, which results in the reopening of CNG channels.

The series of reactions involved in phototransduction are illustrated in Figure 1.5. Phototransduction begins when a photon activates rhodopsin (Rh*). Immediately afterwards, Rh* activates the G-protein, transducin (T). Special structural features of transducin mitigate this interaction. Like most other G-proteins, transducin exists as a heterotrimeric complex, with an α, β, and γ subunit (Fung et al., 1981). In its inactivated state, the α-subunit is bound with GDP. The α subunit is acylated at its N-terminus, and the γ-subunit is farnesylated at the C-terminal end (Fukada et al., 1990; Kokame et al., 1992; Neubert et al., 1992). These lipid modifications anchor transducin to the membrane disks. Activation of transducin by Rh* catalyzes a GDP to GTP exchange on the T_α subunit. Immediately following this exchange, T_α-GTP disassociates from $T_{\beta\gamma}$ and Rh* dissociates from both, allowing the same Rh* to activate additional transducin molecules. This constitutes the first step of signal amplification in the phototransduction cascade.

Transducin exists at a 1:10 ratio to rhodopsin (Lerea et al., 1986; Lee et al., 1992; Peng et al., 1992). Estimates for the number of T_α-GTP produced by a single R* are the subject of speculation, and the number produced is dependent on temperature. One review reports a range from 10 to 3000 T_α-GTP s^{-1} at room temperature (Pugh and Lamb, 1993). This rate has been revised in recent years to ~120 T_α-GTP s^{-1}, which is more consistent with light scattering, biochemical, and electrophysiological experiments (Leskov et al., 2000; Heck and Hofmann, 2001). The number of T_α units activated is dependent on the lifetime of Rh*. For mouse rods, there are two reported estimates for the lifetime of Rh*. In one estimate, the lifetime of Rh* is reported as 80 ms, resulting in

~20 T_α-GTP per Rh* (Krispel et al., 2006). In an alternative estimate, Rh* is believed to lasts for ~100 ms leading to several hundred T_α-GTP (Makino et al., 2003).

Once active, T_α-GTP directly facilitates the next step of phototransduction: the excitation of membrane bound cGMP phosphodiesterase (PDE) (Fung et al., 1981; Stryer et al., 1983; Li et al., 1990; Catty et al., 1992; Qin et al., 1992). T_α exposes one of the two PDE regulatory subunits, PDE_γ, exposing cGMP catalytic sites, PDE_α or PDE_β (Baehr et al., 1979; Hurley and Stryer, 1982). T_α -GTP binds to approximately one subunit during its entire lifetime. Additionally, T_α -GTP forms a complex with γ-PDE and RGS9 (Tsang et al., 1998), which greatly accelerates the hydrolysis of T_α -GTP to T_α -GDP. Therefore, this step does not produce signal amplification/gain within the phototransduction cascade. The second step of amplification is produced from the conversion of cGMP to GMP by active PDE (PDE* or $PDE_{\alpha\beta}$).

In photoreceptors, cGMP is the gating ligand for cyclic-nucleotide-gated nonspecific Na^+/Ca^{2+} cation channels (CNG channel) that are located on the plasma membrane of the outer segment (Kaupp and Seifert, 2002). In dark adapted rods the intracellular cGMP concentration is from 30-60 μM in amphibian rods, but only about 6 μM of cGMP is free (Nakatani and Yau, 1988). Under these conditions in darkness, ~1% of the CNG channels are in the open state (Nakatani and Yau, 1988; Chen et al., 1993; Yau, 1994). These channels are very sensitive to small changes in cGMP concentration due to PDE* (Yau, 1994), and this sensitivity allows photoreceptors to have a graded range of response that spans over a broad range of light intensities. A single PDE* is extremely efficient in the hydrolysis of cGMP, with a K_m of ~10 μM, and a K_{cat} of 2,200

s^{-1} (Wilden et al., 1986; Leskov et al., 2000). At this rate of hydrolysis the conversion of cGMP to 5'-GMP is limited by the aqueous diffusion of cGMP. This may seem trivial, however the cell must overcome cGMP depletion in the recovery phase of phototransduction. Closing of these channels results in the hyperpolarization of the cell, and subsequently changes the amount of glutamate (a neurotransmitter) that is secreted at the synaptic terminal.

Cationic Currents and Calcium Feedback

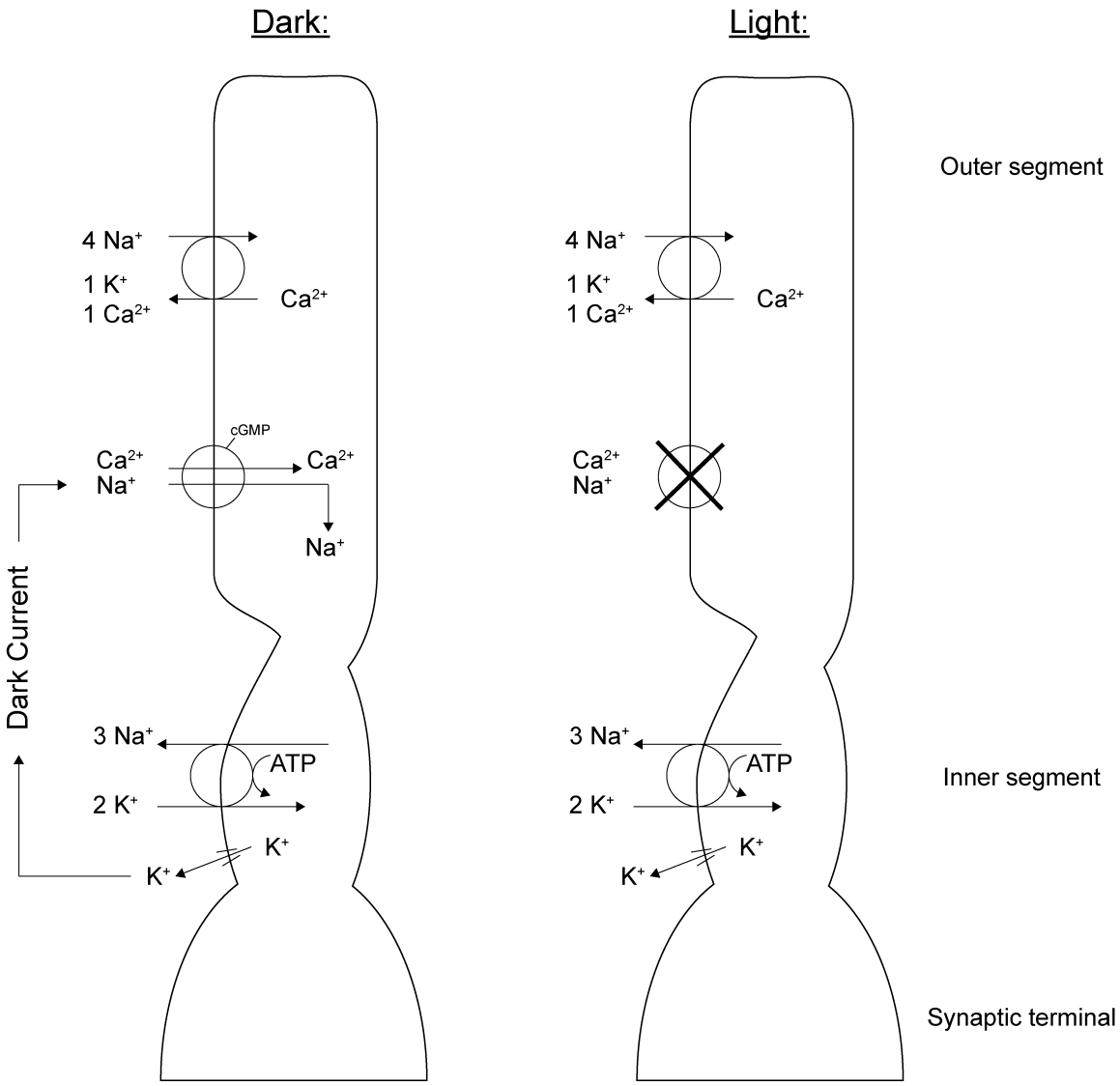

Figure 1.6: Cationic currents with the rod photoreceptor in light and dark conditions. The outer segment contains CNG channels that allow ionic sodium and calcium to flow into the cell. Concurrently, calcium is extruded from the outer segment in a sodium exchanger. K^+ exits the cell in the inner segment through potassium channels. In darkness, this circulation of inward Na^+ and outward K^+ is described as a *dark current*. Phototransduction, brought on by light activation of rhodopsin, results in the closure of the CNG channels. The cell then hyperpolarizes, and the concentration of intracellular free calcium decreases, inducing calcium feedback mechanisms.

In dark-adapted rods, there is a cation influx from Na^+ through the CNG channels and cation efflux of K^+ through potassium channels in the inner segment that is referred to as the *dark current*. A diagram of this current is presented in Figure 1.6. Ionic sodium makes up about 90% of the ionic current, whereas Ca^{2+} makes up the other 10%. Calcium is extruded in the outer segment through a sodium exchanger. Within the inner segment, K^+ is extruded using potassium channel. This current is said to be in a steady state in darkness.

A change to this steady-state current due to light exposure (i.e. phototransduction) is referred to as a *photocurrent*. Bright light exposure closes all of the channels, as shown on the right side of Figure 1.6. The opening and closing of these cGMP gated channels affects the membrane conductance, which is significant when modeling the Nernst/GHK resting membrane potential. In darkness, photoreceptors are partially depolarized. Closing of these channels repolarizes (or hyperpolarizes) the photoreceptor. These changes in membrane potential modulate the glutamic acid release at the rod to rod bipolar synapse.

The CNG channel closure also reduces the intracellular concentration of free Ca^{2+}. Within the photoreceptor, this decrease in free Ca^{2+} induces a *calcium feedback* mechanism that controls the recovery (or deactivation) phase of phototransduction. In salamander rods, the dark-adapted concentration of intracellular calcium is 500-700 nM, whereas following a bright light stimulus, the concentration drops to 30-50 nM (Gray-Keller and Detwiler, 1994; Sampath et al., 1998; Mendez et al., 2001). The most notable of these calcium regulated changes occur in guanylate-cyclase-activating proteins, or

GCAPs (Howes et al., 2002; Makino et al., 2008). When intracellular calcium is lowered through the closure of cGMP-gates channels, then GCAPs stimulates guanylate cyclase (GC), which (as discussed in detail below) promotes the recovery phase of phototransduction. Cyclase converts GTP to cGMP, which allows the CNG channels to reopen. Next, calcium affects recoverin (Rec), a protein that has an inhibitory affect on rhodopsin kinase, and therefore regulates the deactivation of Rh*. This has a small affect on *light adaptation*. Finally, calcium feedback also increases the sensitivity of CNG channels for cGMP, by releasing calmodulin that is normally bound to the CNG channel in the presence of free Ca^{2+} (Hsu and Molday, 1993). This later feedback mechanism also has a small effect on the recovery phase of phototransduction.

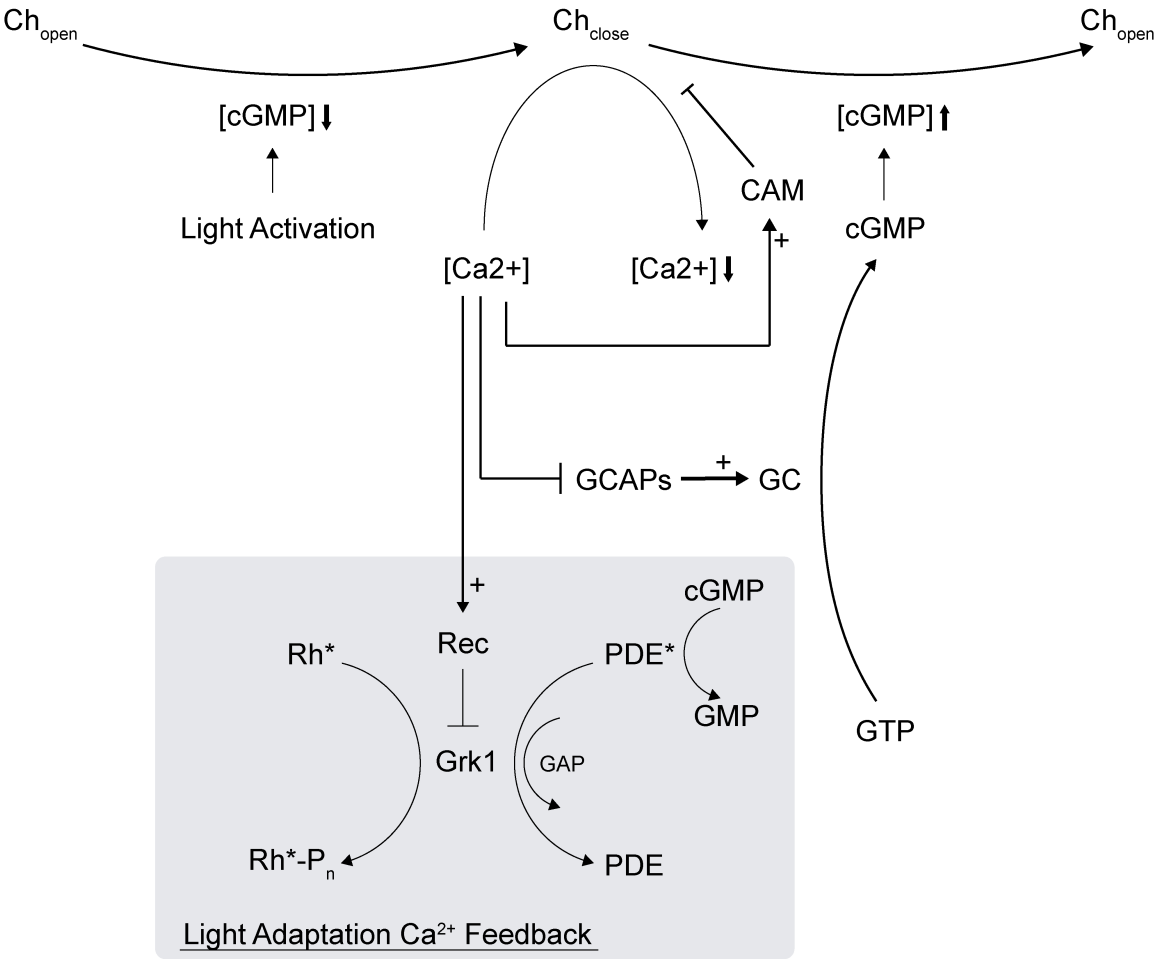

Figure 1.7: A schematic of calcium feedback within rod photoreceptors. Light activation of rhodopsin results in the closure of CNG channels (Ch_{close}). As a direct result the intracellular concentration of free calcium drops. Calcium is involved in the regulation of calmodulin (CAM) binding to CNG channels, guanylate cyclase activating proteins (GCAPS), and recoverin. When intracellular calcium drops, calmodulin unbinds from the channel, which increases the channel's sensitivity to cGMP. Likewise, GCAPS stimulates guanylate cyclase (GC), which allows GC to rapidly convert GTP to cGMP, leading to the reopening of CNG channels. During light adaptation, calcium feedback blocks recoverin (Rec) inhibition of Grk1, meaning that activated visual pigments are more readily phosphorylated. Recently, it has been suggested that Grk1 could also accelerate the deactivation of PDE* (Chen et al., 2015).

The Recovery Phase of Phototransduction

The recovery phase of phototransduction, shown on the right side of Figure 1.5, begins with the deactivation of the visual pigment. Rhodopsin deactivation involves receptor phosphorylation by rhodopsin kinase (Grk1). Phosphorylation of activated rhodopsin inhibits transducin activation, and is said to deactivate the visual pigment. The term "deactivate" may seem like a misnomer, because some *in vitro* studies have demonstrated that phosphorylated rhodopsin can activate transducin with a limited capacity (Miller et al., 1986; Wilden et al., 1986; Bennett and Sitaramayya, 1988; Wilden, 1995). Instead, complete deactivation of rhodopsin requires another reaction, which occurs when visual arrestin (Arr1) binds to the phosphorylated receptors. It is noteworthy that numerous studies provide tentative evidence for this model. These same models emphasize that rhodopsin phosphorylation primarily regulates deactivation of rhodopsin. These hypotheses will be directly tested in this dissertation.

Next in the recovery phase is the deactivation of transducin. The activity of T_{α}-GTP is quenched through GTP hydrolysis to GDP. The rate of T_{α}-GTP hydrolysis is accelerated by its association with a GTPase accelerating protein (GAP) complex. This complex is formed with a regulator of G-protein signaling 9 (RGS9), a transducin GTPase-accelerating protein (He et al., 1998), and Gβ5L (Makino et al., 1999; Keresztes et al., 2004), which is anchored to the outer segment by RGS9-1-Anchor Protein, R9AP (Hu and Wensel, 2002; Cao et al., 2010). Additionally, the affinity of this GAP complex for T_{α}-GTP is increased by PDE_{γ} (Tsang et al., 2006). Coupled to this reaction is the deactivation of PDE*. When T_{α}-GTP is hydrolyzed, it dissociates from PDE_{γ} (Fain,

2011). Next, $PDE_{\alpha\beta}$ rapidly associates with PDE_{γ}, which deactivates the PDE complex. Likewise, T_{α}-GDP can either associate with a free $T_{\beta\gamma}$, or it can become solubilized within the cytoplasm.

As previously mentioned, the closure of the CNG channels decreases the local concentrations of free Ca^{2+} (Sampath et al., 1998; Sampath et al., 1999). Furthermore, it was explained that calcium feedback (Figure 1.7) promotes the guanylate-cyclase-activating proteins (GCAPs) stimulation of guanylate cyclase (GC). In mouse rods, there are 2 GCAPs: GCAP1 and GCAP2, that regulate cyclase activity (Howes et al., 2002; Makino et al., 2008). Cyclase performs the enzymatic conversion of GTP to cGMP. The stimulation by GCAPS accelerates the rate of cGMP production. As the intracellular cGMP concentrations return to normal, CNG gated ion-channels reopen, which, in turn restores the dark current and depolarizes the photoreceptor. As free Ca^{2+} flows into the cell, GCAPs inhibition of cyclase is restored.

Special Circumstances: Light and Dark Adaptation

Photoreceptors are designed to function over a wide range of light intensities. In low light, these cells exhibit photoresponses with slow integration times, which aids in relaying visual information to the brain. However, when the ambient light intensity increases, a slow integration time would cause the rod photoreceptors to maximally hyperpolarize and the cells would remain that way until the light intensity was reduced. Therefore, photoreceptors must undergo *light adaptation*, thereby modulating the phototransduction machinery to extend the graded response range into brighter light

intensities. Two distinct characteristics are observed in light adapted rod photoreceptors. First the photoresponses are accelerated. This acceleration includes a faster raising phase and a faster recovery phase in the light responses. Second, there is a significant reduction in the response amplitudes for light adapted rods when compared to dark-adapted rods. Likewise, there is a noticeable reduction in the dark current during light adaptation.

Dark current reduction results in a decrease in intracellular Ca^{2+} and photoreceptors become continuously impacted by calcium feedback mechanisms. Reduced intracellular calcium creates a set of conditions where Mg^{2+} binds to GCAPS, which stimulates cyclase, which elevates the baseline activity of GC and the acceleration in the photoresponses (Peshenko and Dizhoor, 2004, 2006; Dizhoor et al., 2010).

Recoverin inhibition of Grk1 has an important role in light adaptation. Under these conditions, there is an increase in the rate in which Grk1 phosphorylates Rh* (Kawamura, 1993; Chen et al., 1995a). Likewise, Grk1 is believed to regulate the lifetime of Rh* (Chen et al., 2012). More specifically, the recovery phase of phototransduction was accelerated when Grk1 was over expressed (Sakurai et al., 2011), and when recoverin was removed (Makino et al., 2004; Chen et al., 2012).

Phototransduction promotes the translocation of three proteins within the cell: the α-subunit of transducin (T_α), visual arrestin, and recoverin. In darkness, α-transducin is centrally localized to the outer segment, and translocate out of the outer segment following bright light exposure (Whelan and McGinnis, 1988; Sokolov et al., 2002). The same is true for recoverin (Strissel et al., 2005). Conversely, arrestin is primarily localized in the inner segment while the photoreceptors are dark-adapted. A small

fraction can be found in the outer segment. During light stimulation, arrestin migrates into the outer segment (Whelan and McGinnis, 1988; Sokolov et al., 2002; Nair et al., 2005; Strissel et al., 2006).

The mechanisms for light adaptation occur under two principle conditions. Background light adaptation is produced by continuous stimulation of the phototransduction cascade; this occurs in all light conditions, from the very faint to well lit. This form of adaptation has the normal hallmarks, including the shortened integration time course for responses (Leibrock et al., 1994). Likewise, the amplitude of photon responses is reduced in the presence of background illumination.

For bright bleaching light conditions, in which a more significant fraction of the visual pigment has been bleached, there are additional consequences (Leibrock et al., 1994). For example, a 90% bleached retina only contains 10% of its visual pigment in a light sensitive formation. This would produce a 10-fold reduction is sensitivity due to loss of *quantum catch*, which reflects the fact that only the remaining 10% of the pigment is photosensitive. The desensitization however, far exceeds the loss of sensitivity due solely to the loss of quantum catch (Gouras, 1972; Harosi, 1996; Nymark et al., 2012). One of the consequences of bleaching light intensities is the accumulation of opsin (Cornwall and Fain, 1994; Matthews et al., 1996; Lamb et al., 2015). Individual molecules of opsin have the ability to activate transducin. The activity is very small, such that one opsin molecule is only $\sim 10^{-7}$ as effective as a single Rh* in stimulating transducin (Cornwall and Fain, 1994; Cornwall et al., 1995; Jones et al., 1996; Matthews et al., 1996).

However, when a substantial fraction of rhodopsin is bleached, the decay to opsin produces an effect that is identical to background light adaption.

Dark adaptation is the systematic reversal of all of the light adaptation mechanisms. These reactions are required to restore the sensitivity of rods, and restore the photoreceptors' ability to detect single photons. Dark adaptation requires the regeneration of rhodopsin, the resequestering of transducin and recoverin to the outer segment, the resequestering of arrestin to the inner segment, and ultimately, the restoration of the dark current. There are likely more complex processes involved, however, these additional steps remain elusive since late stage dark adaptation is poorly understood.

Rhodopsin Phosphorylation, Dephosphorylation, and Dark Adaptation

Dark adaptation involves a series of processes that are essential to restoring a light adapted rod photoreceptor's sensitivity when transitioning to low levels of illumination. In general, these processes are poorly understood, but it is known that during dark adaptation, visual pigment must be regenerated, dephosphorylated, and decoupled from arrestin. The current understanding of dark adaptation comes from experiments designed to study phototransduction and through examination of the processes involved in light adaptation. There is a conflict in this approach: since the study of light adaptation primarily reflects on the methods that are not involved in dark adaptation. Therefore, we

infer that dark adaptation must involve a reversal of all of the known light adaptation mechanisms, but this approach lacks direct examination of dark adaptation processes.

A large body of research has shown that light activation of rhodopsin results in visual pigment phosphorylation (for review see Hurley et al., 1998). Phosphorylation constitutes the first of two steps needed to deactivate rhodopsin. In rod photoreceptors, rhodopsin kinase, GRK1, sequentially phosphorylates a cluster of six to seven serine/threonine residues located near the carboxyl-terminus of rhodopsin (Kuhn, 1974; Chen et al., 1995b; Hurley et al., 1998; Mendez et al., 2000a; Mendez et al., 2000b; Kennedy et al., 2001; Azevedo et al., 2015). Following phosphorylation, arrestin-1 binds to rhodopsin, which results in the complete deactivation of rhodopsin (Wilden et al., 1986; Wilden, 1995). The multitude of phosphorylation sites (that promote arrestin binding), provide a multifaceted (and mutually inclusive) control on rhodopsin's active lifetime, which is manifested in highly reproducible single quantal responses (SQR) (Doan et al., 2006; Azevedo and Rieke, 2011). This feature is important in rods, since SQRs allow rods to function in all low light conditions.

During continuous illumination, mouse rods have a significant fraction of rhodopsin in a phosphorylated state (Lee et al., 2010). Following 90 minutes of "bright" office-lighting light adaptation, Lee et al. (2010) showed that 45% of the opsin (the apo-protein of the visual pigment) was light-sensitive rhodopsin (either un-bleached or regenerated), and the remaining 55% was in the form of bleached rhodopsin. At the same time, these authors observed that 80% of the total opsin was phosphorylated. Minimally, this means that at least 25% of the visual pigment was phosphorylated rhodopsin. The

majority of the phosphorylated rhodopsin contains 2 or more attached phosphates. It is reasonable to form the assumption that complete dark adaptation requires dephosphorylation of regenerated phosphorylated rhodopsin, which evokes the question: what effect does rhodopsin phosphorylation have on dark adaptation?

A number of *in vitro* experiments have investigated rhodopsin phosphorylation and phototransduction. Generally, these studies show that phosphorylation of rhodopsin alone is not enough to quench T_{α} activation (Miller et al., 1986; Wilden et al., 1986; Wilden, 1995) and that arrestin is required to terminate Rh* activity (Bennett and Sitaramayya, 1988). Electrophysiological experiments on $Arr1^{-/-}$ mice rods showed flash responses that had very prolonged activation (Xu et al., 1997). The response only partially recovers, and the phototransduction cascade continues for several seconds. This provides strong evidence that phosphorylated rhodopsin (P-Rh) might be able to initiate phototransduction upon reactivation. However, all these interpretations omit the interaction between P-Rh and arrestin. It is a widely held belief that arrestin would immediately quench all activity produced as a result of P-Rh activation.

The role of arrestin must be further examined. Arrestin has a strong affinity for activated phosphorylated rhodopsin (P-Rh*) and a significantly lower affinity for P-Rh (Vishnivetskiy et al., 2007). NMR experiments confirm this affinity by revealing that arrestin transiently binds to P-Rh, and strongly binds to P-Rh* (Zhuang et al., 2013). Curiously, Arrestin-1 exists in a basal state that transitions into a binding-competent conformation by encounters with P-Rh* (Gurevich et al., 2011). In the intact rod, arrestin-1 in the basal state competes with GRK1 and slows Rh* (Metarhodopsin II)

deactivation (Doan et al., 2009). This conjures up a different set of questions: can P-Rh activate Arrestin-1, and convert it to a binding competent state? Would the aforementioned set of conditions increase the rate of P-Rh* deactivation? Moreover, would there be a difference in the rate of excitation and recovery between ground-state Rh and P-Rh?

The primary focus this dissertation is to characterize the relationship between rhodopsin dephosphorylation and dark adaptation in mouse retina. Inhibition of rhodopsin dephosphorylation by genetic means in mice is problematic because the rhodopsin phosphatase gene has not been definitively identified (Ramulu et al., 2001). In this study, I have identified a methodology to significantly inhibit rhodopsin dephosphorylation. I employ this methodology to test the hypotheses that recovery of sensitivity during dark adaption is inhibited by phosphorylation of rhodopsin. Likewise, I will test the hypothesis that arrestin-1 exhibits high affinity binding to P-Rh and will therefore prevent photolyzed P-Rh from initiation of phototransduction.

CHAPTER TWO: EXPERIMENTAL METHODS

The methods outlined in this chapter cover all the procedures and analytical methods that were used while conducting this research project. Included in each section is the rationale behind each type of experiment, the theory that describes the experiment, a description of the instrument(s) and/or experimental procedure(s), a description of the data collection process, and the techniques used during data analysis. All experiments described and reported in the *Methods* and *Results* chapters, respectively, were performed using tissues isolated from mouse retinae.

Retinae were then measured using an array of different instruments and under several experimental conditions. Spectrophotometric measurements on the visual pigment were made using a microspectrophotometer (MSP). Electrophysiological measurements of rod photoreceptors were performed with *trans*-retinal electroretinograms (ERG), and with single cell suction pipettes. Rhodopsin phosphorylation from these isolated retinae were measured using *iso*-electrically focused (IEF) immunoblots. Finally, transducin translocation was measured from isolated rod outer segment using Western blots.

Animal strains and husbandry

All experimental procedures performed on wild-type and transgenic mice were in accordance with protocols approved by the Animal Care and Use Committees of Boston University School of Medicine (Boston, MA, USA) and the University of Southern California Keck School of Medicine (Los Angeles, CA, USA) and they comply with the standards set forth in the Guide for the Care and Use of Laboratory Animals (Alvarez and

Pardo, 1997; Worlein et al., 2011; Carbone, 2012) and the Animal Welfare Act (United States. et al., 2013).

Three strains of mice, "wild-type" (WT) C57BL/6J (J denoting Jackson Lab's inbred strain), cone photoreceptor function loss-3 (*cpfl3*$^{-/-}$), and G-protein receptor kinase 1 knock-out (*Grk1*$^{-/-}$) were used in these studies. The *cplfl3*$^{-/-}$ strain has a spontaneous missense mutation within the alpha subunit of cone transducin, GNAT2 (guanine nucleotide binding protein ([G protein]), that abolishes cone phototransduction. This mutation was generated and characterized within Jackson Lab's C57BL/6J colony (Chang et al., 2006). Hereafter, *cpfl3*$^{-/-}$ mice will be referred to as *Gnat2*$^{-/-}$ mice; reflecting the proteomic phenotype. The *Grk1*$^{-/-}$ strain has rhodopsin kinase (GRK1) genetically knocked out of the C57BL/6 genome (Chen et al., 1999). Photoreceptors lacking GRK1 are unable to phosphorylate activated rhodopsin molecules (Chen et al., 1999; Dryja, 2000).

Wild-type mice were 6-10 weeks of age at the time of experiments, *Gnat2*$^{-/-}$ mice were between 3-12 weeks of age, and *Grk1*$^{-/-}$ mice were between 3-12 weeks of age. All three strains were used at Boston University School of Medicine, were maintained on a 12 h light – 12 h dark cycle, and were dark adapted for 12 h before all experiments. Only wild-type mice were used at the USC Keck School of Medicine, and were maintained in continuous darkness for 24 h a day. All animals were dark adapted overnight prior to use.

Tissue collection

At the beginning of each *ex vivo* experiment and as indicated for *in vivo* experiments, mice were euthanized in dim red light by cervical dislocation followed by decapitation. Eyes were removed from the animal and placed in a 30 mm plastic Petri dish containing physiological solution (described in *Physiological Solutions* section below). From this point, all dissections and manipulations of tissue were performed under infrared illumination with the aid of infrared imaging systems. The eyes were hemisected, and then placed in physiological solution. Unless otherwise stated, retinae were carefully isolated and removed from the retinal pigment epithelium (RPE). Retinae were then kept in darkness until use, in a light tight container containing a nutrient rich physiological solution.

For a limited set of *in vivo* experiments, dark-adapted mice were rendered unconscious using vaporized isoflurane (2-chloro-2-(difluoromethoxy)-1,1,1-trifluoro-ethane). Afterwards, animals were further sedated with an intraperitoneal injection of ketamine (100 μg/g body weight) and xylazine (10 μg/g body weight) mixture. Afterwards the pupils were dilated with an application of 2.5% AK-dilate™ (phenylephrine hydrochloride ophthalmic solution, USP) and 0.5% Tropicacyl® (tropicamide ophthalmic solution, USP). Eyes were then exposed to light and the visual pigment was bleached (see *Bleaching Ex Vivo and In Vivo Retinae* section below). Afterwards mice were returned to darkness as indicated by the experiment before the tissue was harvested as previously described.

Physiological Solutions, Retinoid Preparation, and Tissue Incubation

Isolated retinae were maintained in Ames culture medium (Ames and Nesbett, 1981; Azevedo and Rieke, 2011). Ames medium was first formulated to simulate the extracellular solution that surrounds rabbit retinae, but has since been shown to be quite effective for mouse photoreceptors (Azevedo and Rieke, 2011). Ames culture medium contains 120 mM Na^+, 3.6 mM K^+, 2.4 mM Mg^{2+}, 2.3 mM Ca^{2+}, 125.4 mM Cl^-, 0.5 mM $H_2PO_4^-$, and 2.4 mM SO_4^{2-}, as well as critical vitamins, and amino acids. This aqueous medium was prepared from powdered stock (8.8 g/L) and was buffered to pH 7.4 by one of two buffering agents. The first agent was $NaHCO_3$ (1.9 g/L), which was added to the aqueous Ames medium. This addition of $NaHCO_3$ adjusted the final Na^+ concentration to 143 mM, and contributed a HCO^- concentration of 23 mM. The pH was then adjusted to 7.4 by heating the solution to 37°C and bubbling with a gas mixture of 95% O_2 and 5% CO_2. The second buffer used was HEPES. Here, 4.36 g/L of HEPES buffer and 0.90 g/L (~15.4 mM) of NaCl were added to the Ames medium, and the pH was adjusted to 7.4 by drop-wise addition of 1M NaOH. This solution was not bubbled with a mixture of 95% O_2 and 5% CO_2, because doing so would affectively lower the pH to ~5.6. Instead, 100% O_2 was used, which had no effect on the pH (originally set to 7.4).

Additional compounds were added when performing *trans*-retinal ERG experiments. These pharmacological agents were added to the medium to block certain electrical components of the ERG response These were: 50 μM of racemic DL-(+)-2-Amino-4-phosphonobutyric acid (DL-AP4) and 100 μM of $BaCl_2$. Rational for the use of these specific agents is found below in *the Trans-retinal Electroretinogram* section.

Preparation of 11-cis Retinal

A stock solution of 11-*cis* retinal was prepared by dissolving 1 mg of crystalized 11-*cis* retinal in ethanol (EtOH) in a small glass conical vial. The concentration of this stock solution was determined using a conventional spectrophotometer. In ethanol, 11-*cis* retinal has an extinction coefficient of 24,900 M^{-1} cm^{-1} at 380 nm (Wald et al., 1955; Kane and Napoli, 2010). Afterwards the volume of EtOH was adjusted (through dilution) to achieve a stock solution of 11-*cis* retinal with a concentration of 15 ± 5 mM. Aliquots of stock solution were purged with nitrogen gas, then wrapped with aluminum foil, sealed in a light-tight 35 mm film canister, and stored at -80 °C until use. This concentrated stock solution was measured weekly to verify that it was not degraded by storage.

Diluted aliquots of working solution to which tissue was exposed were made by adding 2 µL of 11-*cis* retinal stock solution to a 1 mL glass conical vial. Dilution was preformed through serial additions of Ames medium that contained 1.9 g/L $NaHCO_3$ and 10.0 g/L fatty-acid free BSA. Ames solution was added serially, in increments as follows: 10 x 5 µl increments, then 4 x 50 µL, then 3 x 100 µL, and finally 1 x 450 µL. After each incremental addition, the vial was swirled vigorously. In total, this procedure yielded 1 ml solution containing ~30 µM 11-*cis* retinal. This solution was either used at full concentration, or following further dilution as indicated.

Tissue Incubation

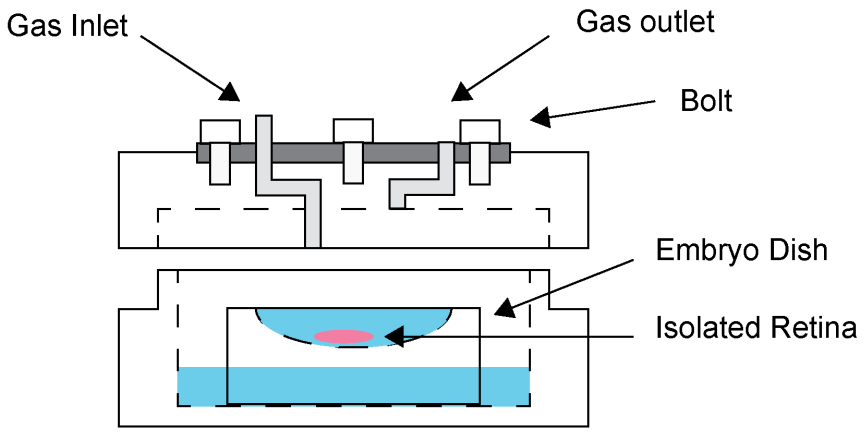

Figure 2.1: A light-tight incubation chamber for isolated retinae. This chamber was designed to maintain the health and viability of isolated retinae by bathing the tissue in physiological solution. The chamber contains a gas exchange system. The bottom chamber was large enough to hold an embryo dish. The embryo dish was filled with 3 mL of Ames culture medium. For pigment regeneration experiments, 3.33 g/L Fatty Acid Free BSA and 10 µM 11-*cis* retinal was also added to this solution. A more detailed description of this chamber is in the text.

Isolated retinae were maintained and incubated in a light tight chamber. A diagram of this chamber is presented in Figure 2.1. This chamber was fabricated by machining a solid piece of opaque black Delrin. The chamber had an interlocking lid between the top and bottom pieces that formed a light-tight internal chamber. The inside of the top and bottom pieces were hollowed out (indicated by the dashed lines). The top piece also had two spiral cut channels (not illustrated). These spiral channels were covered by a small piece of Delrin. This cover was secured to the top of the chamber with three opaque black nylon screws. Combined, these two spiral channels and the small piece of Delrin formed two light mazes that were used as in a gas exchange system. One

maze was used for injecting gas into the chamber, and the other for ejecting excess gas from the chamber. This gas exchange system was necessary with $NaHCO_3$ buffering in order to maintain CO_2/O_2 tension in the solution at physiological levels as well as to stabilize pH. The bottom piece of the chamber was large enough to hold an embryo dish (catalog # 70543-30, Electron Microscopy Science, Hatfield, PA). The embryo dish was filled with 3 mL of Ames culture medium and a buffering agent. During pigment regeneration experiments, 3.33 g/L fatty acid free BSA (Sigma) and 10 μM 11-*cis* retinal was also added to this solution. Surrounding the embryo dish was 10 mL of physiological solution. The purpose for this solution is to help maintain the CO_2/O_2 tension. Additionally, it is believed this this extra solution keeps the chamber humid.

Bleaching *Ex Vivo* and *In Vivo* Retinae

Bleaching Ex Vivo Retinae

A significant number of experimental procedures required photo-activation (bleaching) of a substantial fraction of the rhodopsin in retinae that had been isolated from the mouse eye cup. Empirically, it was determined that rapid (high intensity) bleach rates are detrimental to the health of mouse photoreceptors. Therefore, rapid bleach rates were avoided to ensure that photoreceptor damage by this means was minimized (Makino, 2012; Nymark et al., 2012). For these experiments, following dissection, isolated retinae were placed in a 30 mm plastic Petri dish that contained HEPES buffered Ames culture medium. The center of the Petri dish containing the retina was illuminated by light from an optical bench. The light bench was composed of an adjustable intensity

tungsten/halogen light source, a 500 nm interference filter, and multiple calibrated neutral density filters. Emitted light formed a circular 5 mm diameter (bleaching) field at the level of the preparation. The unattenuated (no neutral density filters) 500 nm wavelength filtered light intensity at the level of the retina was calibrated to be 1.92 x 10^8 photons μm^{-2} s^{-1}. Calibration was accomplished with a 350 Linear/log Optometer radiometer using a Model 221 detector from which the filter had been removed (UDT Instruments, Baltimore, MD). The bleaching intensity was then adjusted at the beginning of each experiment to 5.53 x 10^5 photons μm^{-2} s^{-1} using neutral density filters. At this intensity the rate of bleaching of rhodopsin was 0.3% of total pigment content per second.

The fraction of pigment bleached, F, under these experimental conditions was calculated from the equation:

$$F = e^{-Ipt}, \tag{2.1}$$

where I is the incident light intensity (photons μm^{-2} s^{-1}), p is the photosensitivity of rhodopsin, and t is the duration of light exposure in seconds. The photosensitivity has been determined empirically *in situ* at 500 nm to be 5.7 x 10^{-9} μm^2 $photon^{-1}$ for mouse rod photoreceptors (Woodruff et al., 2004; Nymark et al., 2012). The time, t, for a given bleaching exposure was determined by back-calculation for any desired bleach fraction F. Shown in Figure 2.2 is a dataset that demonstrate the accuracy of this methodology. Following bleaching, retinae were incubated in darkness as indicated in Ames culture medium at 35 °C (as described in Figure 2.1).

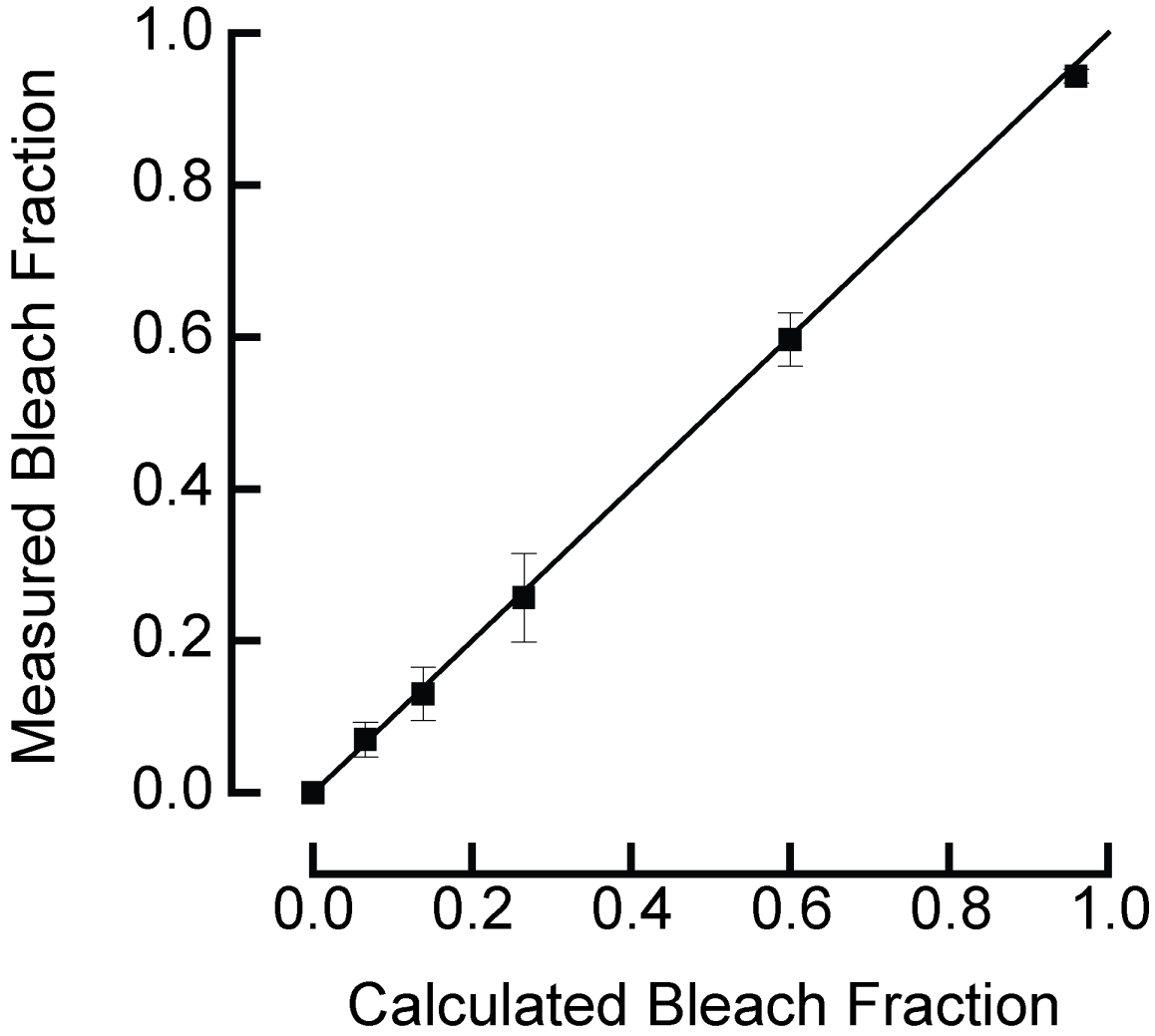

Figure 2.2: Microspectrophotometric (MSP) measurements of rhodopsin following exposure to prescribed light intensities. The data confirms how light exposure results in the bleaching of rhodopsin as described by equation (2.1). Plotted on the abscissa is the calculated bleach fraction. The ordinate represents the measured bleach fraction that is provided by MSP recordings (described in the *Microspectrophotometry* section of this chapter). This figure was produced from data that has been previously reported (Nymark et al., 2012).

Bleaching In Vivo Retinae

During *in vivo* experiments, 90% of the visual pigment was bleached through light exposure. The procedures were more complicated. Unlike *ex vivo* retinal bleaches, which can be accurately determined using equation (2.1), *in vivo* bleaches need to be empirically determined for each experimental setup. There are inevitable optical issues that can not be directly avoided or easily corrected. Therefore, the relationship describing light exposure and bleached fraction *F* needed to be empirically determined.

For *in vivo* experiments, the eyes of anesthetized animals (see the *Tissue collection* section above for detail) were exposed to calibrated 500 nm light in order to bleach a large fraction of the visual pigment over the course of 3-4 minutes. During this time, the body temperature of the animal was not monitored. Several different exposure intervals and light intensities were tested on different animals to determine the light exposure and bleached fraction *F* relationship. The amount of bleaching was determined in the following way. Following the exposure to bleaching light, the animals were sacrificed, and the retinae were isolated from the eyecup and from the RPE to inhibit pigment regeneration. Once isolated, retinae were transferred to an Eppendorf tube (one tube per retina) and treated with a solution that facilitated the solubilization of rhodopsin.

The solubilization solution was composed of 1 mL of PBS buffer solution (pH 7.4) that contained 10 mg/mL of n-Dodecyl-Beta-D-maltopyranoside (SOL-GRADE) detergent and 10 μL of protein C inhibitor cocktail (p8340). Each retina was immersed in 200 μL of solubilization buffer. The Eppendorf tube, containing a single retina and solubilization buffer was then placed on a rocker shaker table for 2 hours. Afterwards, the

solubilized rhodopsin concentration was measured. Solubilized rhodopsin was measured using a standard absorption spectrophotometer. The spectrophotometer was setup to scan across the range from 280-600nm in 1 nm steps. One measurement was performed on solubilized rhodopsin from retina. Afterwards, the remaining unbleached rhodopsin was exposed in the cuvette for 2 minutes to very bright white light, and then a fully bleached spectrum was recorded.

In order to standardize each spectrophotometric measurement for comparative analysis, the data from each recording was baseline corrected. For this purpose, the optical density at 600 nm was used for background subtraction. The optical density at this wavelength is not due to rhodopsin absorbance but instead results from fluctuations in the spectrophotometer's measurement beam intensity. Beyond baseline corrections, the data was normalized to account for sample loading.

One of the potential issues with this experimental method is that the volume of excised retina (i.e. the amount of retinal tissue placed into the Eppendorf tube) will affect the concentration of solubilized rhodopsin. Likewise, the spectrophotometric absorbance will be directly proportional to the concentration of solubilized rhodopsin. Since the volume of excised retinal tissue varied in each sample, the data needed to be normalized in order to allow for comparative analysis. The data normalization process required exploiting the structural properties of proteins and one subsequent assumption about the sample. First, it is well known that rhodopsin contains aromatic amino acids (such as phenylalanine, tryptophan, histidine, and tyrosine). Three of these aromatic amino acids (tryptophan, tyrosine, and phenylalanine) absorb photons that have wavelengths around

280 nm (Smith, 1929). The assumption in the normalization process was that the measured absorbance at 280 nm due to these aromatic amino acids was directly proportional to the amount of solubilized rhodopsin (from excised retinal tissue). From these criteria, it is possible to normalize each sample by the recorded optical density at 280 nm.

The normalizing factor should not be determined from a single recorded data point. Instead, the normalized factor was determined from fitting a function to the aromatic absorbance. More specifically, a linear slope function was fit to the measured optical density between 285 - 295 nm. Afterwards, the slope and y-offset of this fit were used to calculate the optical density at 285 nm. This calculated value was used to normalize each spectrum to 1.0 at 285 nm (rather than at rhodopsin absorption peak around 500 nm).

This methodology is demonstrated in Figure 2.3. Dark adapted preparations are graphed with black traces (with an averaged normalized absorbance at 500 nm of 0.076). For comparison, a fully bleached retina is graphed in with a pink trace (with a normalized absorbance at 500 nm of 0.005). Two different partial bleach conditions, shown in the blue and green traces, were used to calibrate the *in vivo* bleaches (with averaged normalized absorbance of 0.058 and 0.048, respectively). These spectra further indict that these two partial-bleach conditions photo-activated 23.5 % and 35.6 % of the visual pigment, respectively. By modifying equation (2.1) with a correction factor, it was possible to determine that the eye attenuated the incident bleaching light by 1.55 $\log_{10}$ units. Following these calculations, it became possible to determine the conditions that

would produce a 90% bleach. These predictions were verified with the spectrum (orange trace), having a normalized absorbance of 0.008 that corresponded with to an 89.3 % bleach.

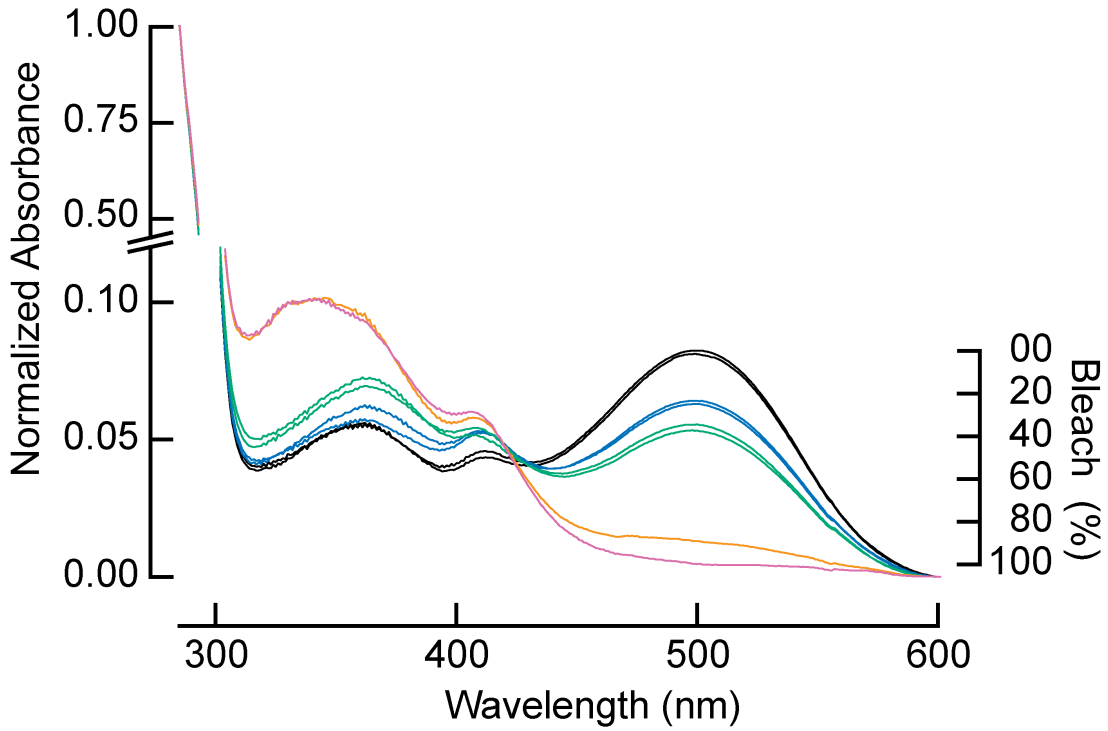

Figure 2.3: Visual pigment bleaches on *in vivo* retinae. This data demonstrates how *in vivo* bleaches were empirically determined. Solubilized rhodopsin was prepared from bleached *in vivo* retinae and the absorbance was measured using a spectrophotometer. Each trace was baseline subtracted, and then normalized by each sample's absorbance at 285 nm. Dark adapted preparations are shown in the black traces. A fully bleached (> 99%) retina is shown in the pink trace. Two different bleach conditions were used to calibrate these bleaches. The first condition, depicted in the blue traces, bleached 23 % of the visual pigment. A second light exposure condition depicted in the green traces, bleached 35 % of the visual pigment. From these data, it was possible to determine the relationship between light exposure and the resulting rhodopsin bleach fraction for *in vivo* experiments. To confirm this relationship, an *in vivo* retina was exposured to the prescribed amount of light needed to bleach 90 % of the visual pigment. The outcome is shown in the orange trace, and correspond with a bleach of 89 %, thus confirming the relationship. The ordinate of the left hand side represented the normalized absorbance. The scale on the right hand side represents the *in vivo* bleach (%) for each condition.

Microspectrophotometry

Rhodopsin is the only protein in the rod photoreceptors that is capable of detecting photons and initiating phototransduction. Light absorption causes rhodopsin to be photoisomerized ("*bleached*") and subsequently renders it essentially insensitive light in the visible range of wavelengths. This decrease in the concentration of light-sensitive rhodopsin within the outer segment means that the rod photoreceptors have a reduced ability to absorb additional photons. This loss of *quantum catch*, in combination with other factors, results in light adaptation. Recovery of sensitivity in subsequent darkness (i.e. dark adaptation), is a complex process that, among other things, requires regeneration of the rhodopsin. Studying light adaptation and dark adaptation requires monitoring the changes in the concentration of rhodopsin within the outer segment.

A tool was needed to measure the relative concentration of rhodopsin in intact rod cells under different conditions. Microspectrometry (MSP) was the tool of choice, because the instrument can perform direct absorbance measurements of rhodopsin and its photoproducts from intact photoreceptors.

Principles of Microspectrophotometry

Rod photoreceptors contain ~3 mM of rhodopsin within the outer segment (Harosi, 1975). This pool of rhodopsin, when measured, has a characteristic spectral absorbance profile (Govardovskii et al., 2000). When bleached, the measured absorbance profile of rhodopsin changes. At first, bleached rhodopsin will be transformed into a metarhodopsin photoproduct state, of which MI, MII (Rh*), and MIII have been

identified. When the overall concentration of rhodopsin decreases, so does the spectral absorbance due to rhodopsin. All of these changes in absorbance are measureable. When multiple measurements are compared, changes in rhodopsin absorbance can be tracked as a function of time. MSP works by measuring the absorbance of rhodopsin (or meta-photoproducts) as a function of wavelength.

Absorbance, or OD, of rhodopsin in isolated patches of rod photoreceptors were made according to Beer's Law:

$$OD = log_{10}(\frac{I_{blank}}{I_{sample}}). \quad (2.2)$$

where OD was the optical density, I_{sample} was the transmitted photon beam intensity that passes through a patch of outer segments, and I_{blank} was the transmitted intensity of the photon beam when positioned in an adjacent space in the preparation that contains only culture medium but no outer segments. Optical density was measured as a function of wavelength λ over the range 300 – 700 nm in 2 nm steps.

The polarization of the incident photon beam used to measure the optical density can affect the absorbance profile of rhodopsin (Harosi and MacNichol, 1974; Kolesnikov et al., 2003). This effect occurs due to the specific orientation of rhodopsin molecules within the outer segment's membranous disks. This makes the outer segment dichroic; meaning that light is absorbed preferentially depending on the plane of polarization of the incident photons. This phenomenon and how to pertains to MSP experiments are illustrated diagrammatically in Figure 2.4A. Differences in resulting absorption spectra due to the outer segment's dichroic nature are illustrated in Figure 2.4B.

A

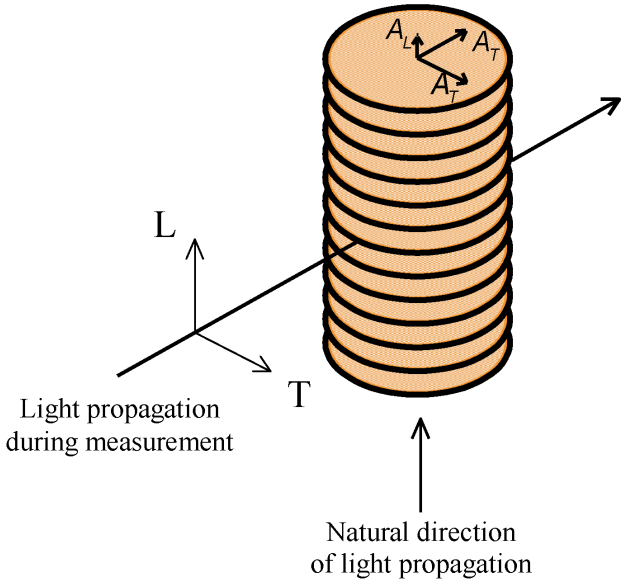
A_L
A_T
A_T
L
T
Light propagation
during measurement
Natural direction
of light propagation

B

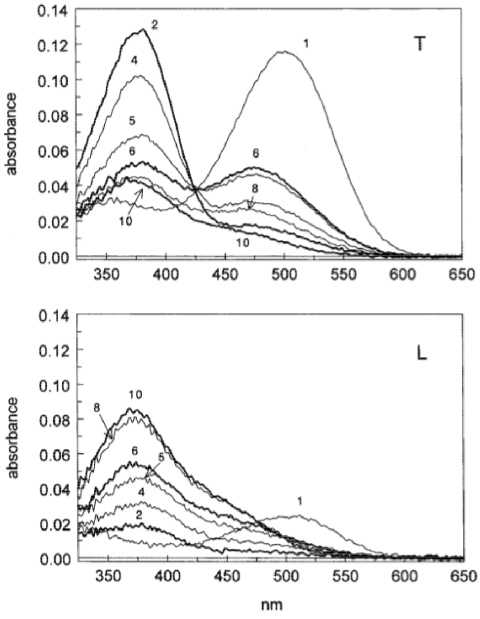
T
L
absorbance
absorbance
nm
0.14
0.12
0.10
0.08
0.06
0.04
0.02
0.00
350
400
450
500
550
600
650

Figure 2.4: Microspectrophotometry (MSP) recordings of rhodopsin are affected by the polarization of the photon beam used for absorbance measurements. *A:* Illustrated is a graphical depiction of the rhodopsin rich disks contained within the rod outer segment. This drawing depicts two different vectors of light propagation into these disks. The natural direction of light propagation is shown coming from below the membrane stacks along the longitudinal axis of the outer segment. The photons within this light always have an electric field that is aligned along the (radial or) transverse axis of these stacks. The MSP measurement beam is the second light propagations vector in this drawing, and it is incident on the membrane disks from the side. The photons within the MSP measurement beam will have an electric field that is either aligned with the membranous discs (T polarization), along a photoreceptor's longitudinal axis (L polarization), or a combination of these two directions. Rhodopsin preferentially absorbs light that has a T polarization. This figure was reproduced with permission from Petri Ala-Laurila. *B:* MSP measurements of rhodopsin taken using T polarization (top panel) or L polarization (bottom panel). Select traces in both graphs are numbered. Matching numbers indicate the measurements were taken under identical conditions. Traces numbered 1 are dark-adapted spectra. Low numbers correspond to small durations of light exposure (seconds to minutes range). Likewise, the larger numbers represent durations of light exposure that occurred over tens of minutes. The difference between the top and bottom panel was due to the dichroic property of rod outer segments. These findings were previously reported (Kolesnikov et al., 2003), and reproduced here with the permission of the authors.

Description of the Microspectrophotometer Apparatus

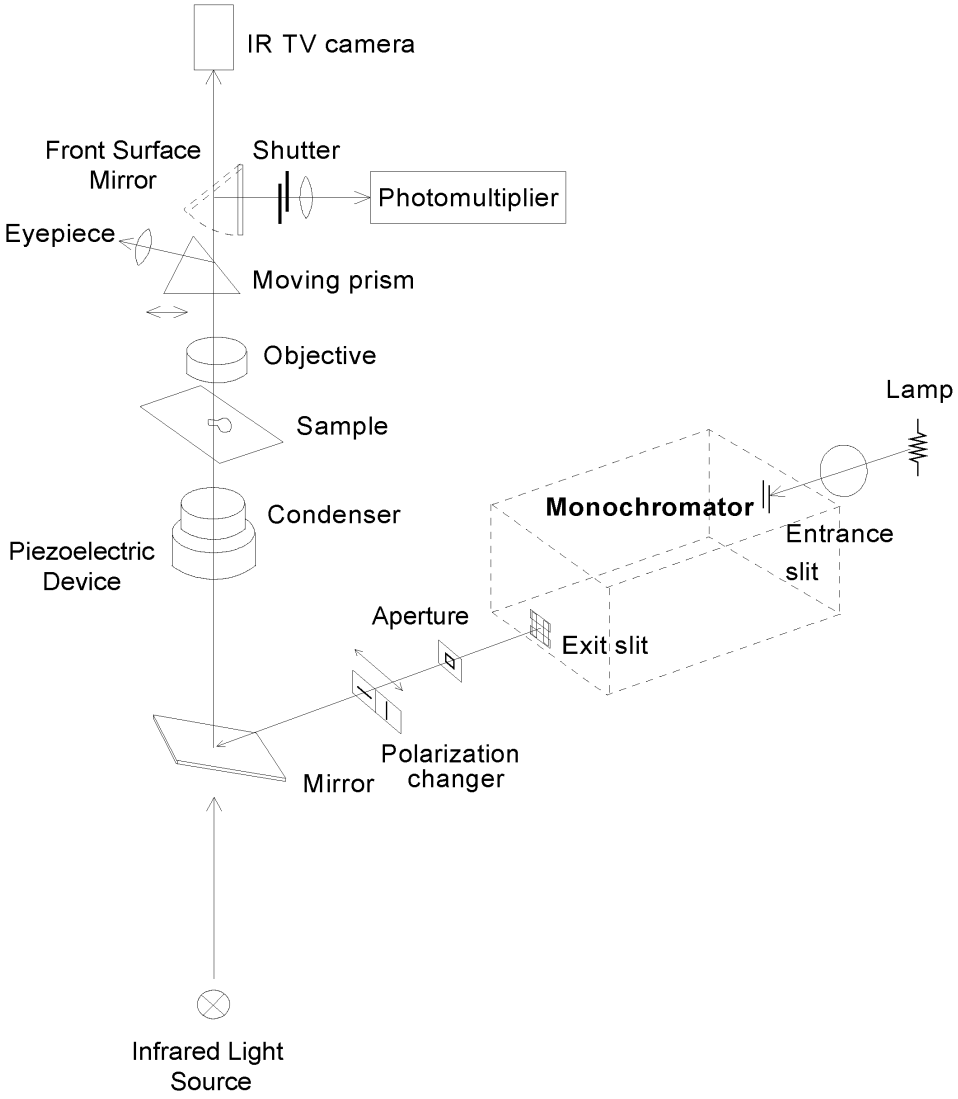

Figure 2.5: A schematic illustration of the microspectrophotometer. Drawn on the right side of this drawing is a light (xenon arch light) source. This light source produced a beam of light that was used for MSP measurements. During measurements a computer controlled shutter allowed the white light beam to enter a programmable monochromator. The output monochromatic light beam passed through an adjustable rectangular aperture and a polarization prism. This light was reflected off a half silvered mirror and passed through a UV condensing objective positioned below the sample stage. The condensing lens was mounted on a computer controlled piezoelectric device to maintain focus across all wavelengths. The image of the aperture was focused onto the rod outer segments. Transmitted light is collected by an immersion objective above the preparation. A movable front surface mirror reflects the transmitted beam of light into a photomultiplier tube (PMT). The measured PMT current was recorded (as a function of wavelength) by a remote workstation (not shown). This instrument also had an infrared imaging system. Below the lower condensing lens was an IR LED. This light source allowed for beam and sample adjustments. The IR camera located above the microscope allowed for visualization of the rectangular slit and the rod outer segments. This instrument has previously been described (Frederiksen et al., 2012).

The microspectrophotometer is illustrated schematically in Figure 2.5. The instrument works as follows. Incident light for the measuring beam of light was provided by white light from a xenon arc lamp (Cairn Instruments, Kent, UK) that passes through a programmable monochromator. The intensity of the light exiting the monochrometer was attenuated using a neutral density quartz wedge (not shown in Figure 2.5). The beam of monochromatic light was then passed through an adjustable rectangular aperture and a Glan-Thompson polarizing prism. The prism was rotated to give the measurement beam a T or L polarization (see Figure 2.4). Unless otherwise stated, T polarization was used as it allows the maximum absorbance amplitude for rhodopsin. A mirror reflected the beam of polarized light through a UV transmitting quartz condensing lens (Achromatic UV-Kondensor, Zeiss) that focused the aperture at the plane of the preparation. Chromatic aberrations were corrected by mounting the objective to a computer controlled piezoelectric device that was used to maintain the beam focus at all wavelengths. The sample chamber in which the retina was placed was a machined 2 mm thick disc of Plexiglas with a quartz cover-slip window located on the bottom. Retinae were mounted on top of this quartz coverslip, and flattened with a tissue anchor (Warner Instruments, Hamden, CT, USA) and continuously perfused with Ames medium. Rod photoreceptor outer segments where positioned into the light path of the monochromatic beam. The rectangular aperture is adjusted to project a box that was dimensionally close to ~10 x 6 μm in size, and which simultaneously illuminated the outer segments of multiple rods. An immersion microscope objective was in contact with the superfusate covering the retina and was located above the sample stage. It collected light that was passed through

the rod photoreceptors (immersible Fluor 20X objective, Nikon). This objective directed transmitted light via a movable front surface mirror, through an electronically controlled shutter and onto the surface of a photomultiplier tube (PMT). The PMT recorded the transmitted light as a photocurrent that is digitally stored (as a function of wavelength) by a remote workstation.

An additional feature of the MSP instrument was that it incorporated an infrared imaging system for viewing the preparation of rod outer segments. This consisted of an infrared light source and camera that was attached to the microscope optics. The imaging system aids the user in positioning/orienting the rod outer segments into the optical path of the measurement beam. During the time of absorbance measurements, the infrared imaging system was deactivated.

During recordings, the monochromator was programmed to scan linearly between 300 – 700 nm in discrete 2 nm steps. Each spectral measurement consisted of ten separate scans, each performed in less than 1 s. These scans were averaged to minimize noise. All of the data was stored on a remote work station. It was determined and previously reported that each series of 10 measurement bleached < 0.1% of the visual pigment (Nymark et al., 2012). Further analysis of the data was performed in a custom made LabVIEW™ software suite.

Trans-Retinal Electroretinogram

Electroretinography (ERG) is an electrophysiological technique that records the voltage changes in the whole retina when it is exposed to a light stimulus. ERG

recordings were made on isolated retinae. *Trans*-retinal ERG measurements provide a means to determine the flash sensitivity from the whole retina under condition that were the same as those for biochemical determinations of the extent of rhodopsin phosphorylation (described in detail below). ERG measurements on wild-type retinae record the electrical responses from rod and cone photoreceptors, and from other retinal neurons, including bipolar, horizontal, amacrine, Müller, and ganglion cells. Additional steps were required in order to exclusively isolate the electrical responses from rod photoreceptors.

ERG recordings presented in this dissertation were made on *Gnat2*$^{-/-}$ mice, in which the cone electrical response is absent. Isolation of photoreceptor responses was achievable with the aid of a pharmacological cocktail added to the profusion system. This pharmacological cocktail added 50 μM DL-AP4 (DL-(+)-2-Amino-4-phosphonobutyric acid; Tocris Biosciences, Bristol, UK) to the superfusate; a glutamate receptor agonist which blocked bipolar and horizontal cell transmission (Nakajima et al., 1993; Heikkinen et al., 2012). The activity of voltage-gated channels of Müller cells was inhibited by adding 100 μM $BaCl_2$ to the superfusate (Bolnick et al., 1979; Baylor et al., 1984; Newman, 1989; Burns et al., 2002; Nymark et al., 2005; Heikkinen et al., 2012).

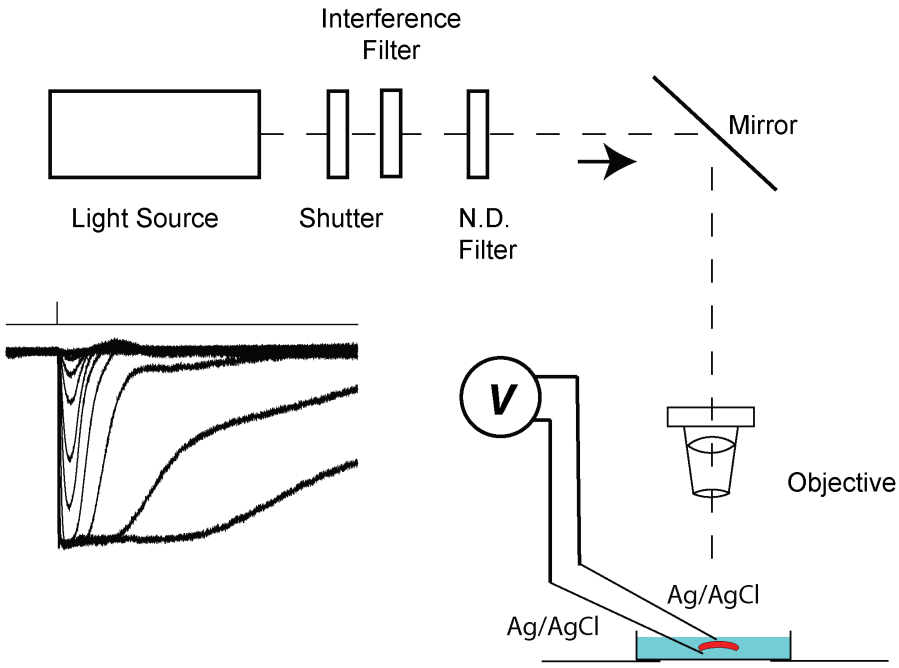

Figure 2.6: Schematic of a *trans*-retinal electroretinogram (ERG) recording instrument. A tunable light source provides a stimulus to the measured retina. The duration of light exposure is controlled by a shutter, and the intensity is further controlled using neutral density filters. An interference filter selectively limits the stimulus wavelengths (in this case to 500 nm). Afterwards, the light is projected onto the plane of a flat mounted retina. The response is recorded using two silver-chloride electrodes (positioned above and below the retina). These electrodes are connected to a differential amplifier, and the signal is digitalized and stored on a remote workstation. A representative dataset (recorded in the presences of the pharmaceutically cocktail) is shown on the left.

A schematic representation of the equipment used for ERG measurements is shown in Figure 2.6. A tunable bright light source provided light stimulation. The stimulus intensity was attenuated using calibrated neutral density filters. These filters were capable of attenuating the light by up to 9 orders of magnitude (9 $\log_{10}$ units) in 0.1 log unit intervals. The light also passed through a 500 nm filter (half band, 10 nm). An electronic shutter controlled the duration of light stimulus, restricting the duration of stimulation to 20 milliseconds. The stimulus flash was reflected off a mirror into a condensing lens, and was focused at the plane of the retina. The spot size was ~5 mm in diameter (sufficiently large to illuminate the entire retina), and was of uniform in intensity. Following its isolation, each retina was positioned in a custom recording chamber, in which a retina was flat mounted. A recording and reference electrode were positioned above and below the retina. These electrodes were connected to a differential amplifier, and the flash responses were recorded using a Warner Instruments DP-311 differential amplifier (1000 X gain). Responses were low-pass filtered at 1000Hz, before being digitized and recorded at 2 kHz using a Digidata 1322A acquisition board (Axon Instruments, Sunnyvale, CA).

An illustration of the recording chamber is provided in Figure 2.7. The recording chamber was custom fabricated from Plexiglas. The chamber had a recessed area that was designed to accommodate a submerged flat mounted retina that was suspended on lens paper (not shown). Below the retina was a cavity designed to accommodate a small volume of fluid. A 1 mm hole separated the (open) upper chamber from the lower cavity. Both the chamber and the cavity were filled with Ames culture medium and were

buffered with bicarbonate and HEPES, respectively, at pH 7.4. During recordings, one electrode would be placed in the lower cavity, and another was positioned in solution above the retina. A temperature probe was also submerged in the chamber to monitor the temperature. The chamber temperature was maintained at 35 ± 1 °C.

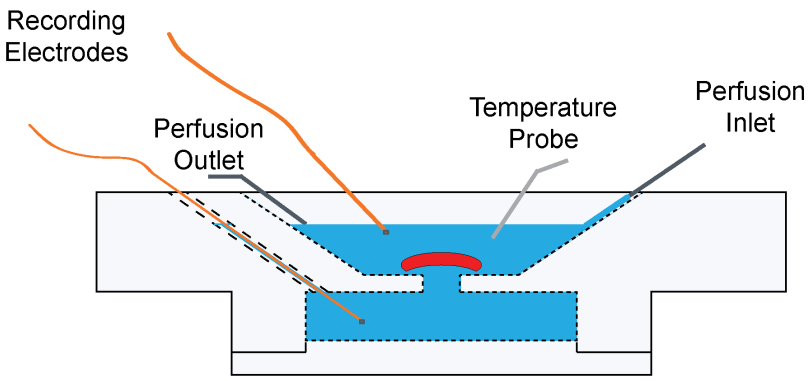

Figure 2.7: The ERG recording chamber. Placed within the recording chamber is a retina that was positioned photoreceptor side up, and flat mounted on top of lens paper (not shown) using a slice anchor (not shown for clarity). The chamber was filled with physiological solution *via* the perfusion inlet. Excess solution was removed by aspiration of the surface. A cavity below the retina provided an electrolytic space in which a reference electrode was placed.

Calibration of the Optical Bench for ERG Stimulation

The intensity and spatial extent of the flash stimulus were calibrated at the beginning of each experiment in the following way. The electronic shutter was engaged to the open position, and a circular aperture (positioned in one of the conjugate planes of

the optical system) was used to limit the spot size to 1000 μm in diameter at the plane of the preparation. The maximum intensity of the light at the plane of the preparation was measured with the detector of a radiometer while the voltage to the lamp was adjusted to provide the same intensity at the beginning of each experiment. The unattenuated 500 nm wavelength filtered light intensity at the level of the retina was calibrated to be 1.27×10^7 photons μm^{-2} s^{-1}. Calibration was accomplished with a 350 Linear/log Optometer radiometer using a Model 221 detector that had the filter removed (UDT Instruments, Baltimore, MD).

Analysis of ERG Data

The recordings from each ERG experiment were processed using a custom made MATLAB® graphical user interface. Briefly, this software was designed to remove the DC offset from each recorded trace and to provide the average response for each test flash intensity. Seven trials were averaged for the dimmest flashes, four trials for modest light intensities, and a single flash trial was used for the brightest light intensities. The software also recorded the maximal response amplitude of each of these averaged traces. A peak finding routine located the maximum-recorded amplitude and then averaged 10 data points before and after the peak. The purpose of this averaging was to reduce noise-induced artifacts.

Single Cell Suction Pipette Recordings

Measurements of light activated changes in membrane current were made extracellularly from single cells that were attached to patches of retina. Such measurements can be used to determine the sensitivity and kinetics of flash responses as well as determine characteristics of single quantum responses.

Description of the Suction Electrode Apparatus

A schematic representation of the single cell suction pipette apparatus is shown in Figure 2.8. Light flash stimuli were provided by an optical apparatus that was similar to the one used for the ERG measurements. Briefly, the tunable xenon bright light source provided a stimulus beam. The intensity of light was attenuated using calibrated neutral density filters, the wavelength was set to 500 nm using an interference filter (half-band, 10 nm), and a shutter restricted the duration of light stimulus to 20 milliseconds. The stimulus flash was reflected off a mirror, into an objective lens that focused the light at the plane of the sample preparation. The samples consisted of small pieces of chopped retinae that were superfused with Ames culture medium. During the course of any experiment, individual cells where drawn outer segment first into a tight-fitting glass micropipette (detailed below). The micropipette was connected to a headstage via an Ag/AgCl pellet in an electrode holder (Warner Instruments; Hamden, CT). The headstage converts the photoreceptor's photocurrent into a voltage signal, which is then amplified using a patch clamp amplifier (Model: List Patch Clamp L/M EPC7, List Electronics, Darmstadt, West Germany). Responses were then low-pass filtered at 60Hz, before being

digitized at 2 kHz using a Digidata 1322A acquisition board (Axon Instruments, Sunnyvale, CA), and stored digitally on a remote workstation.

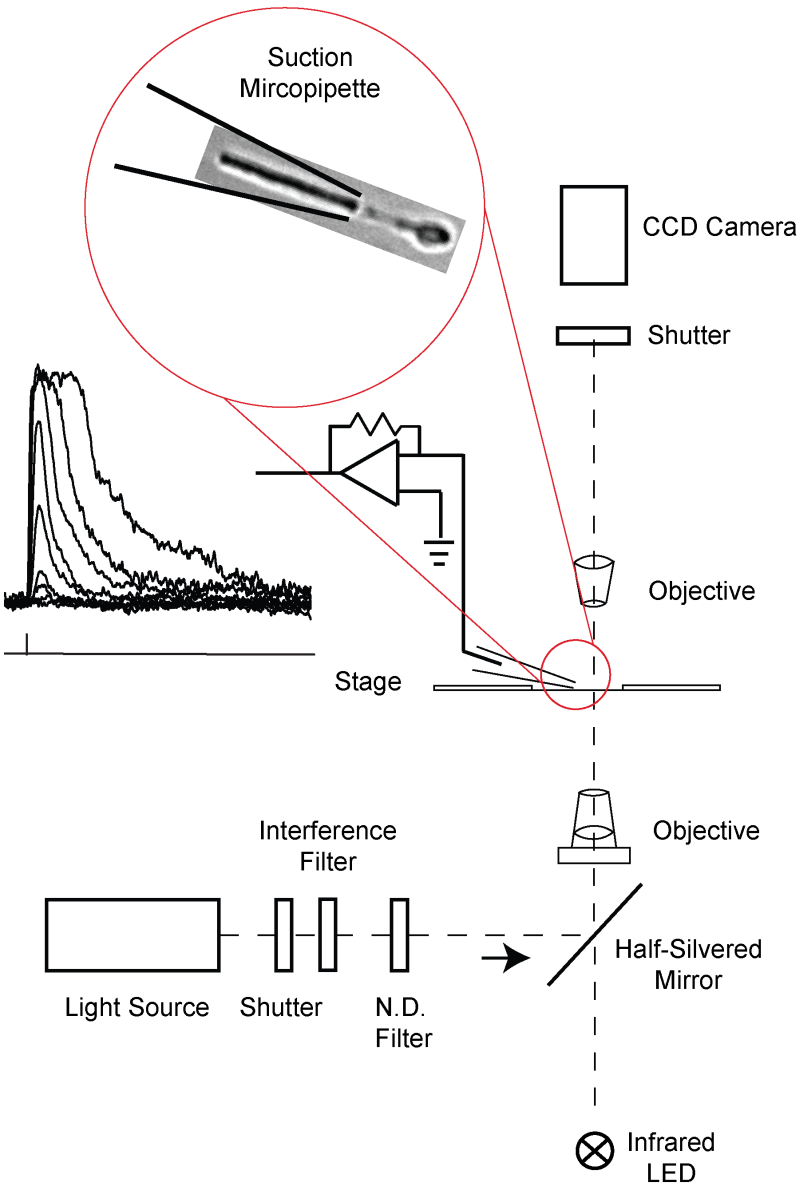

Figure 2.8: Schematic of the single cell suction electrode instrument. In this instrument, an adjustable light source was used to provide a stimulus to the cells. A shutter controlled the duration of light exposure. Within the light path was an interference filter that set the stimulus wavelength. A set of neutral density filters was used to attenuate the light intensity. The stimulus light was reflected off a mirror and projected onto the photoreceptors. The integrated infrared imaging system was used when positioning the cells and in drawing the cells into the micropipette. Following stimulation, the responses from the cell were amplified, digitalized, and stored on a remote workstation. A representative dataset is shown on the left side of the figure.

Single cell recordings were made from prepared isolated retinae. In general, working with whole isolated retina is difficult because the photoreceptors are densely packed together. Therefore, retinae were cut up into small workable patches using a surgical scalpel. These small pieces of retina were then suspended in HEPES buffered Ames culture medium, and were then injected into the sample chamber. A diagram of the recording chamber can be found in Figure 2.9. The retinal patches were given ~10 minutes to allow them to spontaneous settle at and self-adhere to the bottom of the chamber. After this short period of settling, the perfusion system was engaged that provided gassed $NaHCO_3$ buffered Ames culture medium that was heated to 35 ± 1°C.

Suction pipettes were fabricated by heat-pulling a 1 mm OD (0.75 mm ID) glass capillary tube to a fine point using a Flaming Brown micropipette puller model P80/PC (Sutter Instruments). The pointed tip of this micropipette was fire polished to form a smooth surface such that the orifice is just slightly smaller than the outer diameter of the outer segment. A tight contact between outer segment membrane and pipette glass is needed to form a seal, thus providing electrical isolation of the solution inside the pipette from that in the external solution.

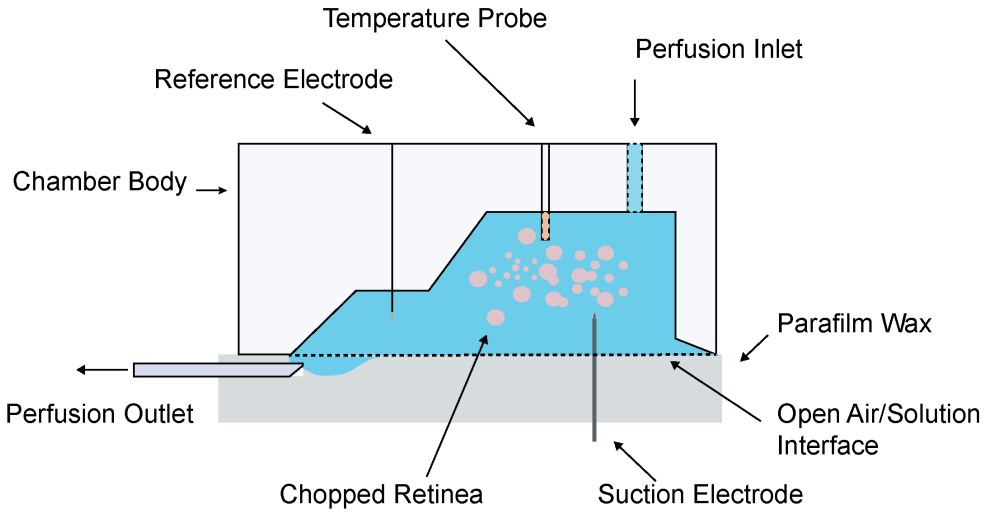

Figure 2.9: A top view of the single cell suction pipette sample chamber. The sample chamber was designed to provide the retinal patches with nutrients, to provide suction pipette accessibility, all while maintaining a low (electrical) noise recording environment. The body of the chamber was milled from plastic into the shape as depicted. This chamber body was mounted on top of a 2 mm thick glass plate (plate not shown). The top of the chamber was covered by a thin cover slip. With the aid of these two panes of glass, there was a hollow cavity that was filled with solution and chopped pieces of retinae (pink pieces). This cavity was perfused with heated (35 °C) bicarbonate buffered Ames solution. Integrated within the chamber body was a temperature sensor and a reference silver-chloride electrode. As physiological solution was fed into the chamber, excess solution protrudes from the chamber and was drawn away by suction *via* perfusion outlet. This suction outlet consists of a clean glass capillary tube that was broken on an angle to promote a mixture of solution with air as superfusate is drawn away. In this way, excess solution was removed without purging the entire volume of chamber. At the same time, this system reduced the electrical noise.

The size of the orifice at the tip of the pipette was empirically determined using a *bubble number*. The bubble number was determined by attaching each pipette to a short length of polyethylene tubing that was connected to a 10 mL plastic syringe. The tip of the pipette was immersed in a small volume of EtOH, contained in a scintillation vial.

Depressing the plunger of the syringe gradually increased the air pressure within the pipette. The plunger was depressed until the tip of the pipette bubbled. The pressure at which air bubbles exited from the tip of the pipette was recorded by the milliliter markings on the syringe barrel. This value constituted the *bubble number*. For these experiments, the size of the opening was set to produce a bubble number of 5.7 ± 0.1. If the bubble-number was greater than 5.7, then the opening was larger than ideal. Likewise, smaller openings had smaller bubble-numbers.

At the time of the experiment, recording pipettes are filled with Ames culture medium that is buffered with HEPES. The pipette is then mounted into a microelectrode holder (World Precision Instruments Inc, Sarasota, FL). These holders also contain a silver-chloride pellet electrode, and a port that connects to an external tube. Negative air pressure is applied by mouth to this tube to draw the rod outer segment into the orifice of the pipette. The Ames solution within the pipette created a salt-bridge connection to the sliver-chloride electrode. The port connection allows the experimenter to orally apply the correct suction/pressure needed to pull cells in and to adjust the position of the outer segment within the pipette tip.

Calibration of the Optical Bench for Suction Electrode Stimulation

The procedures for calibrating the suction electrode optical bench were nearly identical to those described in *Calibration of the Optical Bench for ERG Stimulation*. The differences are as follows. A 100W xenon/halogen lamp was used as a light source. A circular aperture was positioned in one of the conjugate planes of the optical system and was used to limit the spot size to 1000 μm in diameter at the plane of the preparation. The

unattenuated 500 nm light intensity at the level of the retina was calibrated to be 4.18 x 10^7 photons μm^{-2} s^{-1}.

Measurements of Response Families from Single Cells

The procedures for measuring and processing suction electrode response families were identical to those described in *Analysis of ERG Data*. The only difference was that the MATLAB® analysis suite was configured to correspond with the specific light intensity used in these experiments and to the specific neutral density filters for this apparatus's optical bench.

Measurements of Quantal Responses from Single Cells

Single photoreceptors were stimulated with dim light in order to measure the kinetics and frequency of discrete quantal electrical responses that result from discrete activations of rhodopsin molecules. After having been drawn into a micropipette, each rod photoreceptor cell was stimulated with dim light. Under these very dim flash intensities the distribution of photo-isomerizations per flash is predictable by discrete Poisson statistics. Data obtained from these experiments contains 100 trails under light stimulation, and 100 electrical instrument noise trials in absence of stimulation.

Single quantal responses (SQR) were estimated by measuring the mean and time dependent variance from stimulated photoreceptors (Baylor et al., 1979; Rieke, 2000; Ala-Laurila et al., 2007). This analysis begins by first calculating the mean response $r(t)$,

mean squared response $r^2(t)$, and that total variance $\sigma^2(t)$ for both the stimulated and non-stimulated datasets as a function of time. In the treatment of this data as a Poisson process the variance from each (stimulated) trail is a combination of the variance of a light induced responses and the noise induced instrument variance. From these trails the variance is formulated as,

$$\sigma_{Total}^2 = \sigma_{Light}^2 + \sigma_{Dark}^2 \tag{2.3}$$

Here the total variance, $\sigma^2_{Total,}$ is the linear combination of the light induced physiological response variance, σ^2_{Light}, and the dark variance in the absence of light stimulation, σ^2_{Dark}. The dark variance $\sigma^2_{Dark}(t)$ was determined from the 100 trails recorded in the absence of light stimulation. Under these assumptions, the light induced variance was calculated as,

$$\sigma_{Light}^2 = \sigma_{Total}^2 - \sigma_{Dark}^2. \tag{2.4}$$

By determining the light induced variance, it becomes possible to determine the mean number of R^* per flash by scaling the mean light response $r_{Light}(t)$ by the light induced variance $\sigma^2_{Light}(t)$ as :

$$\overline{R^*} = \frac{r_{Light}^2}{\sigma_{Light}^2}. \tag{2.5}$$

In order to properly interpret the results of these types of experiments across multiple test conditions, it is necessary to determine the response amplitude produced from single R^* events. This is determined by scaling the mean response $r(t)$ by the mean R^* per flash as shown by,

$$SQR(t) = \frac{r_{Light}(t)}{\overline{R^*}}. \tag{2.6}$$

To obtain the activation constant, A, SQR(t) of a given treatment were averaged,

smoothed (Origin 8.5.1) and normalized to the dark current (i_{dark} = 1, baseline = 0). The rising phases of these traces, $y(t)$, were fitted with an activation model (Pugh and Lamb, 1993):

$$y(t) = 1 - 0.5\, A(t\text{-}t_{eff})^2, \quad (2.7)$$

where t is the time and t_{eff} is a temporal offset.

Isoelectric focused immunoblots to determine rhodopsin phosphorylation

The motivation for isoelectric focusing immunoblots (IEF) experiments was to track the rate of dephosphorylation during dark adaptation. Samples were generated from isolated retinas that were bleached from in the intact (*in vivo)* eyes or from isolated *ex vivo* retinal preparations. Isoelectric focusing immunoblots were used to segregate rhodopsin lysates from whole retinae based on the number of post-transnationally attached phosphates. As described in the introduction, mouse (and human) rhodopsin has six Ser/Thr sites on rhodopsin's carboxyl-terminus. Rhodopsin kinase, *Grk1,* phosphorylates these residues during the deactivation of the visual pigment. Each of these bound phosphates affects the overall electrical charge of rhodopsin, and therefore directly affects rhodopsin's isoelectric point (pI). When performing an IEF experiment, the cell lysates were placed on a gel that had an electrical field induced pH gradient. The electric field also induced the migration of charged rhodopsin molecules. This motion stopped once rhodopsin molecules pass into a section of the gel in which the local pH matched the pI of individual rhodopsin molecules. Afterwards, the external electric field was

removed, and the gel is immunoblotted with mono-clonal rhodopsin antibodies (as described below).

Tissue used for IEF analysis was generated from isolated retinae. At indicated time points, these retinae were transferred to an Eppendorf tube and then flash frozen in liquid nitrogen. Afterwards, these retinae were stored in foil wrapped tubes at -80 °C. The process was similar for *in vivo* bleach experiments, except the retinae were isolated from *in vivo* mouse preparations at a determined time point following bleaching and euthanization.

The relative amount of visual pigment phosphorylation was determined in these samples as follows: Frozen retinae were thawed and homogenized in 400 µL of buffer A (containing: 25 mM HEPES, pH = 7.5, 100 mM EDTA, 50 mM NaF, 5 mM adenosine, 1 mM phenylmethylsulfonyl fluoride (PMSF), and a protease inhibitor cocktail (Roche)) with a polytron homogenizer for ~30 s. Samples were then centrifuged at 4 °C for 15 min at 19,000 x *g*, and the supernatant was discarded. The pellet was washed 3 times with 1 mL of 10 mM HEPES (pH = 7.5) solution. The pellet was thenresuspended in 1mL of buffer B (containing: 10 mM HEPES, ph = 7.5, 1 mM $MgCl_2$, 100 µM EDTA, 2% BSA, 50 mM NaF, 5 mM adenosine, a protein inhibitor cocktail (Roche), and ~900-1200 pmol of 11-*cis* retinal). The samples were placed on a nutator to incubate overnight. Following incubation, the samples were centrifuged and washed with 10 mM HEPES. The pellet was solubilized in 100 µL of buffer C (containing: 10 mM HEPES, pH = 7.5, 100 µM EDTA, 1 mM $MgCl_2$, 10 mM NaCl, 1 % dodecyl-maltoside, and 1 mM dithiothreitol) for a period of 3 hours at 4 °C. Afterwards the samples were again centrifuged, and glycerol

was added to the supernatant to final concentration of 5%. The acrylamide gel (composed of: 5% acrylamide, 0.01% dodecylmaltoside, 13.33% glycerol, Pharmaltye pH range 3-8 (GE Healthcare)) was prepared on a Pharmacia FBE 300 flat-bed apparatus. The samples were loaded, and the proteins were focused for 2 h at 25 W (constant power). The proteins were blotted onto nitrocellulose using capillary action. The membrane was washed with milk to block non-specific antibody binding. Afterwards the membrane was probed with monoclonal antibodies 4D2, and R2-12N that bind to the N-terminus of rhodopsin. The bands were visualized by an ECL system (or LiCOR Odyssey imaging system) and the images digitalized. These procedures were originally described by Concepcion and Chen (2010) and are adapted from (Kuhn and McDowell, 1977; Adamus et al., 1993). IEF measurements were provided by Jeannie Chen's lab at USC.

Quantification of IEF Data

IEF of bleached retinae will produce 7 distinct bands, corresponding to the number of bound phosphates (i.e. 0, 1, 2, … 6). IEF measurements cannot resolve which specific threonine or serine residues are phosphorylated; only the total extent of phosphorylation can be measured by this technique. For example, there are 6 different combinations in which rhodopsin can be singly phosphorylated, all of which have nearly identical isoelectric points. Conveniently the overlapping of pI greatly simplifies the presentation of data. With these constraints in mind, the banding pattern was analyzed using ImageJ.

In each sample lane the total integrated intensity from each band was determined.

The intensity of each band was normalized by the total integrated intensity from all bands. The relative percentages were recorded, and averaged with like samples ($n \geq 3$). IEF analysis was provided by Jeannie Chen's lab at USC.

Transducin Translocation in Isolated Retinae

Mouse rod outer segments (ROS) were isolated as previously described (Moaven et al., 2013). Four retinae were pooled, frozen in liquid nitrogen, and stored in foil-wrapped 1.5 ml microfuge tubes at -80 °C until analysis. At the time of analysis, tissues were thawed and suspended in Ringer's buffer (130 mM NaCl, 3.6 mM KCl, 2.4 mM $MgCl_2$, 1.2 mM $CaCl_2$, 10mM HEPES, 0.02 mM EDTA, pH 7.4) containing 8% OptiPrep™ (Sigma Aldrich). Each sample was vortexed for two minutes. Afterwards the tissue pieces were allowed to settle for one minute. The supernatant containing severed ROS was removed and collected, then 8% OptiPrep was again added and the process repeated four more times. The pooled supernatant was centrifuged on a discontinuous gradient containing 10% and 18% OptiPrep in Ringer's buffer at 70,000 rpm in a Beckman TLA100 rotor for ≥ 1h. The ROS band was collected and diluted in 3 volumes of Ringer's buffer, centrifuged at 50,000 rpm. The pelleted ROS were resuspended in Ringer's buffer containing 1% n-dodecyl-β-maltoside and protease inhibitor cocktail (Roche diagnostics) and incubated at room temperature for 30 min. The ROS sample was combined with equal amount of 2X sample buffer and the proteins separated on SDS-PAGE, blotted onto nitrocellulose, and probed with the following antibodies: rabbit anti-Gβ5 at 1:3,000 dilution (M. Simon) and mouse anti-GNAT1 (TF-15, 1:5,000,

CytoSignal). Signals were detected using an LI-COR Odyssey Infrared Imaging system. ROS procedures, measurements, and data analysis was performed at USC in Jeannie Chen's lab.

.

CHAPTER THREE: RESULTS

The aim of this study was to determine how rhodopsin dephosphorylation affects dark adaptation. Specifically, my goal was to test the hypothesis that rhodopsin dephosphorylation is required for dark adaptation of rod photoreceptors. This hypothesis has been the topic of previous studies designed to correlate rhodopsin dephosphorylation and dark adaptation (Kennedy et al., 2001; Lee et al., 2010). These studies however stopped short of providing a causal relationship. To test this hypothesis, I have developed an approach in which I could substantially block rhodopsin dephosphorylation, and then determine the physiological consequences to dark adaptation. The results presented in this chapter outline the protocols that I have developed that abolished rhodopsin dephosphorylation in isolated *ex vivo* retinae. I then performed electrophysiological experiments, under identical conditions, to understand how rhodopsin dephosphorylation effects dark adaptation.

Rhodopsin Phosphorylation in *Ex Vivo* Bleached Retinae

In order to test the hypothesis of this dissertation, there needed to be a model system in which rhodopsin dephosphorylation could be regulated. Unexpectedly, I discovered that rhodopsin dephosphorylation was effectively blocked by simply isolating the retina and placing it in isotonic Ames solution used for electrophysiological recordings. The data demonstrating this phenomenon is presented in Figure 3.1. Here, rhodopsin phosphorylation was measured from dark adapted and from bleached isolated WT retinae using IEF protocols (see Methods). IEF gels are composed of several lanes,

each designed to evaluate how the tested experimental conditions affect rhodopsin phosphorylation. With this experimental approach, rhodopsin is segregated based on the degree that each molecule is phosphorylated. A single rhodopsin molecule can either be unphosphorylated, denoted as 0P on the ordinate of each gel, or phosphorylated from one to six times, denoted on the ordinate as 1P (2P, 3P, …) or 6P. The first measured condition, presented in the left-most lane, was designed to determine the extent of rhodopsin phosphorylation that is present in dark-adapted retinae. The data show that only unphosphorylated rhodopsin (0P) is present in dark-adapted retinae; a result that is consistent with previous investigations (Kennedy et al., 2001; Ramulu et al., 2001; Lee et al., 2010). The four lanes to the right illustrate the extent of rhodopsin phosphorylation following exposure to bright light and the time-course of rhodopsin dephosphorylation in subsequent darkness. Rhodopsin phosphorylation was measured from these 70% bleached retinae following 0, 60, 120, and 180 minutes of incubation in darkness. The data show that exposing these retinae to bright light result in rhodopsin phosphorylation. This is evident by the multiple bands in each of these lanes. Moreover, the data show that bleached rhodopsin can have up to 6 attached phosphates; one at each of the three serine and three threonine residues on the C-terminus of opsin. These experiments were repeated ($n \geq 3$), and the data was quantified using ImageJ to control for differences in sample loading (quantification data not shown). The extent of rhodopsin phosphorylation in all of these bleached samples was statistically indistinguishable from each other. Thus, the data show that there is no detectable change in rhodopsin dephosphorylation with increasing the duration of dark incubation. These results demonstrate that rhodopsin

dephosphorylation is substantially attenuated by isolation of the retina. A control experiment, shown on the right side of Figure 3.1, was performed on a 70% bleached GRK1$^{-/-}$ retina; a model in which rhodopsin kinase has been genetically knocked out.

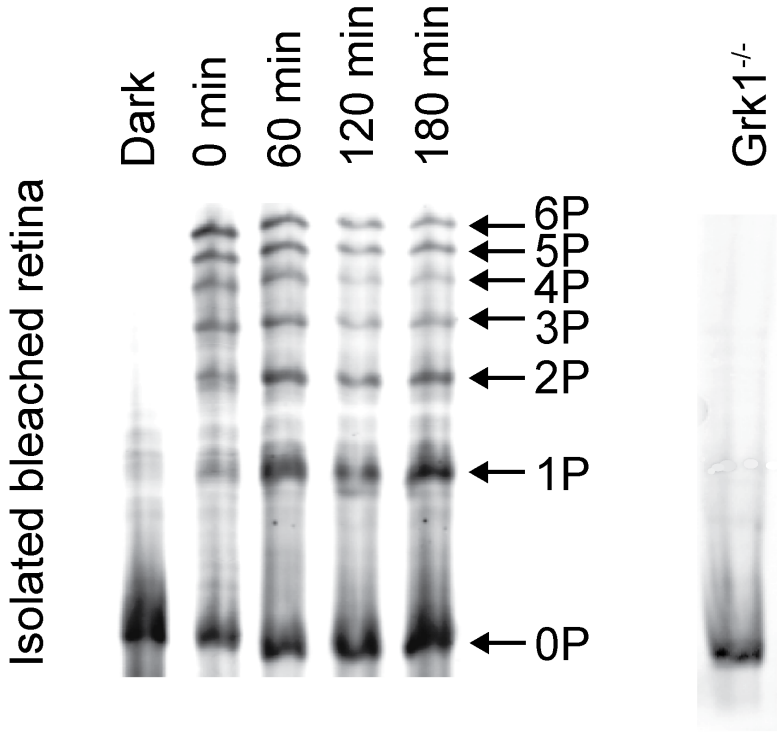

Figure 3.1: IEF measurements of rhodopsin phosphorylation in dark adapted and bleached isolated WT retinae. In these IEF measurements, rhodopsin molecules segregate based on the number of attached phosphate (see methods Chapter). The total number of bound phosphates is indicated on the right side of these gels, and can range for 0 attached phosphates (0P) to 6 attached phosphates (6P). Retinae were either dark adapted (left-most lane) or 70% bleached over the course of 160 seconds (in all remaining lanes). The bleached retinae were incubated in darkness as indicated prior to IEF measurements. A bleached *Grk1*$^{-/-}$ retina, which is devoid of the rhodopsin kinases was used as a negative control.

Rhodopsin Phosphorylation in Bleached *In Vivo* Retinae

Rhodopsin phosphorylation was also measured from intact eyes from living animals. The results presented in Figure 3.2 were obtained from either dark-adapted retinae, or from retinae that were bleached by exposing the eye of living (*in vivo*) animals to light. The exposure to light bleached 90% of the visual pigment. These animals were then allowed to dark-adapt and the retinae were removed at indicated time points (see Methods). Comparison with the results in Figure 3.1 reveal that rhodopsin dephosphorylates within the living mouse, and that it is essentially complete after 3 hours of dark adaptation. It can be seen that no signals were detected from the 3P, 4P, 5P, and 6P bands from IEF samples after 180 minutes of *in vivo* dark adaptation. The experiments in Figure 3.2 are not novel (Ohguro et al., 1995; Kennedy et al., 2001; Lee et al., 2010), but were designed to facilitate a comparison of rhodopsin dephosphorylation as it takes place in bleached intact *in vivo* retinae or in *ex vivo* bleached isolated retinae. For clarity, it is important to reiterate that IEF measurements can not distinguish between phosphorylated opsin and phosphorylated rhodopsin, since the visual pigment must be regenerated before being placed on the IEF gel.

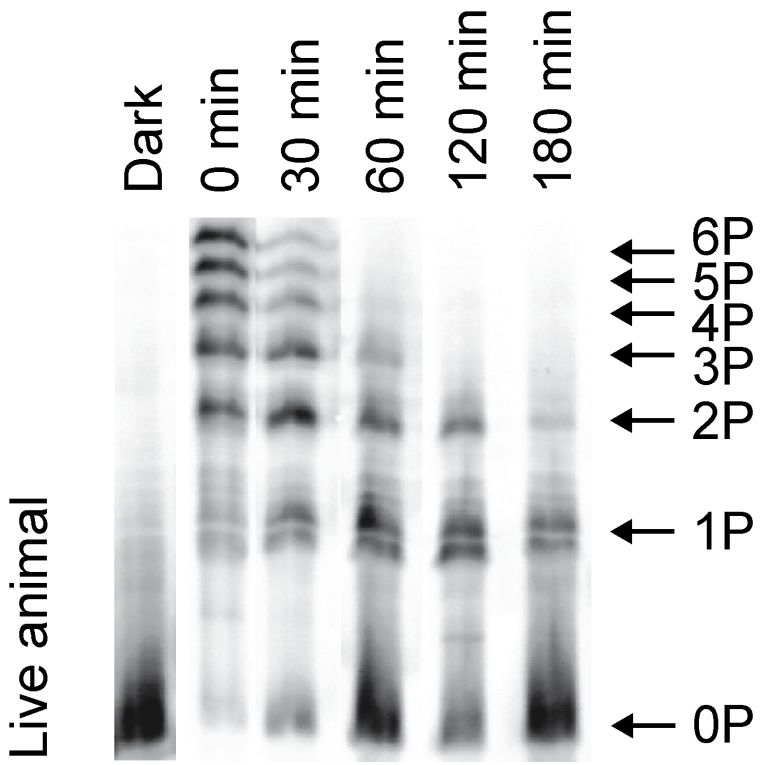

Figure 3.2: IEF measurements of rhodopsin phosphorylation from *in vivo* retinae. Rhodopsin phosphorylation was measured in retinae that were either dark-adapted (*Dark*) or exposed to 500 nm light for 230 seconds in order to bleach 90% of the visual pigment. Animals with bleached retinae were subsequently returned to darkness to dark adapt for the indicated periods of time before they were sacrificed and their retinas extracted and frozen for IEF analysis. In these gels, rhodopsin molecules segregate based on the number of bound phosphates as indicated on the ordinate on the right.

Rhodopsin Phosphorylation in Regenerated *Ex Vivo* Retinae

The results presented in Figure 3.1 show the suppression of rhodopsin dephosphorylation in bleached isolated retinae, while the results in Figure 3.2, illustrate the normal course of dephosphorylation that occurs *in vivo*. One obvious difference between theses preparations is that 11-*cis* retinal was absent in *ex vivo* preparations, and that it was supplied to *in vivo* retinae naturally via the RPE. Since the isolated retina is not in contact with the RPE and no exogenous 11-*cis* retinal was supplied, it was important to determine whether visual pigment regeneration is required before rhodopsin dephosphorylation can occur. I elected to repeat these experiments on *Gnat2*$^{-/-}$ mice in which 11-*cis* retinal was exogenously supplied. *Gnat2*$^{-/-}$ retinae were used since this allowed me to perform a parallel set of electrophysiological experiments on retinae where the cone electrical responses were absent (presented below in *ERG Recordings from Dark Adapting Isolated Retinae*). IEF measurements of rhodopsin phosphorylation were performed on dark-adapted and bleached isolated *Gnat2*$^{-/-}$ retinae, as shown in Figure 3.3. The results presented in the left lane of Figure 3.3, show the phosphorylation profile in dark-adapted retina. IEF measurements confirm that rhodopsin in these retinae exists in the unphosphorylated state, as expected. The IEF data shown in the right most lanes illustrate the time course of dephosphorylation observed subsequent to a bright bleach following 0 min, 100 min, 160 min and

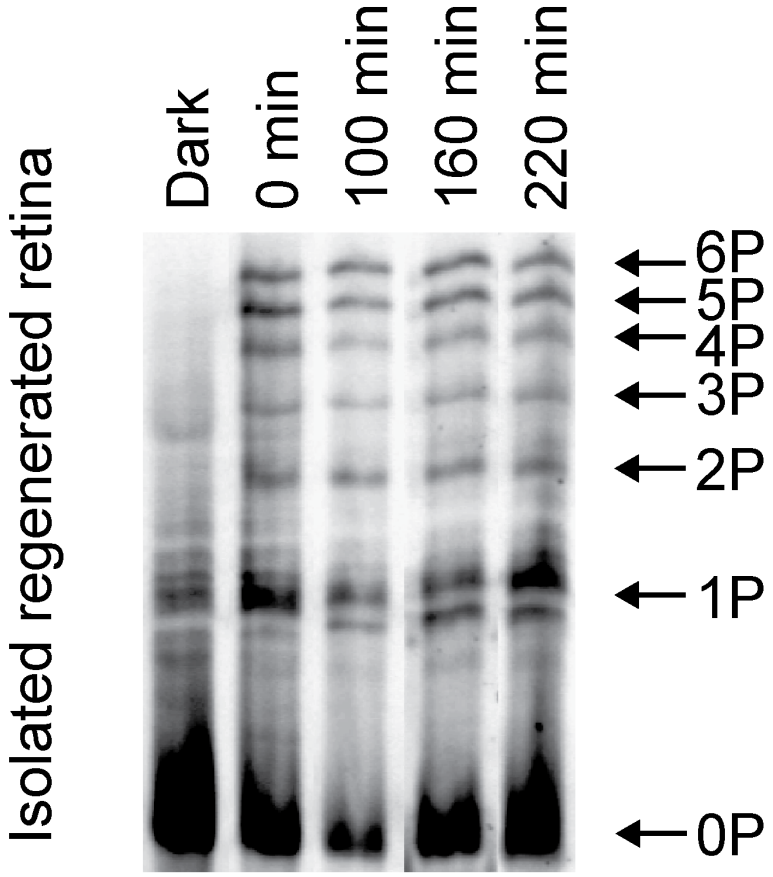

Figure 3.3: IEF measurements of rhodopsin phosphorylation in bleached *Gnat2*$^{-/-}$ rods during dark adaptation with 11-*cis* retinal. (From left to right): Rhodopsin phosphorylation was measured from dark-adapted retinae (Dark) and retinae that were exposed to 500 nm light for 219 s in order to bleached 50% of the visual pigment. A subset of bleached retinae were incubated at 35 ± 1 °C with 11-cis retinal for either 60, 120, or 180 minute in darkness, then subsequently measured with ERG, and flash frozen for IEF analysis as indicated at 100, 160, or 220 minutes, respectively. In these IEF gels, rhodopsin molecules segregate based on the number of bound phosphates as indicated on the ordinate on the right.

220 min of dark incubation. These results are comparable to those presented in Figure 3.1, however for these experiment, the bleach fraction was reduced to 50% because some mouse strains are not tolerant to bleaches in excess of 50% (Nymark et al., 2012).

Quantification of Rhodopsin Phosphorylation

Results in Figures 3.2 and 3.3 were confirmed by multiple observations ($n \geq 3$). The IEF gels from different experiments were digitally scanned and the data was quantified using ImageJ (see Methods). Data presented in Figure 3.4 shows the quantified levels of rhodopsin phosphorylation measured during dark adaptation following light exposure. These measurements were made from bleached isolated (*ex vivo*) *Gnat2*$^{-/-}$ retinae, or from bleached (*in vivo*) retinae obtained from living WT mice. Each figure shows the fractional distribution of rhodopsin phosphorylation. The ordinate for the plots shown in Figure 3.4 is labeled from 0P to 6P; the number preceding each *P* denotes the number of attached phosphates, such that 0P represents the fraction of rhodopsin in the unphosphorylated state, whereas phosphorylated rhodopsin is labelled from 1P-rhodopsin (1P) to 6P-rhodopsin (6P). On the abscissa of each plot is the fraction of total rhodopsin. The data obtained from *ex vivo* retinae (*top* panel of Figure 3.4), clearly shows that rhodopsin phosphorylation remains virtually unchanged regardless of the time spent incubating in darkness in the presence of 11-*cis* retinal. Moreover, there is no discernible redistribution of phosphorylated species of bleached rhodopsin, indicating that rhodopsin phosphorylation appears neither to increase nor decrease as a function of time. The distribution remains essentially unchanged in darkness for periods up to 220 minutes.

This is in contrast to the data obtained from *in vivo* retinae (*bottom* panel of Figure 3.4) that show a clear gradual decline of phosphorylated bleached rhodopsin subspecies with time. This latter result is again consistent with reports that document the normal time course of rhodopsin dephosphorylation that takes place under normal *in vivo* conditions (Kennedy et al., 2001; Ramulu et al., 2001; Lee et al., 2010).

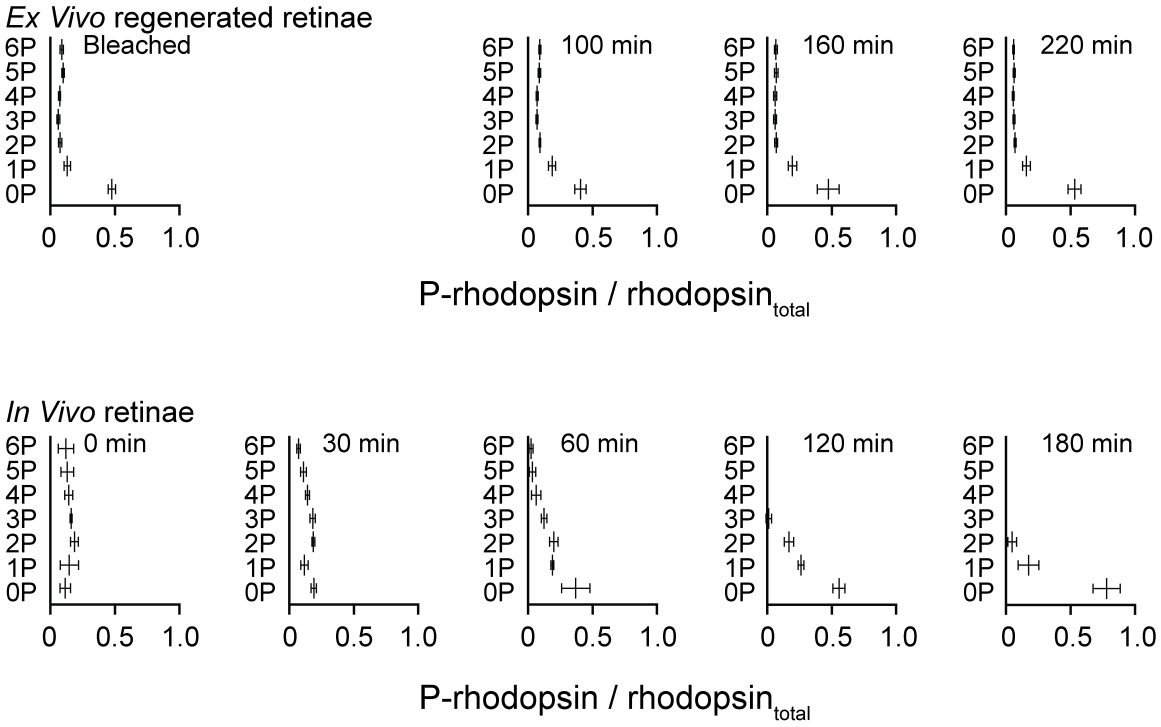
Ex Vivo regenerated retinae
Bleached
100 min
160 min
220 min
6P
5P
4P
3P
2P
1P
0P
0
0.5
1.0
P-rhodopsin / rhodopsin$_{total}$
In Vivo retinae
0 min
30 min
60 min
120 min
180 min
P-rhodopsin / rhodopsin$_{total}$

Figure 3.4: Quantification of rhodopsin dephosphorylation extracted from IEF gel measurements of bleached *in vivo* and *ex vivo* mouse retinae. *In vivo* bleaching was performed by direct projection of 500 nm light into the eye of anesthetized mice. *Ex vivo* bleaching was performed by projection of light on retinae that were isolated from the RPE and placed in Ames solution in a small plastic Petri dish. Dark-adapting *ex vivo* (*Gnat2*$^{-/-}$) retinae that were supplied with (exogenous) 10 μM 11-*cis* retinal and dark-adapting *in vivo* retinae (endogenously supplied 11-*cis* retinal). Each plot graphically shows the distribution of rhodopsin phosphorylation (from 0P to 6P) on the ordinate, as a fraction of total rhodopsin (abscissa) at selected time points. (*Top*): Plots from IEF gels prepared from isolated retina preparations of *Gnat2*$^{-/-}$ mice in 4 different conditions (left to right): 50% bleached retinae (N = 3), 50% bleached retinae incubated in darkness with 10 μM 11-*cis* retinal for 60 min (measured at 100 min, N = 4), for 120 (measured at 160 min, N = 7), and 180 min (measured at 220 min, N = 6). The band intensities from IEF gels were quantified and analyzed using ImageJ. (*Bottom*): Plots of IEF gel data derived from retinae of living WT animals in 5 different conditions (left to right): animals bleached (90%) and then sacrificed after 0 min in darkness (N = 4), sacrificed after 30 min in darkness (N = 4), sacrificed after 60 min in darkness (N = 4), sacrificed after 120 min in darkness (N = 4), or sacrificed after 180 min in darkness (N = 4). Data presented as means ± S.D. Representative IEF data from the *top* and *bottom* panel can be found in Figures 3.3 and 3.2, respectively.

Figure 3.5 plots the average fraction of phosphorylated rhodopsin (P-rhodopsin) as a function of time. *In vivo* determinations were made from wild type retinae that had been bleached by 90%. *Ex vivo* determinations were made on isolated *Gnat2*$^{-/-}$ retinae that were bleached by 50%. Over the course of 180 minutes, bleached *in vivo* retina experienced rhodopsin dephosphorylation (red triangles). The average decline (indicated by the red line) approached 80% over 180 min. In contrast, IEF data representing average results from isolated retinae (black squares) showed no such decline. The black straight horizontal line drawn at 0.5 is not fitted to the data, but simply indicates that the retinae had been exposed to light that bleached 50% of the rhodopsin. Though this line appears superficially to provide a reasonable fit to the data, we observed that a linear regression of the data (not shown) would indicate a slight trend of dephosphorylation over 220 min. However, this fit not was not significantly different from the horizontal line demonstrating no dephosphorylation ($P = 0.248$).

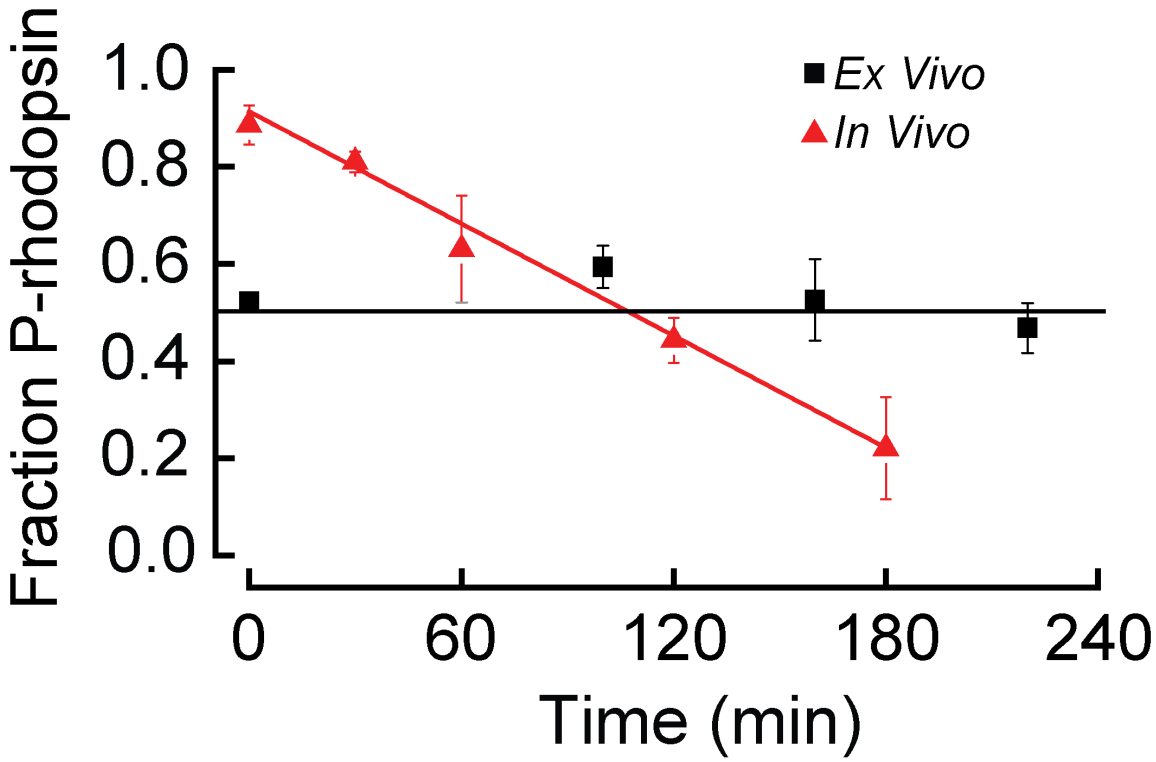

Figure 3.5: Decreased fractional phosphorylation of rhodopsin in dark-adapting retinae. Fractional phosphorylation of opsin plotted *vs* time after bleaching in isolated *ex vivo* retinae (black squares) or in retinae bleached *in vivo* (red triangles). The data points were calculated from Figure 3.4. For each condition, signals from 1P to 6P were summed and divided by signals from all bands (0P to 6P) to obtain the fraction of phosphorylated rhodopsin in that sample. Data reported as Mean ± S.D. Red line was fitted to triangles by method of least squares using the linear function $P_{total} = -0.004t + 0.91$. Black horizontal line is fixed with a slope of 0 and an offset of 0.5.

Measurements of Rhodopsin Phosphorylation under Modified Conditions

The observation that rhodopsin dephosphorylation is severely diminished in isolated retinae is perplexing. Additional experiments were performed to test whether this inhibition of rhodopsin dephosphorylation persists under a wide variety of experimental conditions. The results from these experiments are presented in Figure 3.6. The data in Figure 3.6A shows that incubating 70% bleached isolated retinae with BSA, BSA and 11-*cis* retinal, or at reduced 5.6 pH had no effect on restoring rhodopsin dephosphorylation. Figure 3.6B similarly shows no effect on rhodopsin dephosphorylation when isolated retinae are bleached by 70% using different light intensities. Next, Figure 3.6C shows measurements made from 50% and 70% bleach retinae that where cut into small patches and regenerated with 11-*cis* retinal for 180 minutes. No rhodopsin dephosphorylation was apparent. The inhibition of rhodopsin dephosphorylation was also observed when the RPE was still attached to the retinae, as shown in Figure 3.6D. Measurements were made from 50% bleached isolated retinae in the presences of 11-*cis* retinal and interphotoreceptor retinoid binding protein (IRBP), as shown in Figure 3.6E. Superficially, it would appear that IRBP did promote rhodopsin dephosphorylation. However after the data was quantified, it appeared that IRBP did not have any affect on rhodopsin dephosphorylation. Therefore, it was concluded the bands in Figure 3.6E were faint due to low sample loading. Finally, Figures 3.6F and 3.6G respectively show measurements performed on bleached isolated retinae what were incubated with 0.013 g/L EDTA to lower extracellular calcium, or when 8 mM $CaCl_2$ was added to the superfusate.

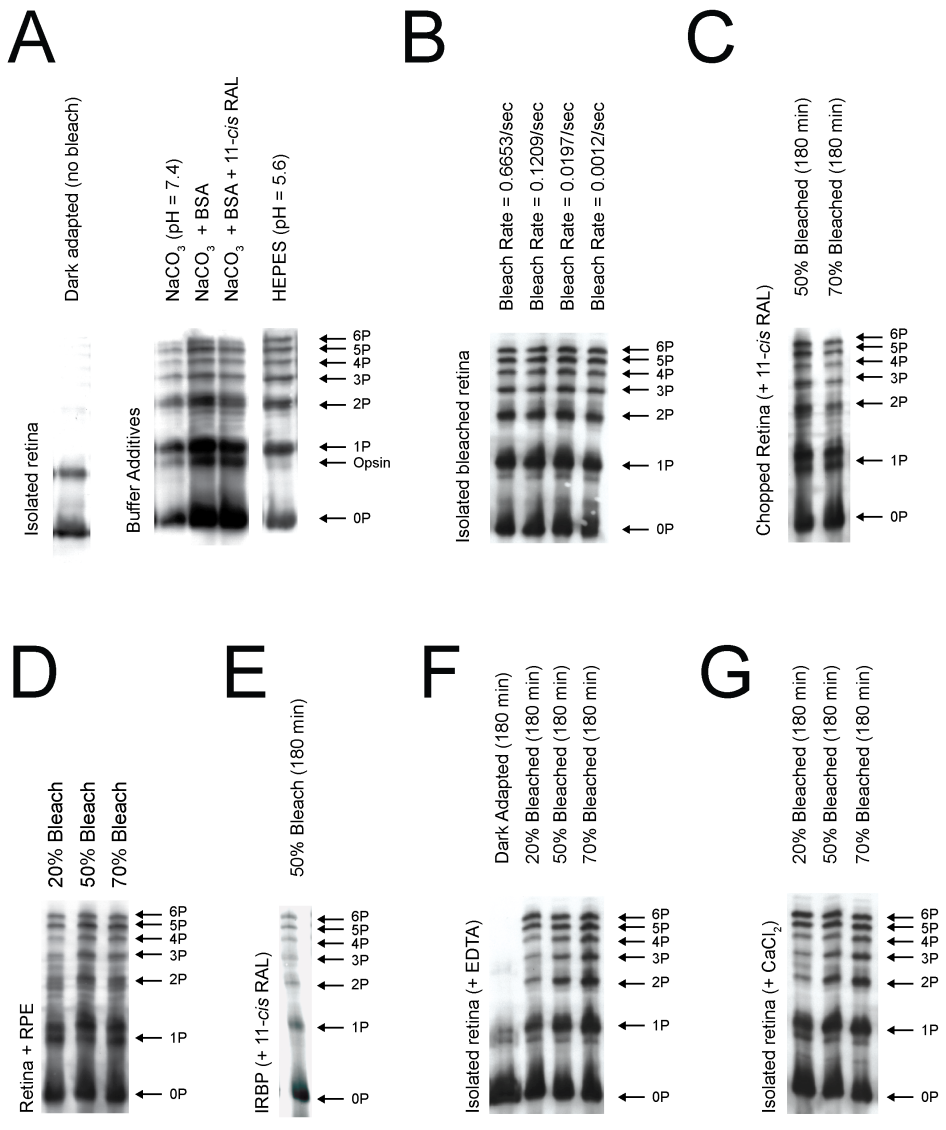
A
Isolated retina
Dark adapted (no bleach)
Buffer Additives
NaCO3 (pH = 7.4)
NaCO3 + BSA
NaCO3 + BSA + 11-cis RAL
HEPES (pH = 5.6)
6P
5P
4P
3P
2P
1P
Opsin
0P
B
Isolated bleached retina
Bleach Rate = 0.6653/sec
Bleach Rate = 0.1209/sec
Bleach Rate = 0.0197/sec
Bleach Rate = 0.0012/sec
C
Chopped Retina (+ 11-cis RAL)
50% Bleached (180 min)
70% Bleached (180 min)
D
Retina + RPE
20% Bleach
50% Bleach
70% Bleach
E
IRBP (+ 11-cis RAL)
50% Bleach (180 min)
F
Isolated retina (+ EDTA)
Dark Adapted (180 min)
20% Bleached (180 min)
50% Bleached (180 min)
70% Bleached (180 min)
G
Isolated retina (+ CaCl2)
20% Bleached (180 min)
50% Bleached (180 min)
70% Bleached (180 min)

Figure 3.6: IEF measurements of rhodopsin phosphorylation from treatment conditions. The gels show rhodopsin segregation based on the total number of attached phosphates as indicated in the right side of each series of gels. For each of the conditions, the tissue was maintained at 35 ± 1 °C. *A:* IEF gels measured after incubation in different conditions as indicated in the panel. The retinae were either dark adapted (left most lane) or bleached 70% and incubated in Ames medium in darkness for 180 min. As indicated, some samples contained BSA, BSA and 11-*cis* retinal, or were buffered with HEPES to lower the pH to 5.6. *B:* IEF measurements from 70% bleached isolated retinae that were bleached at the indicated rates and incubated in darkness for 180 minutes. *C:* IEF gels of retinae that were bleached 50% or 70%, chopped and then incubated in Ames medium containing 11-*cis* retinal in darkness for 180 min. *D:* Eyecups containing both retina and the RPE that were bleached as indicated and incubated in darkness for 180 minutes. *E:* IEF gels of retinae that were bleached 50% and then incubated in Ames medium containing interphotoreceptor retinoid binding protein (IRBP) and 11-*cis* retinal in darkness for 180 min. *F:* IEF gels of retinae that were dark-adapted or bleached as indicated and then incubated in Ames medium containing 0.013 g/L EDTA in darkness for 180 min. *G:* IEF gels of retinae that were bleached as indicated and then incubated in Ames medium containing an extra 8 mM $CaCl_2$ (for a total of 10.3 mM of Ca^{2+}) in darkness for 180 min.

These results are novel and robust. Rhodopsin dephosphorylation is significantly inhibited under conditions that are routinely used in convectional biochemical and electrophysiological conditions. Furthermore, Table 3.1 shows that rhodopsin phosphorylation follows a predictable pattern for each bleaching condition as indicated by the *Trend* column.

# of bound phosphates	20% Bleach	50% Bleach	70% Bleach	Trend (100% Bleach)
6P-Rho	2.7 ± 0.6	5.8 ± 0.7	8.2 ± 1.9	11.6
5P-Rho	2.8 ± 0.3	6.3 ± 0.7	8.7 ± 1.3	12.3
4P-Rho	2.0 ± 0.2	5.6 ± 0.6	8.5 ± 1.8	11.5
3P-Rho	2.1 ± 0.1	6.1 ± 0.7	11.5 ± 1.3	14.5
2P-Rho	3.7 ± 1.2	7.0 ± 0.8	16.9 ± 0.7	20.3
1P-Rho	6.6 ± 0.5	15.7 ± 3.0	20.7 ± 2.8	29.7
0P-Rho	80.1 [%]†	53.1 ± 5.1 [%]	25.2 ± 0.3 [%]	0 [%]

Table 3.1: Rhodopsin phosphorylation in bleached isolated retinae

Retinae were bleached by 20% (n = 4), 50% (n = 6), or 70% (n = 3) and allowed to incubate in Ames medium at 35 ± 1 °C for 3 hours prior to IEF analysis. Each row represents the extent of rhodopsin phosphorylation when isolated retinae were exposed to light in order to bleach 20%, 50%, or 70% of the visual pigment. A scatter plot was constructed for each row (data not shown), where the percentage of P-Rho was plotted against the bleach percentage. Each row of data was fit with a linear function. An extrapolation of these fits uncovered a *trend* that predicts the distribution of rhodopsin phosphorylation when 100% of the visual pigment is bleached. Data reported as Mean ± S.D. † Oversaturated data point, value calculated.

Rhodopsin Dephosphorylation in Physiological Conditions

The isotonic, nutrient rich "physiological" solutions that are typically used for biochemical and electrophysiological experiments do not completely mimic the conditions that are observed in the eyes of living animals. For instance,

electrophysiological experiments are usually performed under conditions of high oxygen tension. Therefore, experiments in this dissertation employed the use of 95% O_2 /5% CO_2 gas mixtures. However, a number of studies have shown that the oxygen tension surrounding the photoreceptors in the retina is substantially lower, ranging between 10-30% (Cringle et al., 2002; Yu and Cringle, 2006; Birol et al., 2007; Lau and Linsenmeier, 2012). In addition, photoreceptor cells of the mammalian retina utilize aerobic glycolysis due to their high metabolic demand (MacGregor et al., 1986; Adler and Southwick, 1992; Hurley et al., 2015). This results in high levels of L-lactate in the interphotoreceptor matrix. This lactate is taken up and used as fuel by Müller cells (Lindsay et al., 2014; Hurley et al., 2015). I wanted to test if adding lactate or if lowering the oxygen tension would affect rhodopsin dephosphorylation in bleached isolated retinae, since these changes would more accurately mimic *in vivo* conditions. Therefore rhodopsin phosphorylation was measured from 70% bleached isolated retinae that were incubated at 35 ± 1 °C with 4.0 mM Na L-lactate and 10 μM 11-*cis* retinal. These results are shown in Figure 3.7A. Likewise, another set of experiments was performed with Ames medium (that did not contain lactate) under conditions of lower oxygen tension. Lower oxygen tension was achieved by saturating the solution with a 20% O_2 / 75% N_2 / 5% CO_2 gas mixture, which did not change the pH (data not shown). The results from these lower oxygen tension experiments are presented in Figure 3.7B. The data shows that L-Lactate promoted rhodopsin dephosphorylation in isolated retinae. Likewise, a modest and statistically significant effect on rhodopsin dephosphorylation was observed when the

oxygen tension was lowered. These results suggest that metabolic processes are critical in promoting rhodopsin dephosphorylation.

The molecular mechanisms that regulate rhodopsin dephosphorylation remain to be discovered. Further studies will need to be conducted to determine why rhodopsin dephosphorylation is blunted in isolated retinae when the oxygen tension is high, and why rhodopsin dephosphorylation is partially restored when the oxygen tension is lowered or when L-lactate is provide in the superfusate. However, in order to test my hypothesis, which states that dephosphorylation of regenerated rhodopsin is required for the recovery of sensitivity during dark adaptation, I exploited my finding that incubating isolated retinae in solutions with high oxygen tension hindered rhodopsin dephosphorylation.

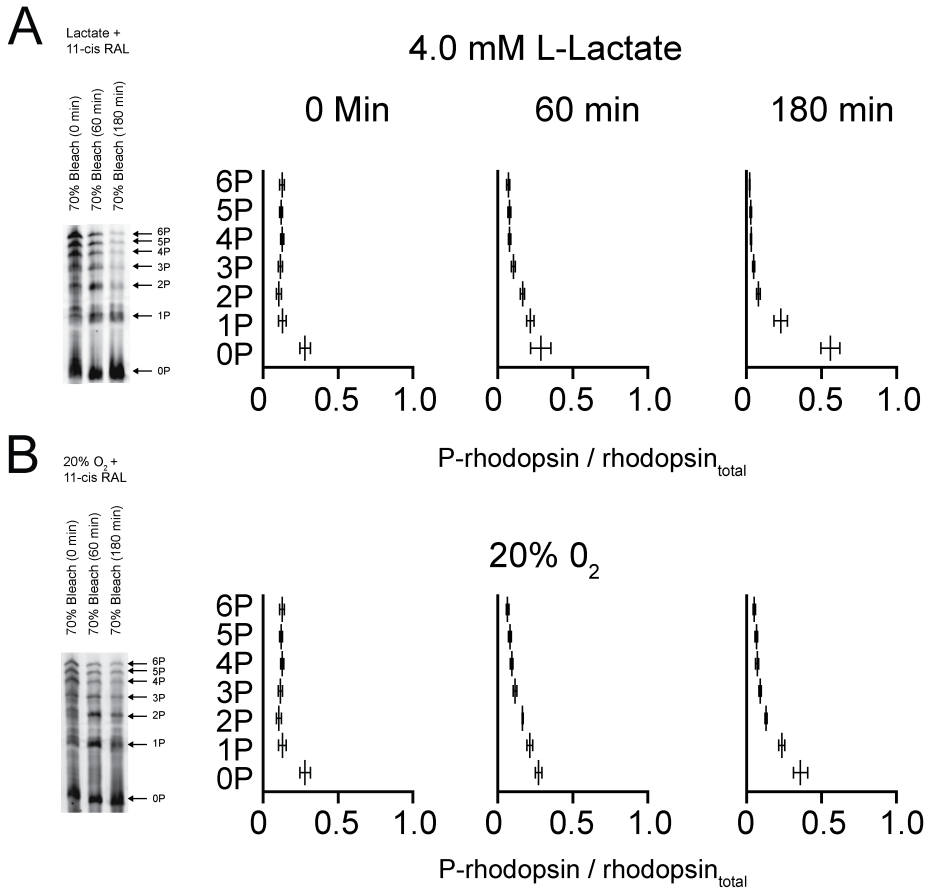

Figure 3.7: IEF measurements of rhodopsin phosphorylation from isolated retinae that were incubated with L-Lactate or 20% oxygen tension. *A:* Retinae were incubated in Ames medium containing 4 mM Na L-lactate, 70% bleached over the course of 160 seconds and immediately frozen (0 min) or frozen after incubated in darkness with 10 μM 11-*cis* retinal for 60 or 180 min. For each lane, signals from 1P to 6P were summed and divided by signals from all bands (0 to 6P) to obtain the fraction of phosphorylated rhodopsin in that sample. The phosphorylated rhodopsin fraction measured at 0 min was 0.72 ± 0.04 (N = 8), corresponding well to the estimated 70% bleach, and 0.71 ± 0.07 (60 min, N = 4) and 0.44 ± 0.06 (180 min, N = 4). These values were subjected to one-way ANOVA. The p-value for one-way ANOVA was $1.7x10^{-6}$, and the p-value for Tukey HSD was $p < 0.002$ for both 180 min vs. 0 min and 180 min vs. 60 min. *B:* Retinae were incubated with Ames medium (without added lactate) under 20% O_2/5% CO_2/75% N_2 and then bleached and incubated in darkness as described in A. The total fraction of phosphorylated rhodopsin was 0.72 ± 0.04 (0 min, N = 8), and 0.73 ± 0.02 (N = 4) for 60 min, and 0.64 ± 0.05 (N = 4) for 180 min. The one-way ANOVA showed a p-value of 0.0049. This was followed by Tukey HSD test, which showed a significant difference between 180 min vs. 0 min and 180 min vs. 60 min ($p < 0.01$ for both comparisons).

Microspectrophotometry

It would be a benefit to the reader to recapitulate the results that have been presented up until now. The data have demonstrated that exposing isolated retina to light results in the phosphorylation of the rhodopsin. Rhodopsin in these isolated retinae does not dephosphorylate (unless given L-lactate or unless the oxygen tension us reduced). In Figure 3.3, I have suggested, without proof, that the visual pigment was regenerated by incubating the bleached retinae with 11-*cis* retinal. The results to follow were designed to determine whether phosphorylation of opsin impacts pigment regeneration. I performed microspectrophotometric (MSP) recordings of the visual pigment on patches of rods from isolated retinae using the same conditions that were used for IEF experiments. The experiments involved measuring the absorbance from bleached isolate retinae. In the first set of experiments, presented in Figure 3.8, I bleached the retinae on the MSP sample stage. Afterwards these retinae were given 60 minutes for the metarhodopsin photoproducts to decay (data not shown). At this point, 10μM 11-*cis* retinal was added to the recording chamber. Figure 3.8A shows absorbance spectra from a representative retina when dark-adapted (black), 50% bleached (red), and regenerated with 11-cis retinal (blue). This data shows that dephosphorylation of opsin was not required for the regeneration of the visual pigment. Furthermore, it demonstrates that all of the visual pigment is regenerated when bleached isolated retinae are incubated on-stage with 11-*cis* retinal.

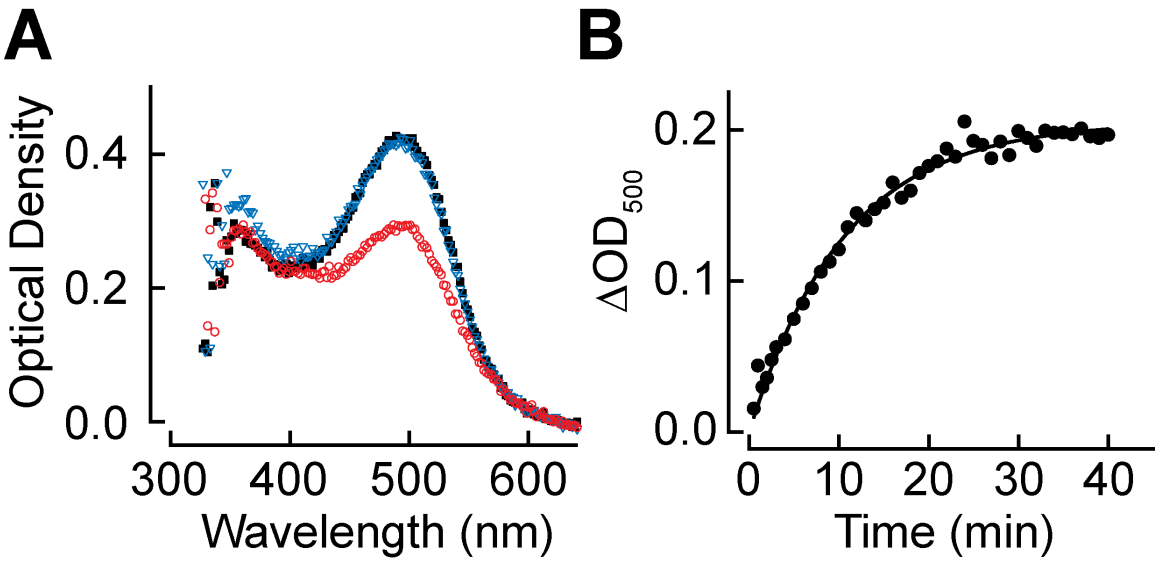

Figure 3.8: MSP measurements of visual pigment regeneration from phosphorylated opsin. *A:* MSP absorbance was measured from dark-adapted isolated retinae (black), following a 50% bleach (red), and after 40 minutes of incubation with 10 μM 11-*cis* retinal. *B:* A representative recording of the visual pigment regeneration process as a function of time spent incubating with 11-*cis* retinal. In these recordings, pigment regeneration was monitored by recording the increase in optical density (OD) at 500 nm. The data was fit using a single saturating exponential function with a time constant of 9.1 ± 0.5 min (Mean ± S.E.; n=5). Dark adapted MSP spectra were recorded at 35 ± 1 °C. Following light exposure (that bleached the visual pigment) the retinae were maintained at this temperature for 60 minutes and the spectra at the end of this time period was recorded. Afterwards, the perfusion system was disengaged, and the retinae were allowed to cool down to room temperature (25 ± 1 °C) for 10 minutes. Once at room temperature 11-*cis* retinal was injected into the recording chamber. After 40 minutes of incubation, the perfusion system was restarted. The superfusate washed the retinae (to remove excess retinoid) and heated the tissue back to 35 ± 1 °C, were the final spectra were recorded.

Next, I needed to perform a set of experiments to confirm that my off-stage incubation system facilitates the regeneration of the visual pigment in bleached isolated retinae. From this experiment I performed measurements on two different groups: one set of measurements on 50% bleached retinae that were incubated in darkness for 180 minutes, and another set of 50% bleached retinae that were incubated with 10 μM 11-*cis* retinal in darkness for 180 minutes. These results are presented in Figure 3.9 A and B,

respectively. Plotted in Figure 3.9A are absorption spectra taken from a cluster of rod outer segments located along the cut edge of a piece of isolated retina which had been 50% bleached and then incubated in darkness for 3 hours in the incubation chamber. Afterwards the retinae were transferred to the MSP stage. Spectrum 1 (blue) is the absorbance spectrum recorded from a 50% bleached retinae. Next, I regenerated the visual pigment by superfusing the retinae with 10μM 11-*cis* retinal on the sample stage. After 40 minutes of incubation the regenerated visual spectrum was recorded (spectrum 2, black). Next, I bleached >99% of visual pigment, and subsequently recorded the spectrum (spectrum 3, pink). As expected, the peak absorbance of spectrum 1 corresponds to a 50% bleach (see Methods and Figure 2.2). Spectrum 3 is likewise consistent with having bleached >99% of rhodopsin at the end of the experiment. The observation that spectrum 2 has approximately twice the optical density (OD) of spectrum 1 confirms that the visual pigment was completely regenerated. This claim is also supported by the data presented in Figure 3.8. This data is proof that opsin dephosphorylation is not needed in order to regenerate the visual pigment. However, one question still remained. Does adding 11-*cis* retinal to the incubation system used for IEF experiments promote pigment regeneration in bleached isolated retinae? Spectrum 4 illustrated in Figure 3.9B was measured 3 hours after an isolated retina had been bleached and incubated with 11-*cis* retinal. The peak absorbance of this spectrum is similar to measurements made from dark adapted retinae. This would suggest that all of the visual pigment had been regenerated. To confirm this, these retinae were incubated again with 11-*cis* retinal that was added to the superfusate. Spectrum 5 (black) shows no additional

increase in absorbance, and thus confirms that the visual pigment can be regenerated in the incubation system. The total amount of rhodopsin in this sample was evaluated by bleaching >99% of the visual pigment, as shown in spectrum 6 (pink). Figures 3.8 and 3.9 also confirm that phosphorylated opsin can be regenerated with 11-*cis* retinal. This observation is consistent with a recent report utilizing carp photoreceptors (Yamaoka et al., 2015). It is noteworthy that the spectrum of phosphorylated rhodopsin is very similar to that of native rhodopsin. This is indicated by comparisons of the MSP traces in Figures 3.9A and 3.9B, with the cyan solid curve calculated for an ideal solution of rhodopsin (Govardovskii et al., 2000).

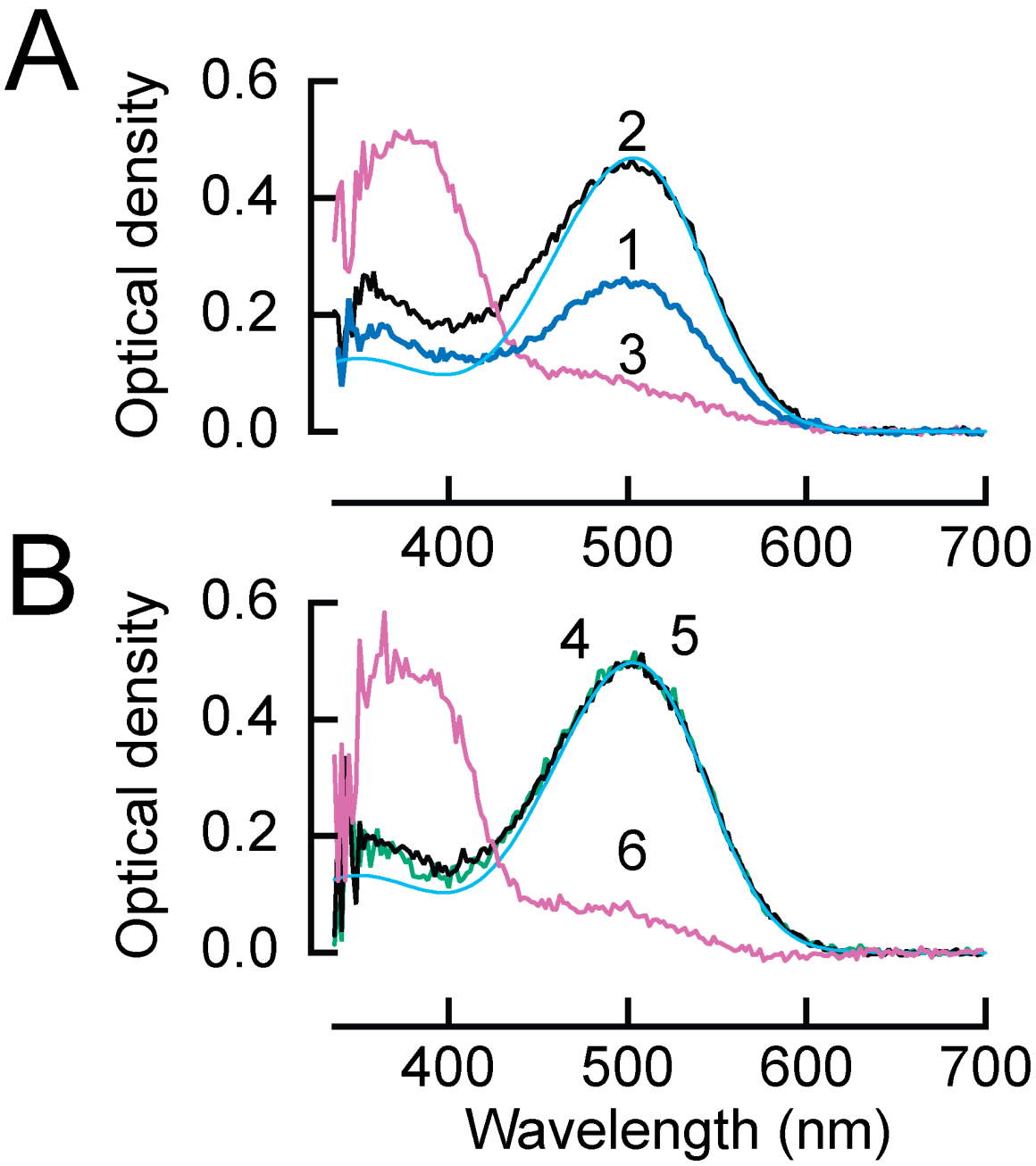
A
B
Optical density
0.6
0.4
0.2
0.0
1
2
3
4
5
6
400
500
600
700
Wavelength (nm)

Figure 3.9: Microspectrophotometric (MSP) absorbance spectra of bleached and regenerated WT (C57BL/6) retinae. *A:* Absorbance spectra of a retina that had been bleached 50% (spectrum 1, blue), then treated with 11-*cis* retinal on the stage of the MSP for 40 min (spectrum 2, black), and finally after exhaustive bleach (spectrum 3, pink). The cyan trace is a normalized rhodopsin spectrum (Govardovskii et al., 2000) calculated at λ_{max} = 503 nm, OD_{α} = 0.47. *B:* Trace 4 (green) shows an absorbance spectrum of a retina that had been bleached 50% and incubated for 3 hours with 10 μM 11-*cis* retinal in darkness in a light-tight incubation container. Spectrum 5 (black) shows the absorbance from the same preparation following 40 min additional exposure to solution containing 10 μM 11-*cis* retinal on the stage of the MSP. Spectrum 6 (pink) shows absorbance following an exhaustive bleach (>99%). The cyan trace is a fitted rhodopsin template (λ_{max} = 503 nm, OD_{α} = 0.50). The optical density at 380 nm can be larger than the template due to lipid bound excess 11-cis retinal in the rod outer segments. In solution (or when bound to lipids) 11-*cis* retinal has an absorbance peak at 380 nm. All experiments were repeat with an $N \geq 3$.

Photosensitivity of Phospho-Rhodopsin

In addition to making spectral measurements of phosphorylated rhodopsin, I also compared the molecular photosensitivity of cells containing 100% rhodopsin and 90% P-rhodopsin with MSP. The purpose of these experiments was to determine if phosphorylation of opsin altered the spectral properties of regenerated rhodopsin. I performed MSP recordings from cells that contained either 100% rhodopsin or 90% P-rhodopsin. Here, the method was to observe the fractional change in the optical density that occurred after light exposures to the calibrated bleaching light. From these data, the fraction of the bleached rhodopsin, *F,* was determined and the photosensitivity *p* was calculated from equation (2.1). The measured photosensitivities for 100% rhodopsin and 90% P-rhodopsin were $(6.0 \pm 1.3) \times 10^{-9}\ \mu m^2\ photon^{-1}$ and $(6.7 \pm 1.2) \times 10^{-9}\ \mu m^2\ photon^{-1}$, respectively. The two measured photosensitivities are statistically indistinguishable from each other (t-test: $t = 0.73$, $p = 0.49$) and are very similar the previously determined photosensitivity for mouse rhodopsin of $5.7 \times 10^{-9}\ \mu m^2$ (Woodruff et al., 2004).

ERG Recordings from Dark Adapting Isolated Retinae

IEF measurements demonstrated that bleached rhodopsin in isolated retinae can remain persistently phosphorylated even when incubated in darkness with 11-*cis* retinal for extended periods. In addition, MSP experiments indicated that rhodopsin was completely regenerated when combined with exogenous exposure to 11-*cis* retinal. I now sought to determine how persistent rhodopsin phosphorylation affected dark adaptation and the recovery of flash sensitivity. The approach involved tracking the recovery of flash sensitivity using whole retina ERG recordings from *Gnat2*$^{-/-}$ mice. ERG recordings

were directly correlated with IEF results (presented earlier in Figures 3.3 and 3.4) by measuring the flash responses and then subsequently freezing the retinae for IEF analysis to determine the extent of rhodopsin phosphorylation. Figure 3.10 shows representative ERG response families measured under several different conditions. The upper-left panel of Figure 3.10 shows a response family from a dark-adapted retina. This can be compared to the panel to the right that shows a similar set of measurements made from a retina that was 50% bleached, and incubated in darkness for 60 minutes. Three differences existed between the dark-adapted and bleached response families. First, the maximum response amplitude is significantly diminished in the bleached retinae. Second, when comparing responses that have similar normalized amplitudes, the waveforms rise and fall at an accelerated rate in the bleached retinae. Finally, the bleached retina is less sensitive to dim flashes (red traces). The families shown at lower left and lower right illustrate the changes in rod sensitivity, which occur when bleached rhodopsin is regenerated. These families were measured 120 and 180 minutes into dark-adaptation, respectively.

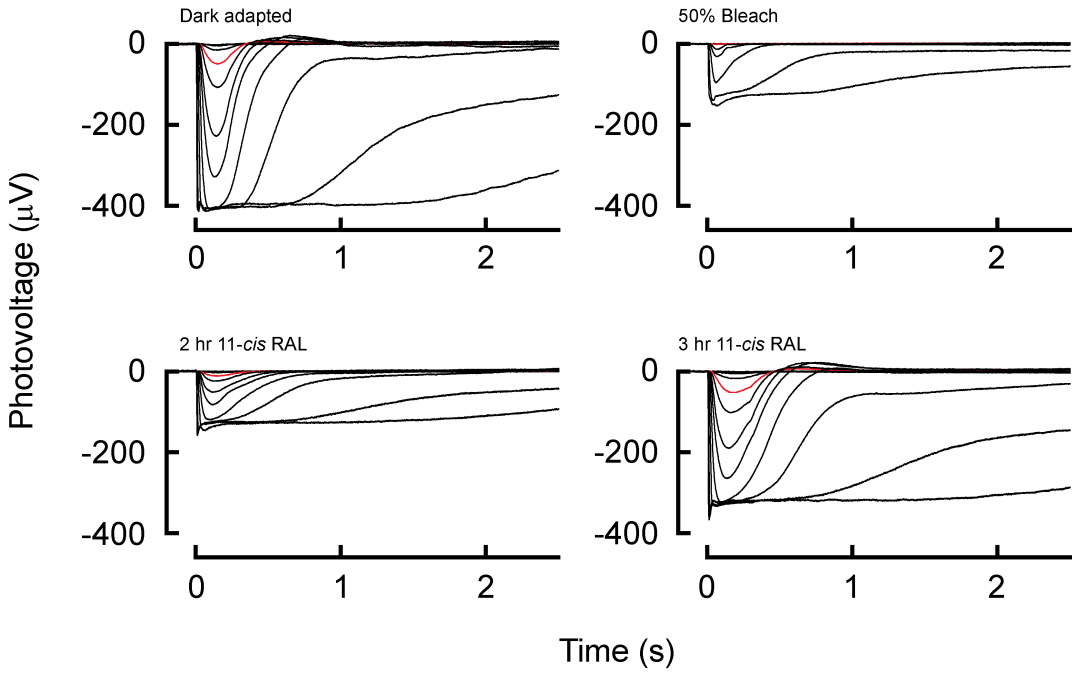

Figure 3.10: Transretinal electroretinograms (ERGs) demonstrating the recovery of flash sensitivity in *Gnat2*$^{-/-}$ mouse rods having persistent rhodopsin phosphorylation. Response families of isolated a-waves from a dark adapted retina (upper-left); from a retina that was bleached 50% and incubated in darkness for 60 min (upper-right); and from a retina that was bleached (50%) and incubated in darkness for 120 min (lower-left) or 180 min (lower-right) in 10 μM 11-*cis* retinal. Red traces in each response family were measured at the same flash intensity. DL-AP4 and Ba^{2+} were added to the superfusate in order to isolate rod photoreceptor (a-wave) responses (see Methods). Flash stimuli was presented at zero seconds, and the retinae were incubated and recorded at 35 ± 1 °C.

Response amplitudes measured after 120 minutes of exposure to 11-*cis* retinal were significantly reduced when compared against the dark-adapted family. Next, I examined the response families after 180 minutes of incubation, in which the bleached retina started to appear as if they were never exposed to light. Under these conditions the response amplitudes on average do not differ from those observed under dark-adapted conditions, and the activation and deactivation of the photoresponses also appears to have been slowed and are similar to those observed in dark-adapted retinae. It is important to emphasize that these rods contain half of their visual pigment in the non-phosphorylated ground state, and the other half of the visual pigment is phosphorylated.

Dark adapted rod photoreceptors are physiologically responsive to very low light intensities. If these bleached isolated retinae have properly dark adapted, then these rods should also be responsive to low light intensities. In order to evaluate the response families further, I examined the ERG response kinetics when stimulated with flashes of very dim light. At these very low light intensities, rod response amplitudes scale linearly with the number of detected photons. Presented in Figure 3.11 are the averaged dim flash responses from each experimental condition. In Figure 3.11A, the average traces from multiple retinae (under identical conditions) where combined into a single trace each. All of these responses where picked from the linear response range. Dim flash responses were measured for dark adapted retinae (black), 50% bleached (pink), and (50%) bleached and incubated with 11-*cis* retinal for 60 (orange), 120 (green), or 180 minutes (blue). The black, green, and blue traces were all measured using the same light intensity, whereas more light was needed to invoke the pink and orange responses. What this data

shows is that the photovoltage is nearly identical between the dark-adapted and the bleached retinae that were incubated for 180 minutes in 11-*cis* retinal; a condition in which 50% of rhodopsin is phosphorylated. In addition, the data shows that there is a substantial increase in the photovoltage between 120 and 180 minutes of incubation. In order to facilitate a direct comparison between all conditions, the traces were normalized by dividing by the absolute value of their peak photovoltage (and smoothed to remove 20Hz acquisition noise) as shown in Figure 3.11B. These normalized traces show that bleaching the retina results in the acceleration of the photoresponses. Furthermore, the data indicates that over the course of 180 minutes, the dim flash response kinetics progressively slow and begin to look more dark-adapted. These traces were further analyzed to determine the response time–to-peaks, and the recovery time constants was fit to the falling phase, which are both presented in Table 3.2. The time-to-peak results suggest that the bleached retinae have dark adapted after 180 minutes of incubation. Collectively, Figure 3.10 and Table 3.2 show that dark adaptation occurs in the rods of bleached isolated retinae, despite the fact that half of rhodopsin is pre-phosprylated prior to photoactivation.

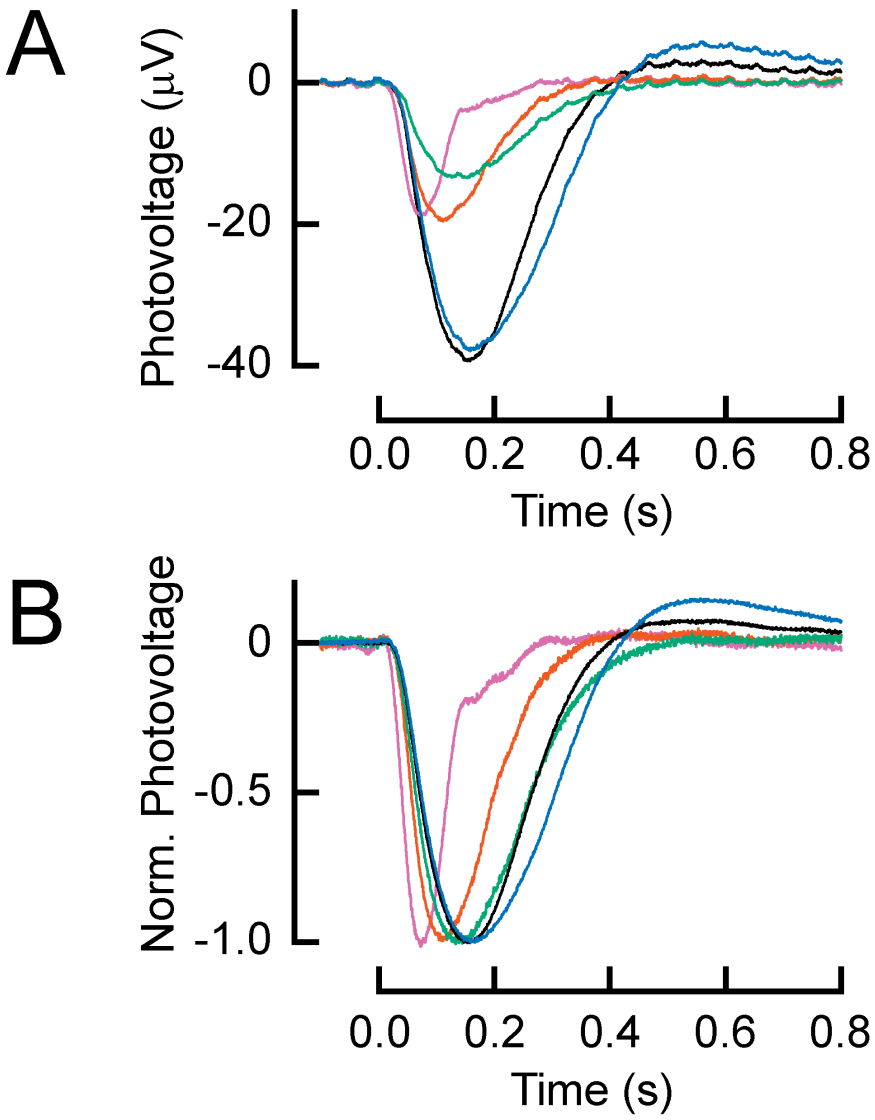

Figure 3.11: Dim flash responses recorded during ERG experiments. *A:* ERG dim flash responses from a dark-adapted retinae (black trace, N = 6, 42 responses), 50% bleached retinae (pink trace, N = 6, 42 responses), and retinae that had been bleached 50% and incubated with 10 μM 11-*cis* retinal in darkness for 1 (orange trace, N = 6, 42 responses) 2 (green trace, N = 8, 56 responses), or 3 hours (blue trace, N = 7, 49 responses). The pink, and orange traces were measured with a flash intensity that was 3.16 fold higher than the light intensity used to elicit the responses in the black, blue and green traces. *B:* Normalized filtered dim flash responses from A.

Preparation	Time to Peak	Recovery Constant (τ_{rec})
Dark adapted	158 ms	0.11 s^{-1}
50% Bleached		
Bleach adapted	72 ms	0.04 s^{-1}
60 min of dark adaptation	111 ms	0.09 s^{-1}
120 min of dark adaptation	133 ms	0.10 s^{-1}
180 min of dark adaptation	166 ms	0.14 s^{-1}

Table 3.2: Dim flash ERG response kinetics

Dim flash response properties from whole retina ERG mouse rods. ERGs were recorded in dark-adapted retinae (N = 6, 42 responses), 50% bleached retinae (N = 6, 42 responses), and retinae that had been bleached 50% and incubated with 10 μM 11-*cis* retinal in darkness for 1 (N = 6, 42 responses) 2 (N = 8, 56 responses), or 3 hours (N = 7, 49 responses). The recovery time constant was fit to the recovery phase of the waveform, and characterizes this phase after the responses recover 20% from maximum. This data should be taken with a bit of caution. There are potential sources of data artifacts that affect the reliability of ERG data. A detailed account of the artifacts is given in the text (in section *Singe Cell Measurements of Sensitivity and Flash Response Kinetics* below).

Further analysis of the data was possible by constructing intensity-response families (IRF) for each dataset. Presented in Figure 3.12 are mean response families from these experiments. Here, the averaged dark-adapted IRF (black squares) is plotted together with the average IRFs for 50% bleached retinae (pink circles), and 50% bleach retinae that were regenerated (with 11-*cis* retinal) for 60 min (orange triangles), 120 min (green diamonds), and 180 min (blue squares). Figure 3.12 demonstrates how bleaching the visual pigment in the retinae reduces the rods sensitivity to light. When bleached retinae are incubated for 1-2 hours, we see a marginal increase in the visual threshold for detection. However, there is an insignificant increase the saturating photovoltage ($p = 0.98$). However, after a 3 hour incubation there is an increase in the response amplitude and the recorded sensitivity appears to be strikingly similar to dark-adapted retinae.

Furthermore, the IRFs from the dark-adapted retinae and the bleached retinae treated for 180 minutes are statistically indistinguishable from each other ($p = 0.93$).

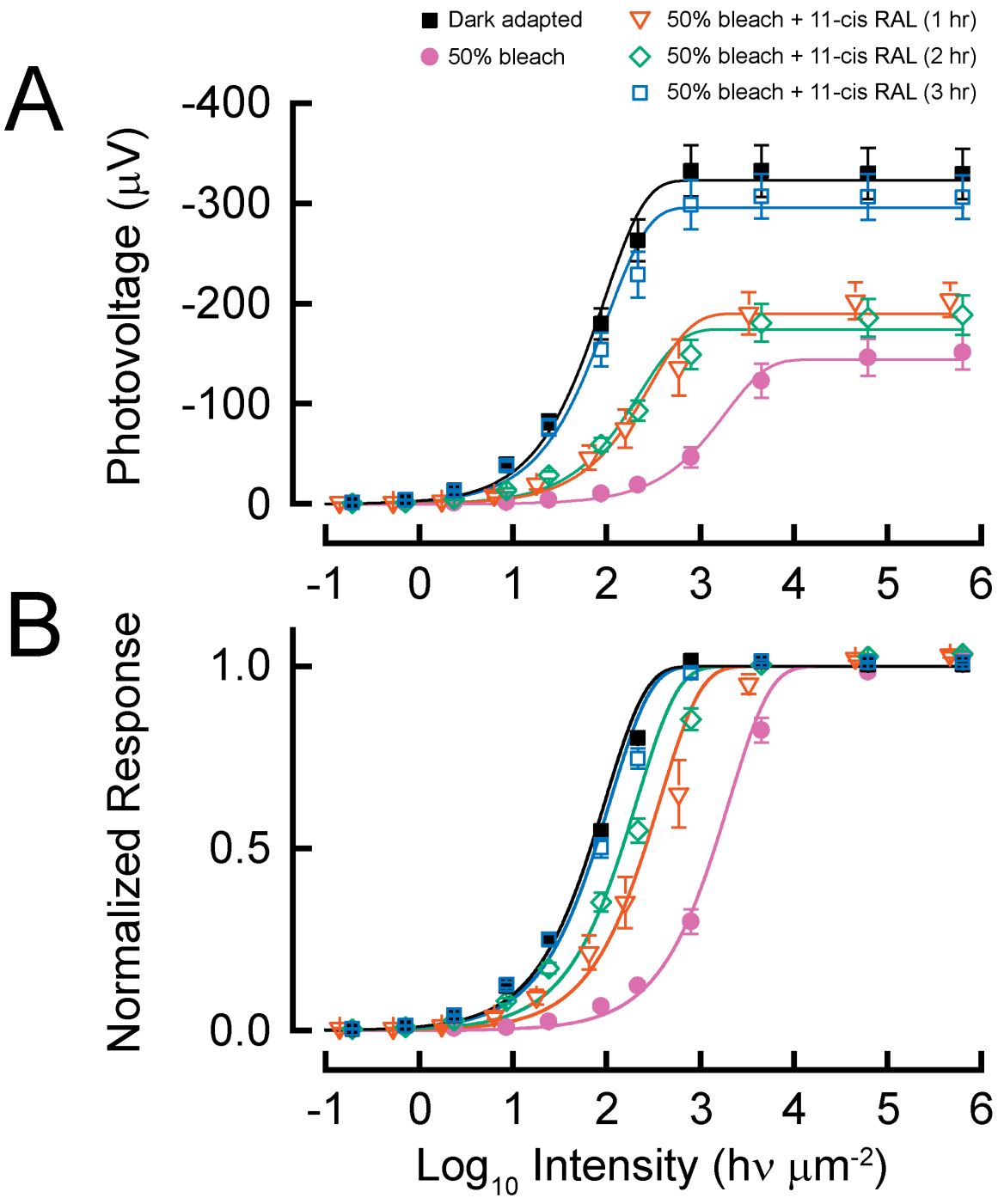
A
B
Dark adapted
50% bleach
50% bleach + 11-cis RAL (1 hr)
50% bleach + 11-cis RAL (2 hr)
50% bleach + 11-cis RAL (3 hr)
Photovoltage (μV)
-400
-300
-200
-100
0
Normalized Response
1.0
0.5
0.0
-1
0
1
2
3
4
5
6
Log10 Intensity (hν μm-2)

Figure 3.12: Transretinal electroretinograms demonstrating the recovery of flash sensitivity in *Gnat2*$^{-/-}$ mouse rods having persistent rhodopsin phosphorylation. *A:* Intensity response relations show the peak a-wave amplitude as a function of the flash light intensity. Each relation is fitted with a exponential saturation function: $V = V_{max}(1\text{-}e^{-I/\tau})$ where V is the voltage amplitude, V_{max} is the voltage amplitude of the saturated response, I is light intensity and τ is a sensitivity fitting parameter. Data were recorded from dark-adapted retinae (black circles, N = 8, *fit:* $V_{max} = 324\ \mu V$, $\tau = 94$ hν μm^{-2}), 50% bleached retinas (pink triangles , N = 6, $V_{max} = 144\ \mu V$, $\tau = 1860$ hν μm^{-2}), and retinae that had been bleached 50% and incubated for 1 hour (N = 6, $V_{max} = 190\ \mu V$, $\tau = 297$ hν μm^{-2}), 2 hours (N = 8, $V_{max} = 174\ \mu V$, $\tau = 223$ hν μm^{-2}), or 3 hours (blue squares, N = 7, $V_{max} = 297\ \mu V$, $\tau = 102$ hν μm^{-2}). An One Way ANOVA was preformed on these data with a $P = 2.02 \times 10^{-6}$. Additionally, a Tukey test was performed and the significance threshold set to $p \leq 0.05$. This analysis indicated that there was no significant difference in response amplitudes when 50% bleached retinae were compared against 50% bleached retinae that were incubated for either 60 or 120 minutes with 11-*cis* retinal. There was a significant difference in response amplitudes when comparing 120 and 180 minutes of dark adaptation. Finally, there was no statistically significant difference between dark adapted retinae and bleached retinae that were incubated with 11-*cis* retinal for 180 minutes. *B:* Normalized IRF of the same data presented in panel A. The recordings were made at 35 ± 1 °C. Error bars are ± S.E.M.

Singe Cell Measurements of Sensitivity and Flash Response Kinetics

ERG data indicates that light exposed rods will dark-adapt over the course of 3 hours when incubated in the presence of 11-*cis* retinal. These observations occurred in spite of the fact that 50% of the visual pigment was phosphorylated. Some caution should be used when interpreting these results. There are some potential sources of artifacts that could be present in the data. For instance, the recorded photovoltages are very sensitive to the positioning of the measurement electrodes. These electrodes must be precisely positioned prior to each experiment. Additionally, it is not outside the realm of possibility that DL-AP4 or $BaCl_2$ could affect the recorded electrophysiology. Finally, if a very small percentage of the rods died during the 180 minutes of incubation, that would result in reduced photovoltages. Therefore, in order to know more about the state of sensitivity and response kinetics under conditions of persistent rhodopsin phosphorylation, I conducted single cell suction electrode experiments under the same conditions used in IEF measurements of rhodopsin phosphorylation. These experiments have several advantages. For example, I can visually identify rods in wild-type retina, and the recordings can be performed in the absences of DL-AP4 or $BaCl_2$. Finally, it is easy identify (and then discard) unhealthy cells since these undesirable cells are unresponsive to light. Figure 3.13A shows response families from such current recordings of rod flash responses in different cells under four different conditions. Response families were measured from dark-adapted single cells, cells that had been exposed to light that bleached ~50% of their rhodopsin, and from cells that contained 50% or 90% phospho-rhodopsin (P-rhodopsin) after regeneration for 180 minutes with 11-*cis* retinal. Multiple

cells were measured in each condition. The data show that when compared against dark-adapted cells (Figure 5.6, left), cells bleached by 50% and incubated in solution for 90 min without 11-*cis* retinal (Figure 3.13A, middle left) have smaller response amplitudes and faster time courses for activation and deactivation. Such responses are characteristic of bleached rods in which the pigment has not been regenerated (Cornwall et al., 1990; Matthews et al., 1990; Jones et al., 1993; Cornwall and Fain, 1994; Nymark et al., 2012). Rods containing 50% P-rhodopsin show response families that are very similar to those observed under dark-adapted conditions, including normal response amplitudes and normal activation and deactivation rates. Furthermore, these incubated retinae do not exhibit any obvious light or opsin adaptation. These data can be compared to cells that were bleached by 90% and incubated with 11-*cis* retinal for 180 minutes. Despite having 90% of the visual pigment in a phosphorylated state, these rod response families are generally similar to those from dark adapted rods. This includes the waveform kinetics and the maximum response amplitude.

Average intensity response relations for each of these adaptation conditions were superimposed and are presented in Figure 3.13B. The response-intensity relationships from a dark-adapted response family and that for a cell 50% bleached and regenerated are again statistically indistinguishable from each other, confirming the observations from ERG experiments. However, the response intensity relation for cells that contained 90% P-rhodopsin was slightly less sensitive as indicated by the fit. In this case, the data illustrates that these photoreceptors are ~2-fold desensitized when compared to dark-

adapted photoreceptors. Responses otherwise display no significant difference from those observed from dark adapted rods. Thus, cells containing a substantial amount of phosphorylated rhodopsin do not display the same effects that occur during opsin adaptation.

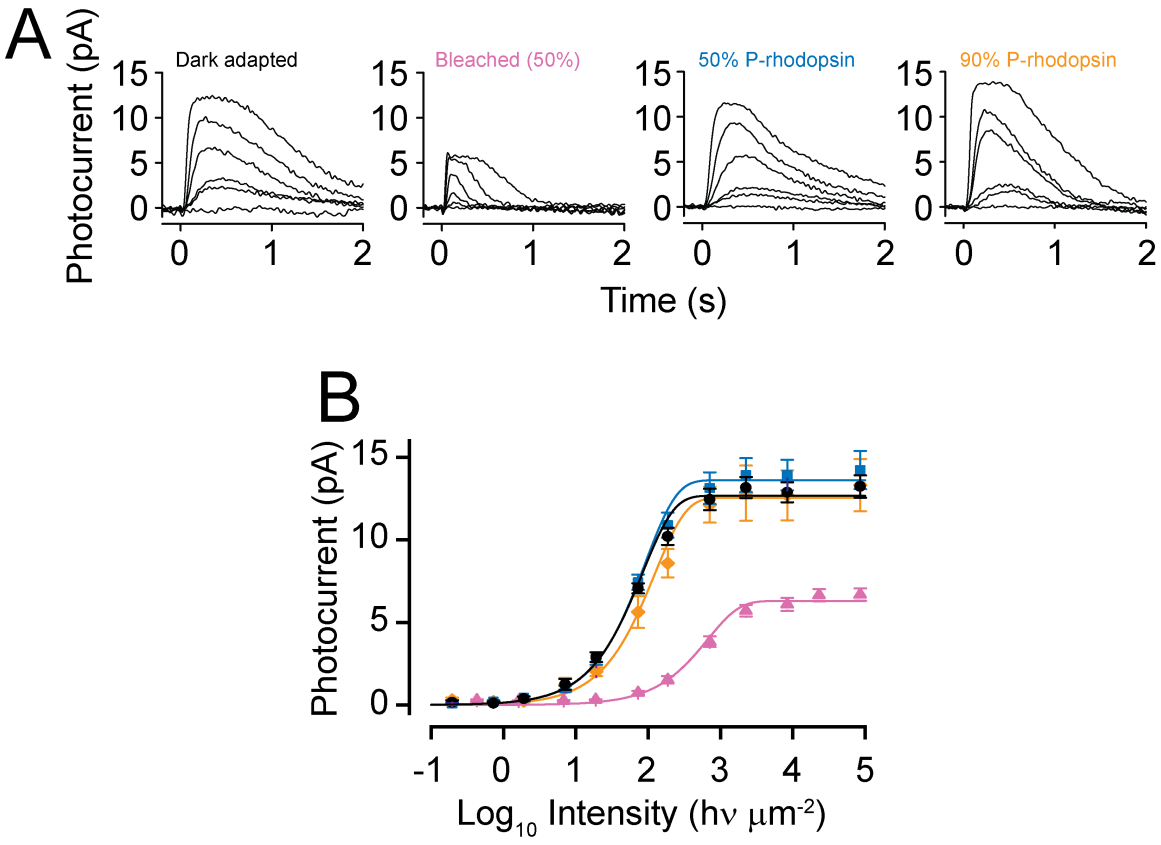

Figure 3.13: Suction electrode recordings demonstrating the flash sensitivity recovery in bleached mouse rods that have regenerated phosphorylated rhodopsin. A: Representative response families from a dark adapted rod (left), from a 50% bleached rod that was incubated in darkness for 90 min (center left), from a rod that was bleached 50% and incubated with 10 μM 11-*cis* retinal in darkness for 3 hours (center right), and from a rod that was bleached 90% and incubated with 10 μM 11-*cis* retinal in darkness for 3 hours (right). *B:* Average response-intensity relations recorded from dark-adapted rods (black circles, N = 8), rods that had been bleached 50% and incubated in darkness for 90 min (pink triangles, N = 4), rods that had been bleached 50% and incubated with 10 μM 11-*cis* retinal in darkness for 3 hours (50% P-rhodopsin, blue squares, N = 10), and rods that had been bleached 90% and incubated with 10 μM 11-*cis* retinal in darkness for 3 hours (90% P-rhodopsin, orange circles, N = 10). Exponential saturation functions: $i = i_{max}(1\text{-}e^{-I/\tau})$ have been fitted to the data, where i is the peak photocurrent, i_{max} is the peak photocurrent of a saturating flash response, I is intensity and τ is a sensitivity fitting parameter. Dark-adapted, black line, i_{max} = 12.9 ± 0.7 pA, τ = 73.8 ± 12.6 hν μm^{-2}; 50% P-rhodopsin, blue line, i_{max} = 13.8 ± 0.7 pA, τ = 81.5 ± 13.1 hν μm^{-2}; 90% P-rhodopsin, orange line, i_{max} = 12.8 ± 0.8 pA, τ = 111.0 ± 22.7 hν μm^{-2}. The recordings were made at 35 - 37 °C. Error bars are S.E.M.

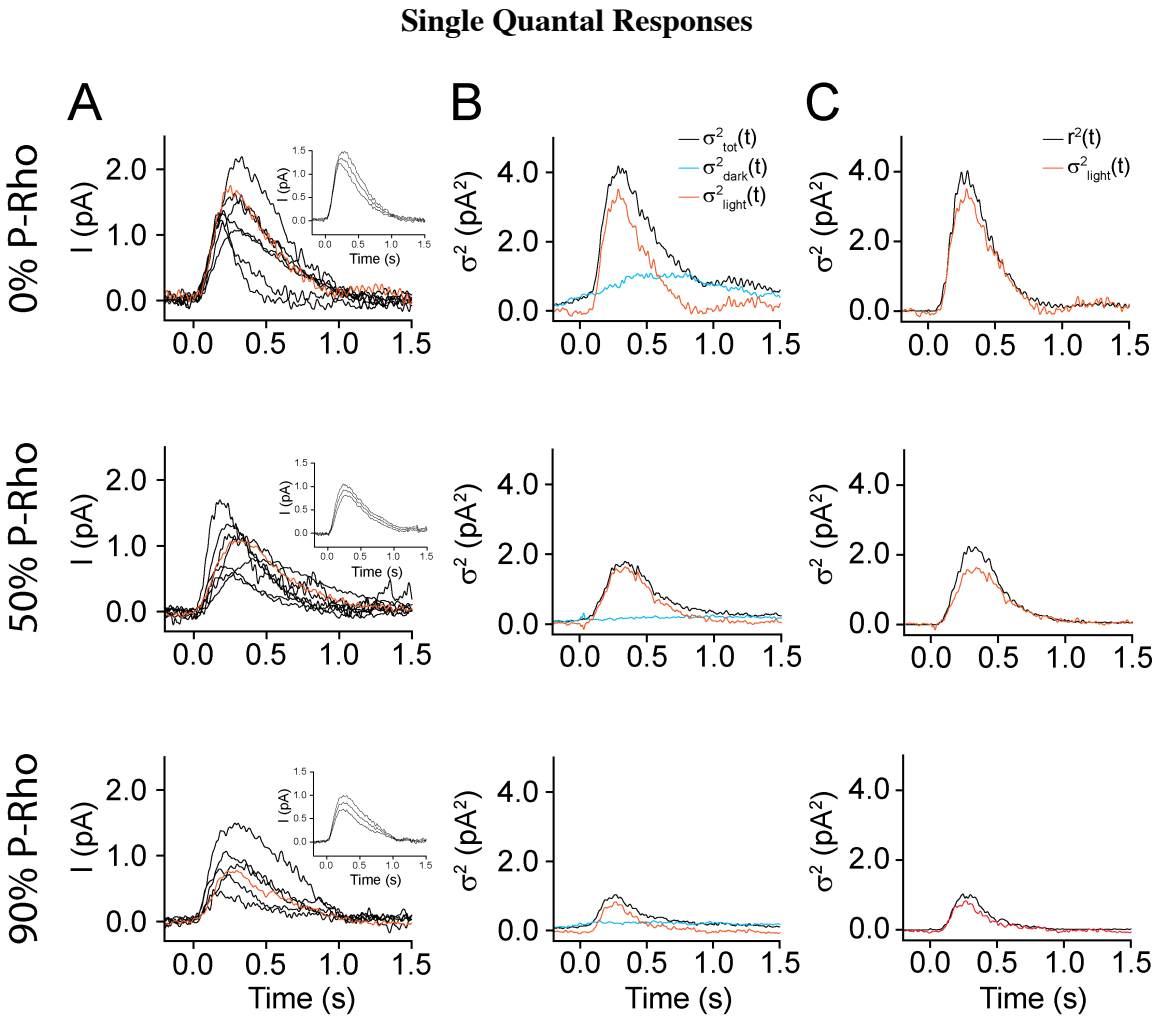

Figure 3.14: Single quantum responses (SQR) recorded from WT rods containing rhodopsin and phosphorylated rhodopsin. *A:* SQRs from rods containing rhodopsin (top), 50% phosphorylated rhodopsin (middle), and 90% phosphorylated rhodopsin (bottom). The red traces show representative SQRs that were analyzed in panels B and C and are shown in Figure 3.15. *Insets:* Mean waveform of all SQRs presented in each panel ± SEM. *B:* Total variance (black), dark variance (blue) and light induced variance (red) from a rod containing rhodopsin (top), 50% phosphorylated rhodopsin (middle), and 90% phosphorylated rhodopsin (bottom). *C:* Comparison of light induced variance (red) and mean square response (black) from a rod containing rhodopsin (top), 50% phosphorylated rhodopsin (middle), and 90% phosphorylated rhodopsin (bottom). See methods for details. All recordings were made at 35 – 37 °C.

In order to explore the mechanism of desensitization further, I recorded thousands of dim flash responses from rods that contained unphosphorylated rhodopsin, 50% P-rhodopsin, and 90% P-rhodopsin. From these data, it was possible to calculate single quantal responses (SQRs) from each of these conditions (see Methods). Presented in Figure 3.14A are the SQRs generated from rods contained 0% P-rhodopsin (top), 50% P-rhodopsin (middle), and 90% P-rhodopsin (bottom). The mean SQR for each of these conditions is shown in the inset. The data shows that SQRs generated from rods containing P-rhodopsin have smaller amplitudes. Likewise, 90% P-rhodopsin rods have smaller response amplitudes when compared against 50% P-rhodopsin rods. However, P-rhodopsin does not appear to affect the time course of the rising phase or the falling phase of SQRs. In order to facilitate a further comparison of the SQR waveforms, a representative recording (red trace) was selected under each condition. Figure 3.14B shows the calculated variance (see Methods) of SQRs for each condition. Specifically, the total variance (black traces), the dark variance (blue traces), and the light induced variance (red traces) are plotted under each condition. Figure 3.14C displays the comparison between the light induced variance (red traces), and the mean squared response (black traces). Figures 3.14B and C demonstrate that the SQR waveforms are similar under all three conditions, albeit with different response amplitudes. These factors indicate that the main source of variance in these SQR recordings was induced by exposure of these rods to light. In other words, the variance is due to light activation of phototransduction. In order to compare SQRs amplitudes, the generated waveforms from these three conditions are plotted together in Figure 3.15A. The data show that

phosphorylation of rhodopsin results in decreased SQR amplitudes. An extrapolation from these data would suggest that P-rhodopsin has half the activation potential when compared to unphosphorylated rhodopsin. To support this claim, I calculated the activation constant under each of these conditions (see the inset of Figure 3.15A). Using the Pugh and Lamb (1993) model (equation 2.7), I determined the activation coefficients of $A_{0\%}$ P-rho $= 4.1\ s^{-2}$, $A_{50\%}$ P-rho $= 3.3\ s^{-2}$, and $A_{90\%}$ P-rho $= 2.9\ s^{-2}$. These fits would indicate that phosphorylation of rhodopsin reduces SQR amplitudes. These observations were similar to biochemical analysis of phosphorylated rhodopsin, which demonstrated that phosphorylated rhodopsin has a reduced ability to activate transducin (Wilden et al., 1986; Bennett and Sitaramayya, 1988; Wilden, 1995). Additionally, in my analysis of the data, phosphorylated rhodopsin was treated as a homogenous population, since 1 to 2 phosphates is sufficient to reduce rhodopsin's ability to activate transducin by 50% (Mendez et al., 2000a). In Figure 3.15B, the SQRs were normalized in order to examine the activation and deactivation kinetics under all three conditions. It is evident from this representative data that the time courses for SQR activation and deactivation are similar under all three conditions. For additional comparison, an additional normalized response from a 50% bleached rod is presented in the pink trace. The bleached response has a faster rate of activation and deactivation when compared against SQRs from 0% P-rhodopsin, 50% P-rhodopsin, and 90% P-rhodopsin. Presented in Table 3.3 is the analysis of the complete SQR dataset from each condition. The table reports the mean SQR response amplitude, the number of R* per flash stimulus, the SQR time to peak, and the mean recovery time constant that was fit to the falling phase of the SQR responses.

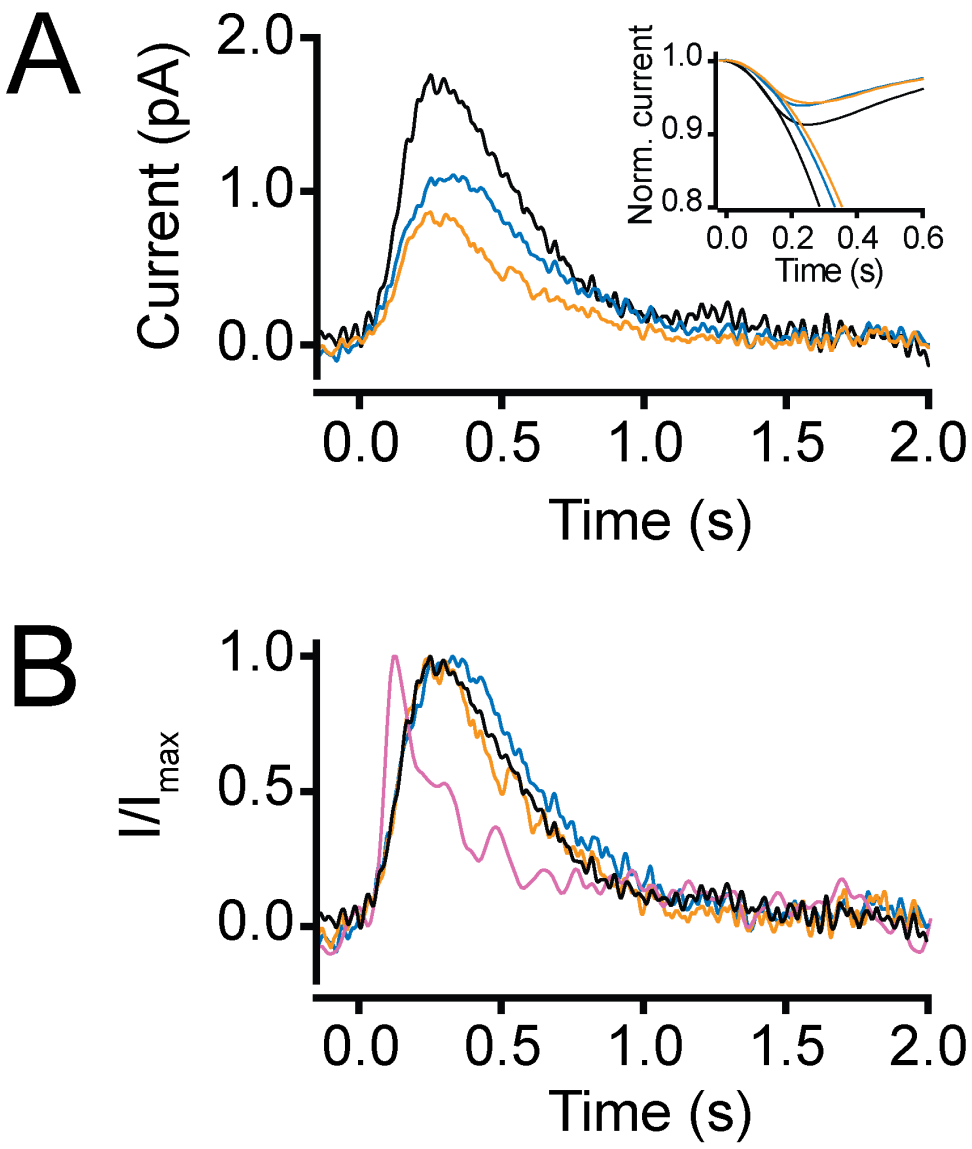

Figure 3.15: Average single quantal responses (SQR) recorded from WT rods containing rhodopsin and phosphorylated rhodopsin. *A:* Representative SQRs from a rod containing rhodopsin (black), 50% phosphorylated rhodopsin (blue), and 90% phosphorylated rhodopsin (orange). The SQRs were calculated from a series of 100 dim flashes per cell. *Inset:* Averaged, smoothed and normalized SQRs fitted with an activation model (Pugh and Lamb, 1993). See text for details. *B:* Normalized SQRs from A. Also shown is a normalized average dim flash response from a 50% bleached rod (pink). The recordings made at 35 – 37 °C.

	Amplitude (pA)	R*[a]	time-to-peak (s)	τ_{rec} (s)[b]
rho	1.50 ± 0.11	1.07 ± 0.14	0.26 ± 0.02	0.37 ± 0.05
50% P-rho	1.02 ± 0.14	1.27 ± 0.19	0.27 ± 0.03	0.35 ± 0.05
90% P-rho	0.81 ± 0.09	0.87 ± 0.09	0.25 ± 0.03	0.40 ± 0.06
ANOVA[c]	F = 7.48; *	F = 0.82; n.s	F = 0.18; n.s.	F = 0.19; n.s.

Table 3.3: Single quantal response (SQR) properties from single cell suction recordings of single mouse rods

SQRs were recorded in dark-adapted retinae containing rhodopsin (rho, N = 8), 50% phospho-rhodopsin (N = 9), and 90% phospho-rhodopsin (N = 6). Values are mean ± S.E.M. [a]R* was calculated according to Eq. 2.5. The incident light was 3.56 * 10^2 photons μm^{-2} s^{-1} in all treatments. [b]τ_{rec} was calculated by fitting an exponential decay function to the falling phase of the response. [c]One way ANOVA with a Tukey test for means comparison. * indicate significance at the 5% level between rho and 50% P-rho, as well as between rho and 90% P-rho. n.s. indicate no significance.

Transducin and Arrestin-1 Translocation

A test needed to be performed to verify whether P-rhodopsin or transducin translocation produced the decreases in SQR amplitudes from rods containing large fractions of P-rhodopsin. Transducin is known to translocate from the outer segment following photoexcitation of rod photoreceptors. This effect is more pronounced during prolonged exposure to light during light adaptation. It is known that this migration of transducin can affect phototransduction. During dark adaptation, transducin slowly recompartmentalizes back into the outer segment. Therefore, I measured transducin and Arr1 concentrations in isolated rod outer segment (ROS) isolated retinae that were either dark adapted or exposed to light that bleached 90% of rhodopsin. Bleached retinae were incubated in the presence of 11-*cis* retinal for periods of 30, 180, and 240 minutes (see Methods). I used western blots to visualize the amount of rod transducin (Gtα) and

arrestin-1 in these ROS at these different times. Sample loading variations were controlled for using proteins found exclusively in rod outer segments. For example, Gβ5L (Keresztes et al., 2004), a component of the transducin GAP complex, is anchored exclusively to the outer segment compartment by R9AP (Cao et al., 2010) and was therefore used as our loading control (Moaven et al., 2013). On the other hand, Gβ5S, an isoform produced from alternative splicing of the same gene, is present in the inner segment and throughout retinal neurons. Gβ5S therefore serves as our quality control for contaminants (Watson et al., 1996). The data, presented in Figure 3.16, shows that dark-adapted retinae have low levels of Arr1 in the outer segments, and high levels of Gtα. These observations are consistent with published observations (see Philp et al., 1987; Sokolov et al., 2002; Slepak and Hurley, 2008). However, when bleached there should be a substantial migration of both of these proteins; transducin moving out of the outer segment and Arr1 migrating into the outer segment. Quantification of the Gtα levels (standardized using the measured concentration of Gβ5L) shows the normalized amount of Gtα was 0.6 ± 0.1 (mean ± SD; N = 4) after 30 minutes of dark adaptation (where dark adapted data was set to 1.0). When bleached retinae were dark adapted for 180 min, Gtα was 0.9 ± 0.2, (N=4), and that this level was maintained at 240 min (0.9 ± 0.2, N=3). The data rules out the possibility that transducin translocation is responsible for the roughly two-fold desensitization observed in single cell experiments between dark-adapted and bleached retinae treated with 11-*cis* retinal. Furthermore, these results indicate that rhodopsin phosphorylation alone is responsible for this persistent desensitization and reduced SQR amplitudes.

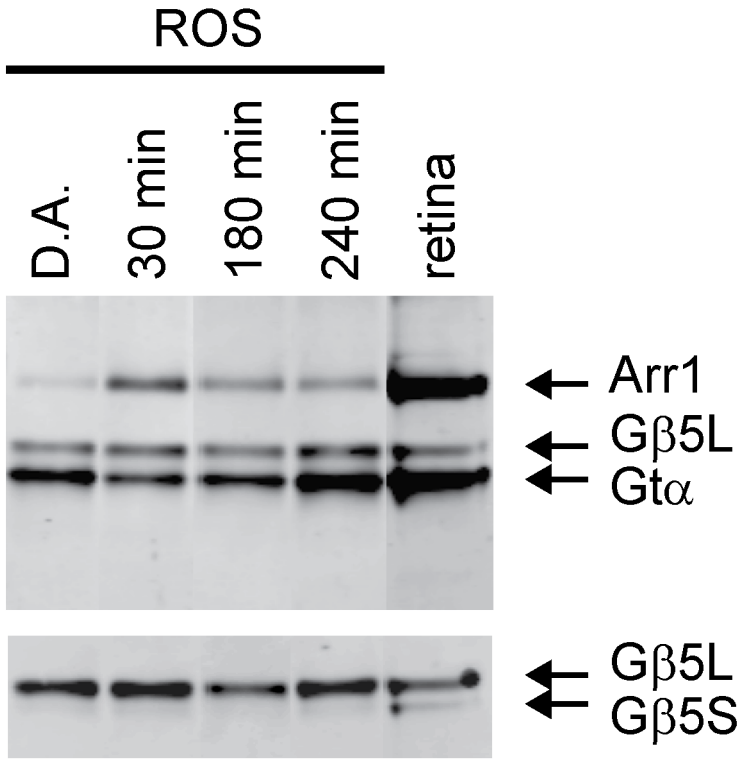

Figure 3.16: Western blots showing transducin translocation. Retinae were either dark adapted or bleached 90% and then incubated in Ames medium containing 11-*cis* retinal in darkness as indicated above the lanes. Retinae were frozen and the rod outer segments (ROS) isolated from the remaining retina. Antibodies were used to visualize the amount of rod transducin (Gtα) in the outer segment. Gβ5L was used as a loading control. Gβ5S serves as a quality control for contaminants. A sample of whole retinal homogenate was carried as control. Signal intensities were quantified using the ImageJ software, and the values for Gtα were normalized against that of Gβ5L. The normalized values for Gtα, when compared to the dark-adapted value (set to 1.0) for 30 min was 0.6 ± 0.1 and for 240 min was 0.9 ± 0.2, (mean ± SD, N=3).

CHAPTER FOUR: DISCUSSION

Throughout the course of my research, I made several novel observations that are presented in this dissertation. First, I was able to use isoelectric focusing (IEF) immunochemistry to show a broad range of conditions that severely diminished rhodopsin dephosphorylation in retinae that were isolated from the eyecup and retinal pigment epithelium (RPE). These conditions are identical to those commonly used in electrophysiological and biochemical experiments. I also discovered that rhodopsin dephosphorylation was substantially restored when the incubation conditions were modified to more accurately represent physiological conditions. I exploited these observations to determine the mechanistic relationship between rod dark adaptation and rhodopsin dephosphorylation. I performed Microspectrophotometry (MSP) recordings that determined that incubating bleached retinae for three hours with 11-*cis* retinal was sufficiently long enough to permit regeneration of 100% of the bleached pigment. Under similar conditions, I performed electroretinogram (ERG) measurements that showed there was a complete recovery in sensitivity after three hours of pigment regeneration. Since a small changes rod in sensitivity can not be resolved from ERG recordings, I subsequently made single cell suction electrode recordings that indicate a slight desensitization in dark adapted retinae that contain phosphorylated rhodopsin. Single quantal response (SQR) measurements shown in Figures 3.13, 3.14, 3.15, and Table 3.3, demonstrated that phosphorylated rhodopsin has about half the activation potential when compared to unphosphorylated rhodopsin. This comparison was measured under several conditions.

The central finding of my work is that mouse rods exposed to bright light followed by long periods of dark adaptation in the presence of 11-cis retinal contain a significant fraction of their rhodopsin in a phosphorylated form, which results in physiological responses with reduced amplitudes, but with kinetics similar to the dark-adapted state. A model that illustrates the possible effects this has on the phototransduction cascade is illustrated in Figure 4.1. This model was based on several biochemistry experiments (Miller et al., 1986; Wilden et al., 1986; Bennett and Sitaramayya, 1988; Wilden, 1995; Binder et al., 1996), and is an extension of models from Lee et al. (2010) and Sommer et al. (2011). Furthermore, this model, and the discussion of data to follow, parallel arguments made in a submitted manuscript that documents this research. The model presented in Figure 4.1 illustrates the coexistence of unphosphorylated rhodopsin (R) and phosphorylated rhodopsin (R-P) within rod photoreceptors. The model is designed to show how these two forms of rhodopsin give rise to different response amplitudes. Following light activation of unphosphorylated rhodopsin (R* or MII), the active pigment initiates the phototransduction cascade. The ability of MII to activate transducin (G) is schematically represented by the two bold vertical arrows. MII is rapidly phosphorylated within ~100 milliseconds to form MII-P (Makino et al., 2003). When phosphorylated, rhodopsin has a reduced ability to activate transducin (as represented by a single bold arrow). Rhodopsin phosphorylation triggers high affinity arrestin-1 (Arr1) binding to form MII-P•Arr1 where the catalytic activity of the visual pigment is quenched fully. All-trans retinal is then gradually released from MII-P•Arr1, leaving phosphorylated opsin (Op-P•Arr1), which has

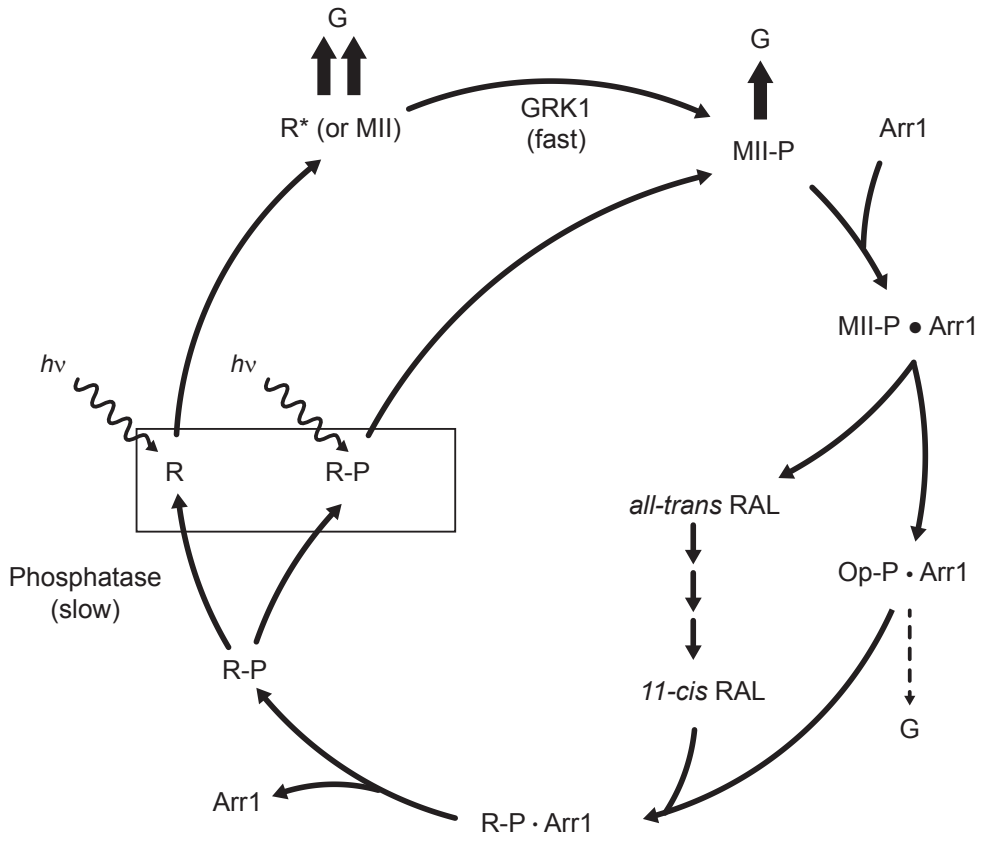

Figure 4.1: A model illustrating the effects of R-P on the phototransduction cascade. When stimulated by light, activated rhodopsin (R* or MII) interacts with the G-Protein transducin (G) to initiate phototransduction (indicated by two bold arrows). Rhodopsin Kinase (GRK1) quickly phosphorylates R* to form MII-P in a process that reduces its capacity to activate transducin (as indicated with only one bold arrow). Shortly thereafter, the catalytic activity of the MII-P is terminated through binding with Arrestin-1 (Arr1) to form MII-P • Arr1. Following this step, phospho-opsin (Op-P • Arr1) is hydrolyzed from all-*trans* retinal, which is recycled in the RPE (not shown). The dashed arrow indicates that opsin itself has very low transduction activity. Pigment regeneration occurs when phospho-opsin (Op-P) recombines with 11-*cis* retinal (supplied from the RPE) to form phospho-rhodopsin (R-P). Phospho-rhodopsin can either be slowly dephosphorylated by rhodopsin phosphatase, or reactivated by light. The latter outcome results in diminished activation of transducin (G).

diminished affinity for Arr1. Opsin has a very weak ability to activate transducin, and under bright bleaching conditions produces opsin adaptation. During bright light exposure large amounts of MII-P•Arr1 will accumulate with the photoreceptor. My model accounts for the observations that dephosphorylation of P-opsin is slow in vivo, and that high levels of P-rhodopsin are formed upon reconstitution of P-opsin with 11-cis retinal (Lee et al., 2010). Regenerated P-rhodopsin can either be dephosphorylated to the ground-state, or reactivated by light. The model shows that photo-activated P-rhodopsin has diminished ability to activate transducin (one bold vertical arrow). This has important implications for rod function during dark adaptation and perhaps light adaptation as well.

There is an extensive body of literature that collectively describes the response activation, kinetics, and reproducibility when single unphosphorylated rhodopsin molecules are photoactivated. Several of these studies provide documentation with regard to how individual phosphorylation sites affect the deactivation of rhodopsin (Mendez et al., 2000a; Makino et al., 2003; Doan et al., 2006). However, these studies were designed to measure single photon responses from rhodopsin that was genetically modified in order to reduce the number of phosphorylation sites on opsin. To my knowledge, my work is the first study that characterizes the amplitude and kinetics of quantal responses arising from the photo-activation of regenerated P-rhodopsin. These measurements were performed in rods that were dark-adapted following pigment regeneration with 11-*cis* retinal. My results indicate that phototransduction gain decreases as the concentration of P-rhodopsin increases within the rods (Figure 3.15 and Table 3.3). An extrapolation of the data indicates that the phototransduction gain would be reduced to 50% in rods that

exclusively contain P-rhodopsin (data not shown), as do my calculations of response activation constants from P-rhodopsin (Table 3.3). These observations are consistent with SQRs measured from rods in which rhodopsin deactivation has been genetically compromised. For example, in $Arr1^{-/-}$ rods, rhodopsin deactivation is incomplete, and the SQRs have recovery phases that stall (and plateau for several seconds) when half of the photocurrent has recovered (Xu et al., 1997; Fu and Yau, 2007). Those observations suggest that phosphorylation of rhodopsin results in about a 2-fold reduction in its ability to activate transducin. My results are also consistent with several biochemical studies which show that phosphorylated rhodopsin has a diminished ability to activate transducin (Miller et al., 1986; Wilden et al., 1986; Bennett and Sitaramayya, 1988; Wilden, 1995). However, in these biochemical studies, the samples contained both phosphorylated rhodopsin and a small fraction of unphosphorylated rhodopsin. The photo-activation of this small portion of unphosphorylated rhodopsin alone could be enough to saturate the measurements of transducin activation, which would be considered an artifact in these reports. Additionally, these studies measured cGMP, which allowed the authors to guess at how much transducin was active in each experiment. This analysis could be tentative since transducin activation and PDE activation are two steps in the amplification of the phototransduction cascade. My IEF results show that phosphorylated rhodopsin is a heterogeneous distribution of phosphorylation states, from 1P to 6P (Table 3.1). Under these conditions, I was able to generated SQRs for phosphorylated rhodopsin, which reflect the actual biological processes that occur in living rods.

A 50% reduction in sensitivity due to P-rhodopsin may seem to be relatively minor when compared to the overall loss in sensitivity produced by bleaching; however, a more significant consequence is expected during the final phases of dark adaption toward absolute visual threshold. The detection of SQRs by rod bipolar cells requires the passage of responses through a nonlinear threshold based on their size (Field and Rieke, 2002). For SQRs to be faithfully transmitted to the bipolar cells, their size must be sufficiently large to decrease glutamate concentrations at the rod-to-rod bipolar synapses (Sampath and Rieke, 2004). Under fully dark-adapted conditions, synaptic saturation renders the rod bipolar current insensitive to small changes in transmitter release from the rod. This threshold nonlinearity in signal transfer therefore is likely to filter out SQRs generated from P-Rhodopsin activation, and reduce the sensitivity at the visual threshold during dark adaptation.

Finally, sensitivity adjustments are also a hallmark of light adaptation, where phototransduction gain is modulated to allow the rods to continue to respond when ambient illumination is increased (Pugh and Lamb, 2000; Fain et al., 2001; Calvert and Makino, 2002; Fain, 2011). My results suggest that P-rhodopsin, which is produced in significant amounts under steady bright light illumination (Lee et al., 2010), reduces overall gain from photolyzed P-rhodopsin and serves as a form of light adaptation.

Does Arr1 Activation or Arr1 Binding Rate Limit Rhodopsin Deactivation?

The deactivation of phototransduction during a single photon response requires a coordinated series of reactions. These processes include: (1) GRK1 binding to MII, (2)

GRK1 catalyzed phosphate attachment to MII (to form MII-P), (3) MII-P activation of arrestin-1, and (4) arrestin-1 termination of MII-P activity. These steps regulate the lifetime of rhodopsin (Figure 4.2A), and therefore shape the kinetics and variability of the single photon responses (Miller et al., 1986; Doan et al., 2006; Gurevich et al., 2011). There are, however, two additional layers of complexity. Arrestin-1 exists in a basal state and must transition into a binding-competent conformation by encounters with MII-P (Gurevich et al., 2011). As a result arrestin-1 activation will be competitively inhibited by GRK1 binding to rhodopsin. It is possible that while GRK1 sequentially adds phosphates onto MII, the interaction between MII-P and arrestin-1 may become favored over GRK1. By comparing SQRs generated by rhodopsin and P-rhodopsin, I had the unique opportunity to investigate two proposed mechanisms for rhodopsin deactivation. These two possibilities are illustrated in Figure 4.3. The first proposed mechanism illustrates a GRK1 catalyzed MII phosphorylation rate limited rhodopsin deactivation model. The alternative model shows arrestin-1 activation and binding to MII-P, as rate-limiting MII deactivation. If rhodopsin phosphorylation rate limits rhodopsin deactivation, then SQRs generated by P-rhodopsin should deactivate faster when compared to SQRs generated by activating non-phosphorylated rhodopsin. The latter process would be slower since deactivation requires additional time for phosphate attachment by GRK1. On the other hand, if arrestin-1 activation is rate limiting, then the SQRs generated from P-rhodopsin will have an identical time course for activation and deactivation to those SQRs observed from unphosphorylated rhodopsin. I observed that SQRs generated from unphosphorylated rhodopsin and P-rhodopsin display indistinguishable time-to-peak and

time constant of deactivation. This similarity of response kinetics suggests that prior to arrestin activation, arrestin-1's affinity for MII is insensitive to phosphate attachment (ie MII-P). The affect of this insensitivity is that arrestin-1 activation is the rate-limiting step in the deactivation of the visual pigment.

A recent study of arrestin-1 interaction with different functional forms of rhodopsin using solution NMR spectroscopy shows that the affinity of arrestin-1 for P-rhodopsin was sufficiently high that active monomeric arrestin-1 in the outer segment is predicted to bind P-rhodopsin in the intact rod (Zhuang et al., 2013). However, my observation that P-rhodopsin SQR kinetics are virtually identical to those of ground-state SQRs indicates that arrestin-1 is not pre-bound to P-rhodopsin in a manner that prevents its signaling.

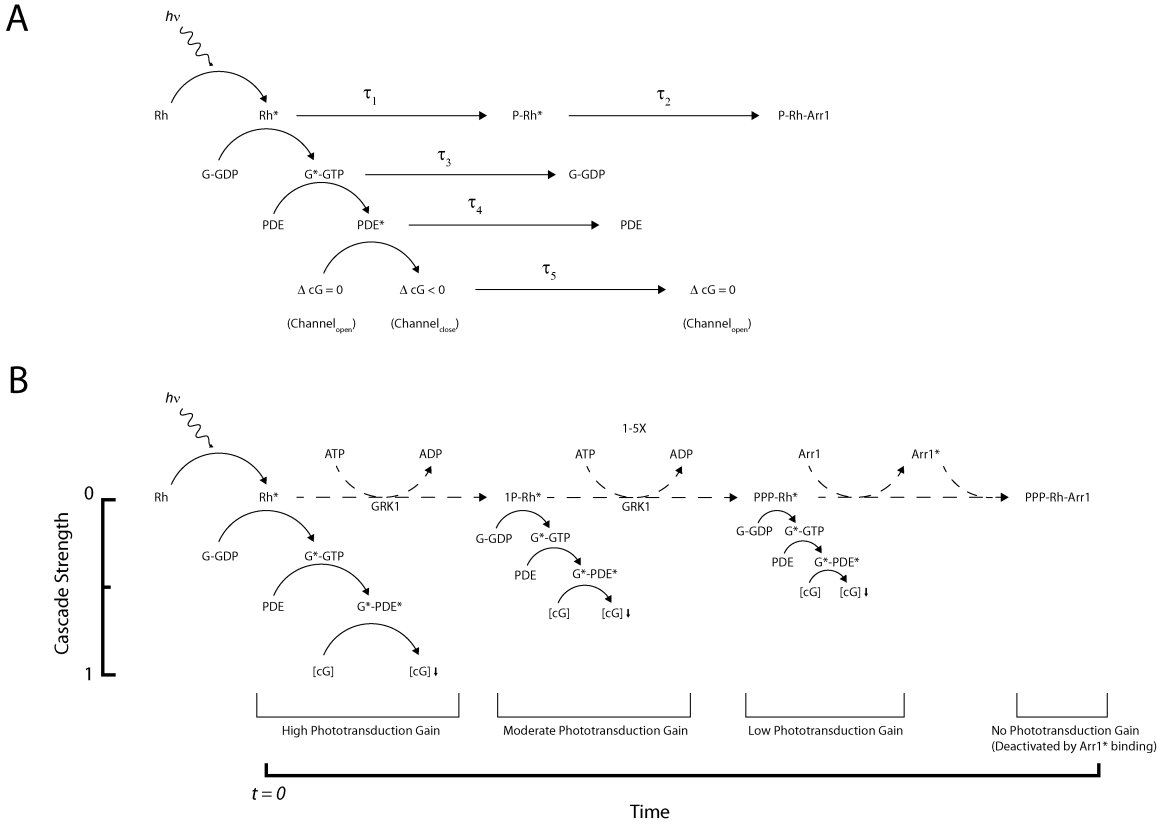

Figure 4.2: Illustration on how rhodopsin phosphorylation regulates the phototransduction cascade. *A:* Light activates rhodopsin (Rh*), which in turn activates the G-protein transducin (G*). This leads to the activation of phosphodiesterase (PDE*) and a local decrease in [cGMP] (cG). This schematic also highlights the importance that the deactivation/decay (τ) of each step in the phototransduction cascade. In this regard, rhodopsin is deactivated by phosphorylation and arrestin-1 binding. While G* and PDE* deactivation (τ_3 and τ_4) each have their own slow intrinsic rate of deactivation, these two process are normally entangled with each other, which increases the deactivation of both process. Overall, there is temporal overlap among all of these deactivation steps. *B:* Illustration demonstrating the effect that rhodopsin phosphorylation has on the overall strength of the phototransduction cascade. This ordinate represents the external excitatory strength (ie, photocurrent, or photovoltage) and does not show the amplification of secondary messengers. Phosphorylation is shown here reducing activated rhodopsin's ability to activate transducin. Additional phosphate attachment further lowers G* amplification. Activated arrestin (Arr1*) binding to P-rhodopsin terminates phototransduction, and the response recovery is dictated by decay (τ) of each process, as shown in panel A. Panel A was adapted with permission from King-Wai Yau (Yau, 1994).

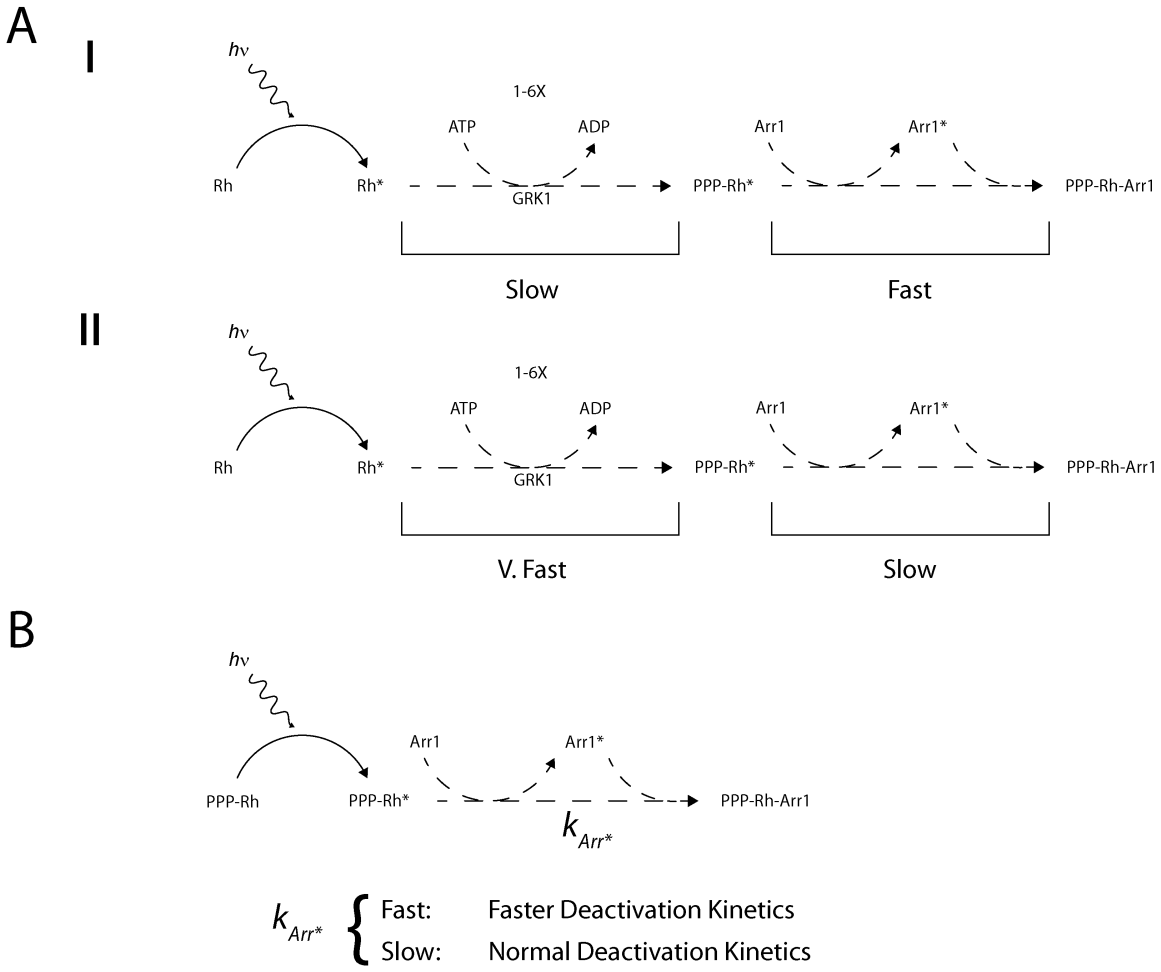

Figure 4.3: Models regulating the lifetime of activated rhodopsin. *A:* Based on previous studies, there are two likely, but incompatible hypotheses for rhodopsin deactivation. In the first model, *I*, rhodopsin phosphorylation by GRK1 is slow, and therefore rhodopsin deactivation is limited by the rate of rhodopsin phosphorylation. In the second model, *II*, arrestin-1 activation is slow and rate limits rhodopsin deactivation. *B:* SQR measured from P-rhodopsin can resolve which model is correct. The activated pigment is already phosphorylated, and only requires arrestin 1 binding to deactivate. If the rate of arrestin-1 activation and binding is fast, then SQRs generated from P-rhodopsin would be faster than SQR from those generated from non-phosphorylated rhodopsin. However, if arrestin-1 activation and binding is slow, than the lifetime of activated rhodopsin would be invariant.

Phosphorylated Rhodopsin, the Visual Cycle, and Light Adaptation

The visual cycle is defined as the ensemble of biochemical reactions that reside in the neural retina and the RPE whereby visual pigment, once bleached, is returned to its fully functional ground state containing 11-*cis* retinal. As rhodopsin cannot be defined as being in its ground state until it has been fully dephosphorylated, I argue that the dephosphorylation of rhodopsin is a critical step in the visual cycle.

Vertebrate rods have the ability to undergo huge changes in their sensitivity in response to differences in background and bleaching light intensity. This endows them with the ability to respond over a range of 3 - 4 orders of magnitude of light intensities. The cellular mechanisms identified within rods which are responsible for these changes include: (1) the transduction driven decrease of cytosolic calcium concentration that, in turn, modulates the activities of cGMP phosphodiesterase, guanylate cyclase, and recoverin within rod outer segments, (2) the prolonged lifetime of photoproducts of rhodopsin bleaching that result in persistent activation of the transduction cascade, (3) bleaching of rhodopsin that by virtue of its decreased concentration within the outer segment reduces quantum catch, and (4) the translocation of transducin from the outer to the inner segment of rods leading to decreased transducin activation by R*. My results show that high levels of P-rhodopsin can persist within rod outer segments for many minutes after bright light exposure, and that P-rhodopsin photoactivation activates transducin with diminished efficiency. These results suggest that this mechanism of adaptation be added to the above list. Except at the highest levels of rhodopsin

phosphorylation, this sensitivity reduction is modest, but it is predicted to have its most significant effects near visual threshold.

Why is Rhodopsin Dephosphorylation Blunted in Isolated Mammalian Retina?

My observation that isolation of the retina from the mouse eye results in substantial inhibition of rhodopsin dephosphorylation is novel and surprising. Importantly, biochemical and electrophysiological measurements of isolated retina and solitary photoreceptor cells under the same conditions I describe here have been routine for over forty years. Thus, my documentation emphasizes that isolation of the retina from the intact animal may have important implications for these studies. Furthermore, I demonstrate that low oxygen tension in the superfusion medium and the presence of lactate both promote dephosphorylation. These latter results clearly suggest the involvement of metabolic mechanisms in the regulation of rhodopsin dephosphorylation, but provide no insights into specific mechanisms. Studies of the metabolic dependence of rhodopsin dephosphorylation in rods is an important topic for further investigation.

The Relevance of Regenerated Phosphorylated Rhodopsin

One of the areas not directly addressed in this study was the biological relevance of my findings. This is important because an earlier study on frog retina suggested that only a negligible fraction of regenerated rhodopsin is phosphorylated *in vivo* (Binder et al., 1996). My data provides evidence that in mouse rods, regenerated phosphorylated rhodopsin exists in significant quantities and that it would actually constitute as a relevant

form of light adaptation. Evidence from Lee et al. (2010), is consistent with my observation, and these authors have shown that during light (and dark-adaptation), a significant portion of rhodopsin in *in vivo* mouse retinae is regenerated in the phosphorylated state. Specifically, Lee et al. (2010) showed that following 90 minutes of bright-light light adaption, approximately 45% of the total opsin was rhodopsin (either un-bleached or regenerated), and the 55% of the remaining was in a bleached form. At the same time, they showed that 80% of the total opsin was phosphorylated. Minimally, this requires that 25% of rhodopsin exists in a phosphorylated state. These observation establish the relevance of my observations within *in vivo* light and dark adaptation.

BIBLIOGRAPHY

Adamus, G., A. Arendt, P.A. Hargrave, T. Heyduk, and K. Palczewski. 1993. The kinetics of multiphosphorylation of rhodopsin. *Archives of Biochemistry and Biophysics.* 304:443-447.

Adler, A.J., and R.E. Southwick. 1992. Distribution of glucose and lactate in the interphotoreceptor matrix. *Ophthalmic research*. 24:243-252.

Ala-Laurila, P., K. Donner, R.K. Crouch, and M.C. Cornwall. 2007. Chromophore switch from 11-cis-dehydroretinal (A2) to 11-cis-retinal (A1) decreases dark noise in salamander red rods. *The Journal of Physiology.* 585:57-74.

Ala-Laurila, P., K. Donner, and A. Koskelainen. 2004. Thermal activation and photoactivation of visual pigments. *Biophysical Journal*. 86:3653-3662.

Alvarez, L.L., and H.G. Pardo. 1997. Guide for the care and use of laboratory animals - Natl-Res-Council. *Psicothema*. 9:232-234.

Ames, A., 3rd, and F.B. Nesbett. 1981. In vitro retina as an experimental model of the central nervous system. *Journal of Neurochemistry*. 37:867-877.

Azevedo, A.W., T. Doan, H. Moaven, I. Sokal, F. Baameur, S.A. Vishnivetskiy, K.T. Homan, J.J. Tesmer, V.V. Gurevich, J. Chen, and F. Rieke. 2015. C-terminal threonines and serines play distinct roles in the desensitization of rhodopsin, a G protein-coupled receptor. *eLife*. 4.

Azevedo, A.W., and F. Rieke. 2011. Experimental Protocols Alter Phototransduction: The Implications for Retinal Processing at Visual Threshold. *Journal of Neuroscience*. 31:3670-3682.

Baehr, W., M.J. Devlin, and M.L. Applebury. 1979. Isolation and characterization of cGMP phosphodiesterase from bovine rod outer segments. *Journal of Biological Chemistry*. 254:11699-11677.

Baldwin, J.M. 1993. The probable arrangement of the helices in G protein-coupled receptors. *EMBO JOURNAL*. 12:1693-1703.

Baylor, D.A., T.D. Lamb, and K.W. Yau. 1979. Responses of retinal rods to single photons. *Journal of Physiology (London, UK)*. 288:613-634.

Baylor, D.A., B.J. Nunn, and J.L. Schnapf. 1984. The photocurrent, noise and spectral sensitivity of rods of the monkey Macaca fascicularis. *Journal of Physiology (London, UK)*. 357:575-607.

Bennett, N., and A. Sitaramayya. 1988. Inactivation of photoexcited rhodopsin in retinal rods: the roles of rhodopsin kinase and 48-kDa protein (arrestin). *Biochemistry*. 27:1710-1715.

Binder, B.M., T.M. O'Connor, M.D. Bownds, and V.Y. Arshavsky. 1996. Phosphorylation of non-bleached rhodopsin in intact retinas and living frogs. *Journal of Biological Chemistry*. 271:19826-19830.

Birol, G., S. Wang, E. Budzynski, N.D. Wangsa-Wirawan, and R.A. Linsenmeier. 2007. Oxygen distribution and consumption in the macaque retina. *American Journal of Physiology - Heart and Circulatory Physiology*. 293:H1696-1704.

Bolnick, D.A., A.E. Walter, and A.J. Sillman. 1979. Barium Suppresses Slow Piii in Perfused Bullfrog Retina. *Vision Research*. 19:1117-1119.

Browning, D.J. Retinal vein occlusions : evidence-based management. xiii, 387 pages pp.

Burns, M.E., A. Mendez, J. Chen, and D.A. Baylor. 2002. Dynamics of cyclic GMP synthesis in retinal rods. *Neuron*. 36:81-91.

Calvert, P.D., and C.L. Makino. 2002. The time course of light adaptation in vertebrate retinal rods. *Advances in Experimental Medicine and Biology*. 514:37-60.

Cao, Y., A.V. Kolesnikov, I. Masuho, V.J. Kefalov, and K.A. Martemyanov. 2010. Membrane anchoring subunits specify selective regulation of RGS9.Gbeta5 GAP complex in photoreceptor neurons. *Journal of Neuroscience*. 30:13784-13793.

Carbone, L. 2012. Pain management standards in the eighth edition of the Guide for the Care and Use of Laboratory Animals. *Journal of the American Association for Laboratory Animal Science : JAALAS*. 51:322-328.

Catty, P., C. Pfister, F. Bruckert, and P. Deterre. 1992. The cGMP phosphodiesterase-transducin complex of retinal rods. Membrane binding and subunits interactions. *Journal of Biological Chemistry*. 267:19489-19493.

Chang, B., M.S. Dacey, N.L. Hawes, P.F. Hitchcock, A.H. Milam, P. Atmaca-Sonmez, S. Nusinowitz, and J.R. Heckenlively. 2006. Cone photoreceptor function loss-3, a novel mouse model of achromatopsia due to a mutation in Gnat2. *Investigative Ophthalmology & Visual Science*. 47:5017-5021.

Chen, C.K., M.E. Burns, M. Spencer, G.A. Niemi, J. Chen, J.B. Hurley, D.A. Baylor, and M.I. Simon. 1999. Abnormal photoresponses and light-induced apoptosis in rods lacking rhodopsin kinase. *Proceedings of the National Academy of Sciences of the United States of America*. 96:3718-3722.

Chen, C.K., J. Inglese, R.J. Lefkowitz, and J.B. Hurley. 1995a. Ca(2+)-dependent interaction of recoverin with rhodopsin kinase. *Journal of Biological Chemistry*. 270:18060-18066.

Chen, C.K., M.L. Woodruff, F.S. Chen, Y. Chen, M.C. Cilluffo, D. Tranchina, and G.L. Fain. 2012. Modulation of mouse rod response decay by rhodopsin kinase and recoverin. *Journal of Neuroscience*. 32:15998-16006.

Chen, C.K., M.L. Woodruff, and G.L. Fain. 2015. Rhodopsin kinase and recoverin modulate phosphodiesterase during mouse photoreceptor light adaptation. *Journal of General Physiology*. 145:213-224.

Chen, J., C.L. Makino, N.S. Peachey, D.A. Baylor, and M.I. Simon. 1995b. Mechanisms of rhodopsin inactivation in vivo as revealed by a COOH- terminal truncation mutant. *Science*. 267:374-377.

Chen, T.Y., Y.W. Peng, R.S. Dhallan, B. Ahamed, R.R. Reed, and K.W. Yau. 1993. A new subunit of the cyclic nucleotide-gated cation channel in retinal rods. *Nature*. 362:764-767.

Cohen, G.B., D.D. Oprian, and P.R. Robinson. 1992. Mechanism of activation and inactivation of opsin: role of Glu113 and Lys296. *Biochemistry*. 31:12592-12601.

Concepcion, F., and J. Chen. 2010. Q344ter mutation causes mislocalization of rhodopsin molecules that are catalytically active: a mouse model of Q344ter-induced retinal degeneration. *PLoS One*. 5:e10904.

Cornwall, M.C., and G.L. Fain. 1994. Bleached pigment activates transduction in isolated rods of the salamander retina. *Journal of Physiology (London, UK)*. 480:261-279.

Cornwall, M.C., A. Fein, and E.F. MacNichol, Jr. 1990. Cellular mechanisms that underlie bleaching and background adaptation. *Journal of General Physiology*. 96:345-372.

Cornwall, M.C., E.F. MacNichol, Jr., and A. Fein. 1984. Absorptance and spectral sensitivity measurements of rod photoreceptors of the tiger salamander, Ambystoma tigrinum. *Vision Research*. 24:1651-1659.

Cornwall, M.C., H.R. Matthews, R.K. Crouch, and G.L. Fain. 1995. Bleached pigment activates transduction in salamander cones. *Journal of General Physiology*. 106:543-557.

Cringle, S.J., D.Y. Yu, P.K. Yu, and E.N. Su. 2002. Intraretinal oxygen consumption in the rat in vivo. *Investigative Ophthalmology & Visual Science*. 43:1922-1927.

Dizhoor, A.M., E.V. Olshevskaya, and I.V. Peshenko. 2010. Mg2+/Ca2+ cation binding cycle of guanylyl cyclase activating proteins (GCAPs): role in regulation of photoreceptor guanylyl cyclase. *Molecular and Cellular Biochemistry*. 334:117-124.

Doan, T., A.W. Azevedo, J.B. Hurley, and F. Rieke. 2009. Arrestin competition influences the kinetics and variability of the single-photon responses of mammalian rod photoreceptors. *Journal of Neuroscience*. 29:11867-11879.

Doan, T., A. Mendez, P.B. Detwiler, J. Chen, and F. Rieke. 2006. Multiple phosphorylation sites confer reproducibility of the rod's single-photon responses. *Science*. 313:530-533.

Doukas, A.G., B. Aton, R.H. Callender, and T.G. Ebrey. 1978. Resonance Raman studies of bovine metarhodopsin I and metarhodopsin II. *Biochemistry*. 17:2430-2435.

Dryja, T.P. 2000. Molecular genetics of Oguchi disease, fundus albipunctatus, and other forms of stationary night blindness: LVII Edward Jackson Memorial Lecture. *American Journal of Ophthalmology*. 130:547-563.

Ebrey, T., and Y. Koutalos. 2001. Vertebrate photoreceptors. *Progress in Retinal and Eye Research*. 20:49-94.

Estevez, M.E. 2007. Molecular mechanisms underlying rapid dark adaptation in cone photoreceptors. Dissertation, Boston University School of Medicine,

Fain, G.L. 2011. Adaptation of mammalian photoreceptors to background light: putative role for direct modulation of phosphodiesterase. *Molecular Neurobiology*. 44:374-382.

Fain, G.L., H.R. Matthews, M.C. Cornwall, and Y. Koutalos. 2001. Adaptation in vertebrate photoreceptors. *Physiological Reviews*. 81:117-151.

Field, G.D., and F. Rieke. 2002. Mechanisms regulating variability of the single photon responses of mammalian rod photoreceptors. *Neuron*. 35:733-747.

Frederiksen, R., N.P. Boyer, B. Nickle, K.S. Chakrabarti, Y. Koutalos, R.K. Crouch, D. Oprian, and M.C. Cornwall. 2012. Low aqueous solubility of 11-cis-retinal limits the rate of pigment formation and dark adaptation in salamander rods. *Journal of General Physiology*. 139:493-505.

Fu, Y., and K.W. Yau. 2007. Phototransduction in mouse rods and cones. *Pflugers Archiv : European journal of physiology*. 454:805-819.

Fukada, Y., T. Takao, H. Ohguro, T. Yoshizawa, T. Akino, and Y. Shimonishi. 1990. Farnesylated gamma-subunit of photoreceptor G protein indispensable for GTP-binding. *Nature*. 346:658-660.

Fung, B.K., J.B. Hurley, and L. Stryer. 1981. Flow of information in the light-triggered cyclic nucleotide cascade of vision. *Proceedings of the National Academy of Sciences of the United States of America*. 78:152-156.

Gouras, P. 1972. Color opponency from fovea to striate cortex. *Investigative ophthalmology*. 11:427-434.

Govardovskii, V.I., N. Fyhrquist, T. Reuter, D.G. Kuzmin, and K. Donner. 2000. In search of the visual pigment template. *Visual Neuroscience*. 17:509-528.

Gray-Keller, M.P., and P.B. Detwiler. 1994. The calcium feedback signal in the phototransduction cascade of vertebrate rods. *Neuron*. 13:849-861.

Gurevich, V.V., S.M. Hanson, X. Song, S.A. Vishnivetskiy, and E.V. Gurevich. 2011. The functional cycle of visual arrestins in photoreceptor cells. *Progress in Retinal and Eye Research*. 30:405-430.

Harosi, F.I. 1975. Absorption spectra and linear dichroism of some amphibian photoreceptors. *Journal of General Physiology*. 66:357-382.

Harosi, F.I. 1996. Visual pigment types and quantum-catch ratios: implications from three marine teleosts. *Biological Bulletin*. 190:203-212.

Harosi, F.I., and E.F. MacNichol, Jr. 1974. Dichroic microspectrophotometer: a computer-assisted, rapid, wavelength- scanning photometer for measuring linear dichroism in single cells. *Journal of the Optical Society of America*. 64:903-918.

He, W., C.W. Cowan, and T.G. Wensel. 1998. RGS9, a GTPase accelerator for phototransduction. *Neuron*. 20:95-102.

Heck, M., and K.P. Hofmann. 2001. Maximal rate and nucleotide dependence of rhodopsin-catalyzed transducin activation: initial rate analysis based on a double displacement mechanism. *Journal of Biological Chemistry*. 276:10000-10009.

Heikkinen, H., F. Vinberg, M. Pitkanen, B. Kommonen, and A. Koskelainen. 2012. Flash responses of mouse rod photoreceptors in the isolated retina and corneal electroretinogram: comparison of gain and kinetics. *Investigative Ophthalmology & Visual Science*. 53:5653-5664.

Howes, K.A., M.E. Pennesi, I. Sokal, J. Church-Kopish, B. Schmidt, D. Margolis, J.M. Frederick, F. Rieke, K. Palczewski, S.M. Wu, P.B. Detwiler, and W. Baehr. 2002. GCAP1 rescues rod photoreceptor response in GCAP1/GCAP2 knockout mice. *EMBO JOURNAL*. 21:1545-1554.

Hsu, Y.T., and R.S. Molday. 1993. Modulation of the cGMP-gated channel of rod photoreceptor cells by calmodulin [published erratum appears in Nature 1993 Sep 16;365(6443):279] [see comments]. *Nature*. 361:76-79.

Hu, G., and T.G. Wensel. 2002. R9AP, a membrane anchor for the photoreceptor GTPase accelerating protein, RGS9-1. *Proceedings of the National Academy of Sciences of the United States of America*. 99:9755-9760.

Hurley, J.B., K.J. Lindsay, and J. Du. 2015. Glucose, lactate, and shuttling of metabolites in vertebrate retinas. *Journal of Neuroscience Research*. 93:1079-1092.

Hurley, J.B., M. Spencer, and G.A. Niemi. 1998. Rhodopsin phosphorylation and its role in photoreceptor function. *Vision Research*. 38:1341-1352.

Hurley, J.B., and L. Stryer. 1982. Purification and characterization of the gamma regulatory subunit of the cyclic GMP phosphodiesterase from retinal rod outer segments. *Journal of Biological Chemistry*. 257:11094-11099.

Jager, F., K. Fahmy, T.P. Sakmar, and F. Siebert. 1994. Identification of glutamic acid 113 as the Schiff base proton acceptor in the metarhodopsin II photointermediate of rhodopsin. *Biochemistry*. 33:10878-10882.

Jones, G.J., M.C. Cornwall, and G.L. Fain. 1996. Equivalence of background and bleaching desensitization in isolated rod photoreceptors of the larval tiger salamander. *Journal of General Physiology*. 108:333-340.

Jones, G.J., A. Fein, E.F. MacNichol, Jr., and M.C. Cornwall. 1993. Visual pigment bleaching in isolated salamander retinal cones. Microspectrophotometry and light adaptation. *Journal of General Physiology*. 102:483-502.

Kane, M.A., and J.L. Napoli. 2010. Quantification of endogenous retinoids. *Methods in Molecular Biology*. 652:1-54.

Kaupp, U.B., and R. Seifert. 2002. Cyclic nucleotide-gated ion channels. *Physiological Reviews*. 82:769-824.

Kawamura, S. 1993. Rhodopsin phosphorylation as a mechanism of cyclic GMP phosphodiesterase regulation by S-modulin. *Nature*. 362:855-857.

Kennedy, M.J., K.A. Lee, G.A. Niemi, K.B. Craven, G.G. Garwin, J.C. Saari, and J.B. Hurley. 2001. Multiple phosphorylation of rhodopsin and the in vivo chemistry underlying rod photoreceptor dark adaptation. *Neuron*. 31:87-101.

Keresztes, G., K.A. Martemyanov, C.M. Krispel, H. Mutai, P.J. Yoo, S.F. Maison, M.E. Burns, V.Y. Arshavsky, and S. Heller. 2004. Absence of the RGS9.Gbeta5 GTPase-activating complex in photoreceptors of the R9AP knockout mouse. *Journal of Biological Chemistry*. 279:1581-1584.

Kokame, K., Y. Fukada, T. Yoshizawa, T. Takao, and Y. Shimonishi. 1992. Lipid modification at the N terminus of photoreceptor G-protein alpha-subunit. *Nature*. 359:749-752.

Kolesnikov, A.V., E.Y. Golobokova, and V.I. Govardovskii. 2003. The identity of metarhodopsin III. *Visual Neuroscience*. 20:249-265.

Krispel, C.M., D. Chen, N. Melling, Y.J. Chen, K.A. Martemyanov, N. Quillinan, V.Y. Arshavsky, T.G. Wensel, C.K. Chen, and M.E. Burns. 2006. RGS expression rate-limits recovery of rod photoresponses. *Neuron*. 51:409-416.

Kuhn, H. 1974. Light-dependent phosphorylation of rhodopsin in living frogs. *Nature*. 250:588-590.

Kuhn, H., and J.H. McDowell. 1977. Isoelectric focusing of phosphorylated cattle rhodopsin. *Biophysics of structure and mechanism*. 3:199-203.

Lamb, T.D., R.M. Corless, and A.D. Pananos. 2015. The kinetics of regeneration of rhodopsin under enzyme-limited availability of 11-cis retinoid. *Vision Research*. 110:23-33.

Lau, J.C., and R.A. Linsenmeier. 2012. Oxygen consumption and distribution in the Long-Evans rat retina. *Experimental Eye Research*. 102:50-58.

Lee, K.A., M. Nawrot, G.G. Garwin, J.C. Saari, and J.B. Hurley. 2010. Relationships among visual cycle retinoids, rhodopsin phosphorylation, and phototransduction in mouse eyes during light and dark adaptation. *Biochemistry*. 49:2454-2463.

Lee, R.H., B.S. Lieberman, H.K. Yamane, D. Bok, and B.K. Fung. 1992. A third form of the G protein beta subunit. 1. Immunochemical identification and localization to cone photoreceptors. *Journal of Biological Chemistry*. 267:24776-24781.

Leibrock, C.S., T. Reuter, and T.D. Lamb. 1994. Dark adaptation of toad rod photoreceptors following small bleaches. *Vision Research*. 34:2787-2800.

Lerea, C.L., D.E. Somers, J.B. Hurley, I.B. Klock, and A.H. Bunt-Milam. 1986. Identification of specific transducin alpha subunits in retinal rod and cone photoreceptors. *Science*. 234:77-80.

Leskov, I.B., V.A. Klenchin, J.W. Handy, G.G. Whitlock, V.I. Govardovskii, M.D. Bownds, T.D. Lamb, E.N. Pugh, Jr., and V.Y. Arshavsky. 2000. The gain of rod phototransduction: reconciliation of biochemical and electrophysiological measurements. *Neuron*. 27:525-537.

Li, T.S., K. Volpp, and M.L. Applebury. 1990. Bovine cone photoreceptor cGMP phosphodiesterase structure deduced from a cDNA clone. *Proceedings of the National Academy of Sciences of the United States of America*. 87:293-297.

Lindsay, K.J., J. Du, S.R. Sloat, L. Contreras, J.D. Linton, S.J. Turner, M. Sadilek, J. Satrustegui, and J.B. Hurley. 2014. Pyruvate kinase and aspartate-glutamate carrier distributions reveal key metabolic links between neurons and glia in retina. *Proceedings of the National Academy of Sciences of the United States of America*. 111:15579-15584.

MacGregor, L.C., L.R. Rosecan, A.M. Laties, and F.M. Matschinsky. 1986. Altered retinal metabolism in diabetes. I. Microanalysis of lipid, glucose, sorbitol, and myo-inositol in the choroid and in the individual layers of the rabbit retina. *Journal of Biological Chemistry*. 261:4046-4051.

Makino, C.L. 2012. Easy does it when bleaching isolated mouse rods. *The Journal of Physiology.* 590:2551-2552.

Makino, C.L., R.L. Dodd, J. Chen, M.E. Burns, A. Roca, M.I. Simon, and D.A. Baylor. 2004. Recoverin regulates light-dependent phosphodiesterase activity in retinal rods. *Journal of General Physiology*. 123:729-741.

Makino, C.L., I.V. Peshenko, X.H. Wen, E.V. Olshevskaya, R. Barrett, and A.M. Dizhoor. 2008. A role for GCAP2 in regulating the photoresponse. Guanylyl cyclase activation and rod electrophysiology in GUCA1B knock-out mice. *Journal of Biological Chemistry*. 283:29135-29143.

Makino, C.L., X.H. Wen, and J. Lem. 2003. Piecing together the timetable for visual transduction with transgenic animals. *Current Opinion in Neurobiology*. 13:404-412.

Makino, E.R., J.W. Handy, T. Li, and V.Y. Arshavsky. 1999. The GTPase activating factor for transducin in rod photoreceptors is the complex between RGS9 and type 5 G protein beta subunit. *Proceedings of the National Academy of Sciences of the United States of America*. 96:1947-1952.

Masland, R.H. 2001a. The fundamental plan of the retina. *Nat Neurosci*. 4:877-886.

Masland, R.H. 2001b. Neuronal diversity in the retina. *Current Opinion in Neurobiology*. 11:431-436.

Matthews, H.R., M.C. Cornwall, and G.L. Fain. 1996. Persistent activation of transducin by bleached rhodopsin in salamander rods. *Journal of General Physiology*. 108:557-563.

Matthews, H.R., G.L. Fain, R.L. Murphy, and T.D. Lamb. 1990. Light adaptation in cone photoreceptors of the salamander: a role for cytoplasmic calcium. *Journal of Physiology (London, UK)*. 420:447-469.

Mendez, A., M.E. Burns, A. Roca, J. Lem, L.W. Wu, M.I. Simon, D.A. Baylor, and J. Chen. 2000a. Rapid and reproducible deactivation of rhodopsin requires multiple phosphorylation sites. *Neuron*. 28:153-164.

Mendez, A., M.E. Burns, I. Sokal, A.M. Dizhoor, W. Baehr, K. Palczewski, D.A. Baylor, and J. Chen. 2001. Role of guanylate cyclase-activating proteins (GCAPs) in setting the flash sensitivity of rod photoreceptors. *Proceedings of the National Academy of Sciences of the United States of America*. 98:9948-9953.

Mendez, A., N.V. Krasnoperova, J. Lem, and J. Chen. 2000b. Functional study of rhodopsin phosphorylation in vivo. *Methods Enzymology*. 316:167-185.

Miller, J.L., D.A. Fox, and B.J. Litman. 1986. Amplification of phosphodiesterase activation is greatly reduced by rhodopsin phosphorylation. *Biochemistry*. 25:4983-4988.

Moaven, H., Y. Koike, C.C. Jao, V.V. Gurevich, R. Langen, and J. Chen. 2013. Visual arrestin interaction with clathrin adaptor AP-2 regulates photoreceptor survival in the vertebrate retina. *Proceedings of the National Academy of Sciences of the United States of America*. 110:9463-9468.

Nair, K.S., S.M. Hanson, A. Mendez, E.V. Gurevich, M.J. Kennedy, V.I. Shestopalov, S.A. Vishnivetskiy, J. Chen, J.B. Hurley, V.V. Gurevich, and V.Z. Slepak. 2005. Light-dependent redistribution of arrestin in vertebrate rods is an energy-independent process governed by protein-protein interactions. *Neuron*. 46:555-567.

Nakajima, Y., H. Iwakabe, C. Akazawa, H. Nawa, R. Shigemoto, N. Mizuno, and S. Nakanishi. 1993. Molecular characterization of a novel retinal metabotropic glutamate receptor mGluR6 with a high agonist selectivity for L-2-amino-4-phosphonobutyrate. *Journal of Biological Chemistry*. 268:11868-11873.

Nakatani, K., and K.W. Yau. 1988. Guanosine 3',5'-cyclic monophosphate-activated conductance studied in a truncated rod outer segment of the toad. *Journal of Physiology (London, UK)*. 395:731-753.

Nathans, J. 1990a. Determinants of visual pigment absorbance: identification of the retinylidene Schiff's base counterion in bovine rhodopsin. *Biochemistry*. 29:9746-9752.

Nathans, J. 1990b. Determinants of visual pigment absorbance: role of charged amino acids in the putative transmembrane segments. *Biochemistry*. 29:937-942.

Neubert, T.A., R.S. Johnson, J.B. Hurley, and K.A. Walsh. 1992. The rod transducin alpha subunit amino terminus is heterogeneously fatty acylated. *Journal of Biological Chemistry*. 267:18274-18277.

Newman, E.A. 1989. Potassium conductance block by barium in amphibian Muller cells. *Brain Research*. 498:308-314.

Nymark, S., R. Frederiksen, M.L. Woodruff, M.C. Cornwall, and G.L. Fain. 2012. Bleaching of mouse rods: microspectrophotometry and suction-electrode recording. *The Journal of Physiology.* 590:2353-2364.

Nymark, S., H. Heikkinen, C. Haldin, K. Donner, and A. Koskelainen. 2005. Light responses and light adaptation in rat retinal rods at different temperatures. *The Journal of Physiology.* 567:923-938.

Ohguro, H., J.P. Van Hooser, A.H. Milam, and K. Palczewski. 1995. Rhodopsin phosphorylation and dephosphorylation in vivo. *Journal of Biological Chemistry*. 270:14259-14262.

Oseroff, A.R., and R.H. Callender. 1974. Resonance Raman spectroscopy of rhodopsin in retinal disk membranes. *Biochemistry*. 13:4243-4248.

Peng, Y.W., J.D. Robishaw, M.A. Levine, and K.W. Yau. 1992. Retinal rods and cones have distinct G protein beta and gamma subunits. *Proceedings of the National Academy of Sciences of the United States of America*. 89:10882-10886.

Peshenko, I.V., and A.M. Dizhoor. 2004. Guanylyl cyclase-activating proteins (GCAPs) are Ca2+/Mg2+ sensors: implications for photoreceptor guanylyl cyclase (RetGC) regulation in mammalian photoreceptors. *Journal of Biological Chemistry*. 279:16903-16906.

Peshenko, I.V., and A.M. Dizhoor. 2006. Ca2+ and Mg2+ binding properties of GCAP-1. Evidence that Mg2+-bound form is the physiological activator of photoreceptor guanylyl cyclase. *Journal of Biological Chemistry*. 281:23830-23841.

Philp, N.J., W. Chang, and K. Long. 1987. Light-stimulated protein movement in rod photoreceptor cells of the rat retina. *FEBS Letters*. 225:127-132.

Pugh, E.N., Jr., and T.D. Lamb. 1993. Amplification and kinetics of the activation steps in phototransduction. *Biochim Biophys Acta*. 1141:111-149.

Pugh, E.N., and T.D. Lamb. 2000. Phototransduction in Vertebrate Rods and Cones: Molecular Mechanisms of Amplification, Recovery, and Light Adaptation. Elsevier Science. 183-255 pp.

Qin, N., S.J. Pittler, and W. Baehr. 1992. In vitro isoprenylation and membrane association of mouse rod photoreceptor cGMP phosphodiesterase alpha and beta subunits expressed in bacteria. *Journal of Biological Chemistry*. 267:8458-8463.

Ramulu, P., M. Kennedy, W.H. Xiong, J. Williams, M. Cowan, D. Blesh, K.W. Yau, J.B. Hurley, and J. Nathans. 2001. Normal light response, photoreceptor integrity, and rhodopsin dephosphorylation in mice lacking both protein phosphatases with EF hands (PPEF-1 and PPEF-2). *Molecular and Cell Biology*. 21:8605-8614.

Rao, V.R., and D.D. Oprian. 1996. Activating mutations of rhodopsin and other G protein-coupled receptors. *Annual review of biophysics and biomolecular structure*. 25:287-314.

Rieke, F. 2000. Mechanisms of single-photon detection in rod photoreceptors. *Methods in Enzymology*. 316:186-202.

Robinson, P.R., G.B. Cohen, E.A. Zhukovsky, and D.D. Oprian. 1992. Constitutively active mutants of rhodopsin. *Neuron*. 9:719-725.

Sakmar, T.P. 1998. Rhodopsin: a prototypical G protein-coupled receptor. *Progress in nucleic acid research and molecular biology*. 59:1-34.

Sakmar, T.P., R.R. Franke, and H.G. Khorana. 1989. Glutamic acid-113 serves as the retinylidene Schiff base counterion in bovine rhodopsin. *Proceedings of the National Academy of Sciences of the United States of America*. 86:8309-8313.

Sakurai, K., J.E. Young, V.J. Kefalov, and S.C. Khani. 2011. Variation in rhodopsin kinase expression alters the dim flash response shut off and the light adaptation in rod photoreceptors. *Investigative Ophthalmology & Visual Science*. 52:6793-6800.

Sampath, A.P., H.R. Matthews, M.C. Cornwall, J. Bandarchi, and G.L. Fain. 1999. Light-dependent changes in outer segment free-Ca2+ concentration in salamander cone photoreceptors. *Journal of General Physiology*. 113:267.

Sampath, A.P., H.R. Matthews, M.C. Cornwall, and G.L. Fain. 1998. Bleached pigment produces a maintained decrease in outer segment Ca2+ in salamander rods. *Journal of General Physiology*. 111:53-64.

Sampath, A.P., and F. Rieke. 2004. Selective transmission of single photon responses by saturation at the rod-to-rod bipolar synapse. *Neuron*. 41:431-443.

Slepak, V.Z., and J.B. Hurley. 2008. Mechanism of light-induced translocation of arrestin and transducin in photoreceptors: interaction-restricted diffusion. *IUBMB life*. 60:2-9.

Smith, F.C. 1929. The Ultra-Violet Absorption Spectra of Certain Aromatic Amino-Acids, and of the Serum Proteins. *Proceedings of the Royal Society of London, Series B, Containing Papers of a Biological Character*. 104:198-205.

Sokolov, M., A.L. Lyubarsky, K.J. Strissel, A.B. Savchenko, V.I. Govardovskii, E.N. Pugh, Jr., and V.Y. Arshavsky. 2002. Massive light-driven translocation of transducin between the two major compartments of rod cells: a novel mechanism of light adaptation. *Neuron*. 34:95-106.

Sommer, M.E., K.P. Hofmann, and M. Heck. 2011. Arrestin-rhodopsin binding stoichiometry in isolated rod outer segment membranes depends on the percentage of activated receptors. *Journal of Biological Chemistry*. 286:7359-7369.

Strissel, K.J., P.V. Lishko, L.H. Trieu, M.J. Kennedy, J.B. Hurley, and V.Y. Arshavsky. 2005. Recoverin undergoes light-dependent intracellular translocation in rod photoreceptors. *Journal of Biological Chemistry*. 280:29250-29255.

Strissel, K.J., M. Sokolov, L.H. Trieu, and V.Y. Arshavsky. 2006. Arrestin translocation is induced at a critical threshold of visual signaling and is superstoichiometric to bleached rhodopsin. *Journal of Neuroscience*. 26:1146-1153.

Stryer, L., J.B. Hurley, and B.K. Fung. 1983. Transducin and the cyclic GMP phosphodiesterase of retinal rod outer segments. *Methods in Enzymology*. 96:617-627.

Tang, L., T.G. Ebrey, and S. Subramaniam. 1995. Sequences and structures of retinal proteins. *Israel Journal of Chemistry*. 35:193-209.

Tsang, S.H., M.E. Burns, P.D. Calvert, P. Gouras, D.A. Baylor, S.P. Goff, and V.Y. Arshavsky. 1998. Role for the target enzyme in deactivation of photoreceptor G protein in vivo [In Process Citation]. *Science*. 282:117-121.

Tsang, S.H., M.L. Woodruff, C.K. Chen, C.Y. Yamashita, M.C. Cilluffo, A.L. Rao, D.B. Farber, and G.L. Fain. 2006. GAP-independent termination of photoreceptor light response by excess gamma subunit of the cGMP-phosphodiesterase. *Journal of Neuroscience*. 26:4472-4480.

United States., United States. Animal and Plant Health Inspection Service., and United States. 2013. Animal Welfare Act and animal welfare regulations. U.S. Dept. of Agriculture, Animal and Plant Health Inspection Service, Washington, D.C. x, 136 p. pp.

Vishnivetskiy, S.A., D. Raman, J. Wei, M.J. Kennedy, J.B. Hurley, and V.V. Gurevich. 2007. Regulation of arrestin binding by rhodopsin phosphorylation level. *Journal of Biological Chemistry*. 282:32075-32083.

Wald, G., P.K. Brown, R. Hubbard, and W. Oroshnik. 1955. Hindered Cis Isomers of Vitamin a and Retinene: The Structure of the Neo-B Isomer. *Proceedings of the National Academy of Sciences of the United States of America*. 41:438-451.

Watson, A.J., A.M. Aragay, V.Z. Slepak, and M.I. Simon. 1996. A novel form of the G protein beta subunit Gbeta5 is specifically expressed in the vertebrate retina. *Journal of Biological Chemistry*. 271:28154-28160.

Whelan, J.P., and J.F. McGinnis. 1988. Light-dependent subcellular movement of photoreceptor proteins. *Journal of Neuroscience Research*. 20:263-270.

Wilden, U. 1995. Duration and amplitude of the light-induced cGMP hydrolysis in vertebrate photoreceptors are regulated by multiple phosphorylation of rhodopsin and by arrestin binding. *Biochemistry*. 34:1446-1454.

Wilden, U., S.W. Hall, and H. Kuhn. 1986. Phosphodiesterase activation by photoexcited rhodopsin is quenched when rhodopsin is phosphorylated and binds the intrinsic 48-kDa protein of rod outer segments. *Proceedings of the National Academy of Sciences of the United States of America*. 83:1174-1178.

Woodruff, M.L., J. Lem, and G.L. Fain. 2004. Early receptor current of wild-type and transducin knockout mice: photosensitivity and light-induced Ca2+ release. *The Journal of Physiology.* 557:821-828.

Worlein, J.M., K. Baker, M. Bloomsmith, K. Coleman, and T.L. Koban. 2011. The Eighth Edition of the Guide for the Care and Use of Laboratory Animals (2011); Implications for Behavioral Management. *American Journal of Primatology*. 73:98-98.

Xu, J., R.L. Dodd, C.L. Makino, M.I. Simon, D.A. Baylor, and J. Chen. 1997. Prolonged photoresponses in transgenic mouse rods lacking arrestin. *Nature*. 389:505-509.

Yamaoka, H., S. Tachibanaki, and S. Kawamura. 2015. Dephosphorylation during Bleach and Regeneration of Visual Pigment in Carp Rod and Cone Membranes. *Journal of Biological Chemistry*. 290:24381-24390.

Yau, K.W. 1994. Phototransduction mechanism in retinal rods and cones. The Friedenwald Lecture. *Investigative Ophthalmology & Visual Science*. 35:9-32.

Yu, D.Y., and S.J. Cringle. 2006. Oxygen distribution in the mouse retina. *Investigative Ophthalmology & Visual Science*. 47:1109-1112.

Zhuang, T., Q. Chen, M.K. Cho, S.A. Vishnivetskiy, T.M. Iverson, V.V. Gurevich, and C.R. Sanders. 2013. Involvement of distinct arrestin-1 elements in binding to different functional forms of rhodopsin. *Proceedings of the National Academy of Sciences of the United States of America*. 110:942-947.

Zhukovsky, E.A., and D.D. Oprian. 1989. Effect of carboxylic acid side chains on the absorption maximum of visual pigments. *Science*. 246:928-930.

CURRICULUM VITAE

Justin D. Berry,

1427 Commonwealth Ave, Apt. #505
Brighton, MA 02135
Year of Birth: 1984
JDBerry@gmail.com, (708) 261-5901

Education

2010 – 2016
Boston University School of Medicine — *Ph.D. Physiology & Biophysics*
Advisor: M. Carter Cornwall

2007 – 2010
Northern Illinois University — *M.S. Physics*
Advisor: Laurence B. Lurio

2003 – 2007
Illinois State University — *B.S. Physics, minor Mathematics*

Research Experience

2011 – 2016

Effects of rhodopsin phosphorylation on dark adaptation and the recovery of sensitivity

Boston University School of Medicine, Dept. of Physiology & Biophysics

Dark adaptation is the process that occurs when light exposed photoreceptors transition into darkness, whereby rod photoreceptors become increasingly more sensitive to dim light illumination. Dark adaptation was believed to require both the dephosphorylation and regeneration of the visual pigment (rhodopsin). My research tested the commonly held hypothesis that the recovery of dim light sensitivity during rod dark adaptation requires the dephosphorylation of regenerated rhodopsin. In these studies, I relied on biochemical measurements that allowed me to developed a methodology to impede rhodopsin dephosphorylation, while otherwise preserving the processes involved in rhodopsin regeneration. Afterwards I performed a series of electrophysiological recordings containing large fractions of phosphorylated rhodopsin. Surprisingly, I discovered that light activation of these phosphorylated rhodopsin triggers a physiological response. I observed only a marginal reduction in the transduction gain from these activated phosphorylated visual pigments. This was a substantial deviation from conventional thinking.

Dr. M. Carter Cornwall, Ph.D. Advisor

2008 – 2010

X-Ray Dynamic and Static Measurements of Supported Phospholipid Bilayers.

Northern Illinois University, Department of Physics

The purpose of my research was to elucidate the physical properties of phospholipid membranes. These studies were designed to probe various surface phenomena, including the dynamic properties such as capillary waves and in-plane diffusion of lipid rafts. Additionally, we determined structural properties of lipid membranes systems that could potentially be used for biological sensors. In this project, I primarily utilized a variety of X-ray spectroscopy techniques to perform measurements. X-rays have a notable advantage over other techniques in that membranes can be studied without introducing probes that can alter the properties of the lipid bilayer. Within the scope of this project, I focused on studying the various properties of phospholipids through a supported triple bilayer system composed of (DPPE) phospholipids. The bilayers were created using a combination of Langmuir-Blodgett and Langmuir-Schaefer depositions, yielding highly reproducible bilayer stacks. Two points of considerable interest were the interactions between the bilayers and the substrate and those between the adjacent lipid bilayers. My method was a novel design and the experiments yielded new scientific insights.

In additional to lipid experiments, I also participated in research and development efforts conducted at Sector 8 at the Advanced Photon Source located at Argonne National Laboratory. The Sector 8 beamline is optimized to perform X-ray Photon Correlation Spectroscopy (XPCS) measures on soft-matter materials. I assisted the beamline research scientists by characterizing and determining the optimization parameters of prototype X-ray focusing optics. During this time, Sector 8 was involved with designing a high efficiency, fast charged coupled device (CCD) area detector. I provided software support for this detector by writing code to allow the raw data output from the camera to be read into preexisting analysis software. I contributed to both of these efforts to increase the applicability of XPCS to include a broader range of materials (including biological and soft-matter).

Dr. Laurence B. Lurio, Masters Thesis Advisor

2007 – 2008

Particle Flow Algorithm Design for the International Linear Accelerator

Northern Illinois Center for Accelerator and Detector Development

In this research project, I was involved with developing code that analyzed subatomic interactions, including analysis of jet energies, shape, and geometry of the collision process that was believed to be the dominant signal for Higgs production at the proposed International Linear Collider. The algorithms were necessary to optimize the detector design. My research required close communication and collaboration with members of the Stanford Linear Accelerator Center. The project was terminated before completion due to budget constraints and funding of ILC project.

Dr. Dhiman Chakraborty, Research Advisor

Research Skills

Developing novel experimental methodologies: In addition to utilizing established methodologies, my research required critical thinking around new approaches, and the ability to integrate concepts into new experimental designs.

Experimental apparatus design and fabrication: My research required machining several novel parts that were essential in performing cutting-edge research. Some designs of mine are now employed as operating apparatuses in other laboratories. I have experience machining with metals, plastics, and (as a hobbyist) wood.

Tissue culturing: I have worked on very sensitive isolated retinae in a way that maintains normal physiological function, and have experience with derived embryonic stem cells (on retinal pigment epithelial cells).

Electrophysiology: I am proficient in single cell suction electrode recordings and electroretinogram measurements of isolated retinae.

Spectroscopy: I am proficient in spectrophotometry, microspectrophotometry, grazing incidence X-ray spectroscopy, X-ray photon correlation spectroscopy. Familiar with ^{1}H NMR, IR spectroscopy.

Computer Programing: I have extensive programing experience with Matlab, and Python. I am competent with labVIEW, C++, and Fortran 90. I have coded my own data analysis software (with graphical user interfaces).

Publications

Effect of Rhodopsin Phosphorylation on Dark-Adaptation in Mouse Rods, **Justin D. Berry**, Rikard Frederiksen, Soile Nymark, Yun Yao, Jeannie Chen, M. Carter Cornwall, (Submitted Sept. 2015, Revised Submission Feb 2016 with Journal of Neuroscience).

Phosphorylation and arrestin binding control the decay of photoactivated rhodopsin and dark adaptation of mouse rods, Rikard Frederiksen, Soile Nymark, Alexander V. Kolesnikov, **Justin D. Berry**, Leopold Adler IV, Yiannis Koutalos, Vladimir J. Kefalov, M. Carter Cornwall, (Submitted Oct. 2015, in revision with Journal of General Physiology)

Substrate suppression of thermal roughness in stacked supported bilayers, C.M. DeCaro, **J.D. Berry**, Y. Ma, G. Chen, Z. Jiang, L. Tayebi, A.R. Sandy, A.N. Parikh, S.K. Sinha, and L.B. Lurio, Phys. Rev. E 84, 041914 (2011).

Thesis/Dissertation

Effects of rhodopsin phosphorylation on dark adaptation and the recovery of sensitivity, **Justin D. Berry**, Boston University School of Medicine. Oral Defense was March 17 2016.Written dissertation was submitted in April 2016.

Soft Matter Studies of Phospholipid Membranes, **Justin D. Berry**, Laurence B. Lurio. Northern Illinois University (2010). ISBN: 9781124022871

Presentations

Research Talks

Dark adaptation of rod photoreceptors in the presence of persistent rhodopsin phosphorylation, **Justin D. Berry**, Rikard Frederiksen, Yun Yao, Jeannie Chen, M. Carter Cornwall, Association for Research in Vision and Ophthalmology Annual Meeting, Orlando, FL, May 2014

Meta III limits opsin availability during pigment regeneration in bleached mouse rods, Rikard Frederiksen, Soile Nymark, **Justin D. Berry**, Alexander V. Kolesnikov, Vladimir J. Kefalov, M.C. Cornwall, Association for Research in Vision and Ophthalmology Annual Meeting, Orlando, FL, May 2014

Dynamic and Static Measurements of a Single and Double Phospholipid Bilayer Systems, **J.D. Berry**, C.M. DeCaro, D. Bricarello, Y. Ma, G. Chen, Z.. Jiang, A.N. Parikh, S.K. Sinha, and L.B. Lurio, Biophysical Society, 54th Annual Meeting, San Francisco, CA, February 2010.

Investigation of Booming and Burping Sand Phenomena, **J.D. Berry**, B.K. Clark, and D.T. Marx, Argonne Symposium for Undergraduates in Science, Engineering, and Mathematics, Argonne National Laboratory, November 2006.

Analyzing the Interaction of Laser and Hollow Cathode Lamp, **J.D. Berry**, T.A.

Juskevice, B.K. Clark, and E. Rosa, Jr., Argonne Symposium for Undergraduates in Science, Engineering, and Mathematics, Argonne National Laboratory, Argonne, IL, November 2005.

Synchronizing a Hollow Cathode Discharge Damp with a Diode Laser, **J.D. Berry**, T.A. Juskevice, B.K. Clark, and E Rosa, Jr., Argonne Symposium for Undergraduates in Science, Engineering, and Mathematics, Argonne Nation Laboratory, Argonne, IL, November 2004.

Poster Presentations

Phosphorylation State Of Opsin Affects The Rate Of Pigment Regeneration In Mouse Rod Photoreceptor Outer Segments, **Justin D. Berry**, Rikard Frederiksen, Soile Nymark, and M. Carter Cornwall, Association for Research in Vision and Ophthalmology, Inc Annual Meeting 2012, Fort Lauderdale FL, May 2012

Enhancement of Diffuse X-Ray Scattering from Supported Phospholipid Bilayers Using Au Nanoparticle Labeling, **J.D. Berry**, C.M. DeCaro, A.M. Brozell, J.E. DeBartolo, Y. Ma, V.N.C. Karunaratne, M. Mukhopadyay, G. Chen, Z. Jiang, J. Strzalka, A.N. Parikh, S.K. Sinha, and L.B. Lurio, Argonne Users Meeting 2009, Argonne National Laboratory, Argonne, IL, May 2009

Synchronization of a Plasma Discharge to a Frequency Modulated Laser, **J.D. Berry**, T.A. Juskevice, B.K. Clark, and E. Rosa, Jr., Illinois State University Undergraduate Research Symposium, Normal IL, April 2006.

Experimental Coupling of Laser Light with a Plasma Discharge, **J.D. Berry**, T.A. Juskevice, B.K. Clark, and E. Rosa, Jr., Illinois State University Undergraduate Research Symposium, Normal IL, April 2005.

Academic Activities

Professional

Graduate Researcher, Advisor: M. Carter Cornwall, Department of Physiology & Biophysics, Boston University School of Medicine, Boston, MA, May 2011 – present

Graduate Teaching Assistant, Department of Physiology & Biophysics, Boston University School of Medicine, Boston, MA, Fall 2014

Visiting Graduate Scientific Researcher, Local Advisor: Jeannie Chen, Zilkha Neuroscience Institute, Keck School of Medicine, University of Southern California, Los Angeles, CA, March 2014

Visiting Graduate Scientific Researcher, Local Advisor: A.P. Sampath, Zilkha Neuroscience Institute, Keck School of Medicine, University of Southern California, Los Angeles, CA, July – August 2013

Graduate Research Assistant, Advisor: Laurence B. Lurio, Department of Physics, Northern Illinois University, DeKalb, IL, June 2008 – August 2010

Graduate Teaching Assistant, Department of Physics, Northern Illinois University, DeKalb, IL, August 2007 – May 2009

Undergraduate Teaching Assistant, Department of Physics, Illinois State University, Normal, IL, August 2006 – May 2007

Volunteer

Tutor, Physics, Department of Physics, Normal Illinois University, DeKalb, IL, September 2007 – May 2010

Scientific Secretary, American Linear Collider Physics Group Conference 2007, Fermi National Accelerator Laboratory, October 2007

Tutor, Physics and Mathematics, Department of Physics, Illinois State University, Normal, IL, September 2005 – May 2007

Presenter, Youth Physics Outreach Program, Illinois State University, Normal, IL, October 2006 – May 2007